University of Naples Federico II University

University of Engineering Department of Chemical Engineering, Materials and Industrial Production

Ph.D in Engineering of Materials and Structures

XXVII Cycle

DEVELOPMENT OF A THREE-DIMENSIONAL ORGANOTYPIC SKIN MODEL FOR *IN VITRO* STUDY OF SKIN DISEASE STATE

Ph.D Thesis

Bernadette Lombardi

Tutor

Prof. Paolo Antonio Netti

DEPARTMENT COORDINATOR

Prof. Giuseppe Mensitieri

ADVISOR

Doc. Ing. Francesco Urciuolo

"Thank you to all those who have fondly supported me and patiently endured me"

Table of Contents

Abstract

The SKIN functions as a protective physical barrier against the outside [1] and has a primary role to protect body from external influences such as pathogenic microorganisms and mechanical injuries [2]. Moreover in the skin, the interaction of keratinocytes, fibroblasts and melanocytes is tightly controlled by various factors and cascades [3]. Under normal conditions, there is a balance between cell types via cell–cell contact and the extracellular matrix (ECM). The ECM provides structural scaffolding for cells, as well as contextual information [4,56]. The disruption of these equilibria can result in an uncontrolled stroma degeneration (as involved in scarring) [7] or uncontrolled proliferation of epithelial cells (as in malignant melanoma) [8].

Wound healing is a highly organized series of processes resulting in tissue integrity and function of the damaged tissue; this process needs a complex microenvironement to be studied. Carcinogenesis is defined as complex, adaptive process, controlled by intricate communications between the host and the tissue microenvironment [6]. Thus, the microenvironment and the stroma play an important role in both wound healing process and tumour development.

In this perspective, in the present PhD thesis a tissue engineering bottom-up approach was used to fabricate a 3D dermis tissue. This model was composed by a cell-synthesized and responsive extracellular matrix that resembles the *in vivo* dermis, and it was used as living platform to study *in vitro* skin alteration and diseases.

The first model of skin alteration dealt with the wound healing process, by exploiting its self-repairing capability. Interestingly, the relationship between cell migration, differentiation marker and ECM production and remodeling during repair process followed the same *in vivo* timing. Moreover, the presence of a responsive dermis allowed possibility to evaluate granulation tissue and to study and understand processes involved in scarring. Indeed, due to the endogenous nature of the stroma, the model proposed could represent a valuable tool to *in vitro* study tissue status at both cellular and extracellular level after a physical damage.

At least, once demonstrated dermis responsivity, we investigated epidermal counterpart. In this perspective, we fabricated a 3D human skin equivalent (3D-HSE) model with the same endogenous stroma as dermis component to study cell-ECM – with native basement membrane (BM) – and cell–cell communications, in the presence of an aggressive form of skin cancer: melanoma. As a fact, carcinogenesis can disrupt these forms of communication , thus altering cell biology of human skin [6,9]

Consequently, we investigated the role of skin cells and BM components on melanoma biology and invasive ability in reconstructed human skin equivalent. We first made-up and characterized a human skin model that resembled the architecture of skin *in situ*, than we carried out an analogous procedure for the equivalent engineered tumor model. On the basis of our results, we can assert that there is communication between skin cells and melanoma cells and the outcome is dictated by the nature of the melanoma cells. Thus, the bioengineered 3D melanoma skin model may become a valuable tool to investigate the underlying mechanics of melanoma infiltration. The proposed study does not recapitulate yet melanoma metastasis process as a whole, however, the present engineered 3D tissue represents a reliable model for investigating the phenotype and behavior of melanoma cells derived from primary sites. Indeed, the 3D melanoma skin model is suitable to study the biological properties of radial growth phase invasion. This study represents a preliminary model for investigating all aspects of melanoma metastasis and it has great potential for improving our understanding of the interactive biology between melanoma cells and their immediate surroundings and evaluating melanoma cells influence on epidermis structure and differentiation.

In conclusion, the present 3D engineered skin model represents a valid platform to study scar formation and a valuable tool for studying healthy and disease skin [10,11] or for screening test *in vitro*. Moreover, this platform could provide an *in vivo* skin substitute in clinical applications [5,12,13].

References

1. Iii JTS, Tompkins RG, Burke JF. Artificial skin. *Rev Med*. 2000;(3):231-244.

2. Metcalfe AD, Ferguson MWJ. Bioengineering skin using mechanisms of regeneration and repair. *Biomaterials*. 2007;28(34):5100-5113. doi:10.1016/j.biomaterials.2007.07.031.

3. Groeber, Florian, Holeiter, Monika, Hampel, Martina, Hinderer, Svenja, Schenke-Layland, Katja. Skin tissue engineering — In vivo and in vitro applications. *Adv Drug Deliv Rev*. 2011;63(4-5):352-366. doi:10.1016/j.addr.2011.01.005.

4. Auger FA, Lacroix D, Germain L. Skin substitutes and wound healing. *Skin Pharmacol Physiol*. 2009;22(2):94-102. doi:10.1159/000178868.

5. Fernandes H, Moroni L, van Blitterswijk C, de Boer J. Extracellular matrix and tissue engineering applications. *J Mater Chem*. 2009;19:5474. doi:10.1039/b822177d.

6. Bissel MJ, Radisky D. Putting tumors in context. *Nat Rev Cancer*. 2001;1(1):46-54. doi:10.1038/35094059.PUTTING.

7. Hari G. Garg MTL. *Scarless in Wound Healing*. Vol 133.; 2000. doi:10.1016/B978-0-444-62644-8.00008-X.

8. Elder D, Elder D. Melanoma Progression. 2016;(2015):1-8. doi:10.1016/j.pathol.2015.12.002.

9. Ruiter D, Bogenrieder T, Elder D, Herlyn M. Melanoma – stroma interactions : structural and functional aspects. :35-43.

10. Seo BF, Lee JY, Jung SN. Models of abnormal scarring. *Biomed Res Int*. 2013;2013. doi:10.1155/2013/423147.

11. Middelkoop E, Bogaerdt AJ Van Den, Ulrich MM, Meeting S. Artificial dermis and cellular aspects of scar formation. 2006;(2):1-14.

12. Balasubramani M, Kumar TR, Babu M. Skin substitutes : a review. 2001;27:534-544.

13. Beaumont KA, Mohana-Kumaran N, Haass NK. Modeling melanoma in vitro and in vivo. *Healthcare*. 2013;2(1):27-46. doi:10.3390/healthcare2010027.

1 Tissue engineering and Skin tissue engineering – *in vivo* and *in vitro* applications

1.1 Tissue engineering: an overview

The terminology 'tissue engineering' was officially coined at a National Science Foundation workshop in 1988 to mean 'the application of principles and methods of engineering and life sciences toward the fundamental understanding of structure-function relationships in normal and pathological mammalian tissues and the development of biological substitutes to restore, maintain or improve tissue function' [1]. Tissue engineering is a radically new concept for the treatment of disease and injury and consists in a multidisciplinary discipline that involves biology, medicine, and engineering [2]. This science born to improve the health and quality of life for millions of people worldwide by restoring, maintaining, or enhancing tissue and organ function [3]. In addition this science can have diagnostic applications by developing of in vitro tissue for testing drug metabolism and uptake pathogenicity [4]. The foundation of tissue engineering for either therapeutic or diagnostic applications gives possibility to exploit living cells in a variety of ways. For this reason, it has been necessary to generate structures that mimic the intricate architecture and complexity of native organs and tissues. With the desire to create more complex tissues with features such as developed and functional microenvironments, cells-cells and cells-matrix communications and tissue specific morphology, tissue engineering techniques are beginning to focus on building modular microtissues with repeated functional units [5] [6]. This science evolved from the field of biomaterials development and refers to the practice of combining biodegradable scaffold, cells and molecules into functional tissues [7].

1.1.1 Classical approach

Classical strategies of tissue engineering employ a "top-down" approach in which cells are seeded on a biodegradable polymeric scaffold. In top-down approaches, cells populate the scaffold and create the adequate extracellular matrix (ECM) and microenvironment often with the aid of growth factors [8], perfusion [5] and mechanical stimulation [9]. One of the first rules to induce formation of adequate microenvironement are the use of biomimetic and biodegradable scaffolding and the use of structural features on the microscale to build modular tissues that can be used as building blocks to create larger tissues [5]. However, despite advances, top-down approaches often have difficulty recreating the intricate microstructural features of 3D-tissues. Indeed, this approach – to produce viable tissue by seeding cells into preformed, porous, and biodegradable scaffolds – presents several problems mainly due to the difficulty in reproducing, adequate microenvironmental conditions in a three-dimensional (3D) thick structure [10 11].

1.1.2 Bottom up approach

An innovative modular approach was proposed to resolves typical problems of top-down approaches and to recreate the intricate microstructural features of tissues. This approach builds tissues by assembling blocks mimicking those units in a bottom–up [5]. The fabrication of those tissue models necessitates tools to create an initial architecture and to systematically manipulate their microenvironments in space and time [12]. Once obtained microtissues, these multicellular spheroids spontaneously aggregate and self-organize and can be used as building blocks to create larger scaffold-free tissues [5 13]. One of the major challenges of this method is to assemble modular tissues with specific micro architectures into macroscale biomimetic engineered tissues. Despite this approach allows possibility to print complex tissues with high shape resolution, their use is limited by lack of mechanical integrity of the cellular aggregates that restricts the size of the resulting tissues. In addition to cell aggregates, the microtissues used as building units include cell-laden microgels [5], cell-seeded microbeads [14], and cell sheet [7]. However there is a strong biological basis for this bottom-up approach as many tissues are comprised of repeating functional units, such as the lobule in

the liver [5]. By mimicking native microstructural functional units, bottom-up approaches aim to create more biomimetic engineered tissues. One of the major challenges by using this approach is to assemble modular tissues with specific micro architectures into macroscale biomimetic engineered tissues [15] [16]. Other challenge is to retain the microarchitecture and cellular behaviour of modular tissues, and at same time, to create engineered tissues with robust mechanical properties. Figure 4 show an example of bottom-up methods witch microscale building blocks can be assembled into larger construct realized by various technology as: soft lithography [17], photolithography [18], membrane technology [19], centrifugal casting [10], micromachining [20], or the combination of multiple processes [21]. Moreover, combination with computer-aided printing systems helps generation of appropriate and complex 3D-templates. Designs must focus on promoting itself-remodelling into the final architecture. Usually these building blocks composed by gel encapsulated cells [16] or spontaneously aggregated cells [22]. Microbioreactors are other important makers of this approach, Indeed, presence of microbioreactors allows long-term control of microscale tissue, formation of adequate microenvironement and accurate control of amounts of biological factors and relate gradients [18] [23] [15]. The primary advantages of this method are the rapid production of millimetre-thick 3D cell structures, a homogeneous cell density, a tissue formation without necrosis in a period of less than a week and the possibility. to culture microtissues in controlled, heterogeneous environments [2425]

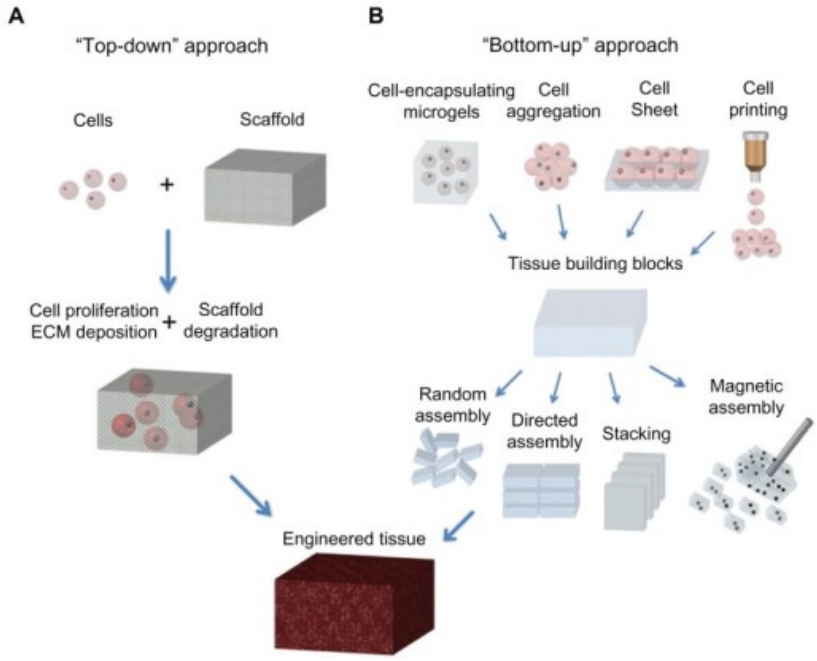

Fig. 1: Bottom-up & Top-down approaches to tissue engineering. In the bottom-up approach there are multiple methods for creating modular tissues, which are then assembled into engineered tissues with specific micro-architectural features. In the top-down approach, cells and biomaterial scaffolds are combined and cultured until the cells fill the support structure to create an engineered tissue [8].

1.2 Human skin and engineering skin tissue

The skin is the largest organ in mammals with a total area of about 20 square feet and has a surface area of 1.5–2.0 m^2. Skin plays a primary role in protecting the body from mechanical damage and his first role is to create a protective barrier at the interface between the human body and the surrounding environment in order to protect the body against toxins, pathogens and external microorganisms [26]. Moreover the skin helps regulate body temperature, allows the sensations of touch, heat, and cold and receives sensory stimuli from the external environment [27]. The skin consists of three layers of tissue: epidermis, dermis with a complex nerve and blood supply, and hypodermis composed mainly of fat and a layer of loose connective tissue. At cellular level, cell types are various (Fig.2) [2]. The barrier function of the skin is provided by its avascular epidermal layer, which is composed mainly of keratinocytes: a-nuclear keratinocytes product keratin and form the surface barrier layer. Melanocytes are found in the basal layer of the epidermis and provide skin colour by production of melanin. Fibroblasts are the first cell type present in dermis and provide strength and resilience to stroma [26].

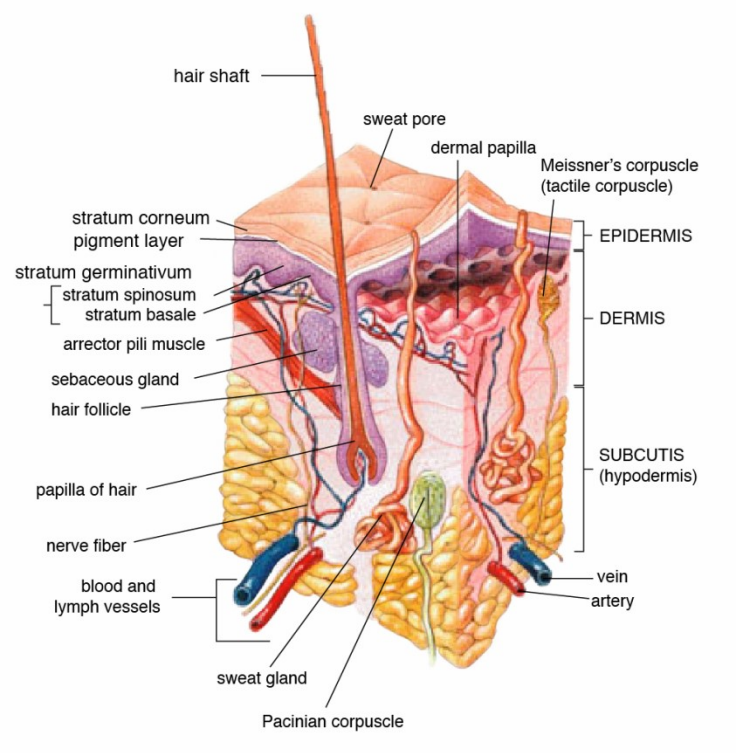

Fig. 2: The epidermis, dermis, and subcutaneous tissue are the three layers that compose the human skin

In the past 30 years, great efforts have been made to create substitutes that mimic human skin [28] and different researches were born by evaluating different aspects of skin and studying all types of cell behaviour. Indeed, engineered human skin models designed require the ability to fabricate tissues that faithfully mimic the *in vivo* counterparts to advance our understanding of human disease processes [26]. These artificial skins have been used for clinical applications, promoting the healing of acute and chronic wounds, to study skin diseases, to shown that cell-cell interactions during early cancer progression and for *in vitro* studies as screening platform [2] [26]. Thus skin substitutes were used both for clinical application promoting in vivo repair by their use as in vivo grafts, than for in vitro test systems [29]. In this perspective, engineering skin (ES) tissue born as valid alternative to use of animal models. Animal models provide valuable translational vehicles for human treatment modalities and disease investigations. However, because there are differences between animal skin and human skin development [26], as for example aberrant scars are specific to humans, the extrapolation to the human situation and development of an animal model has been extremely difficult [30]. The major difference between laboratory animals and humans are differences in the metabolism, different anatomical architecture compared to human skin and the presence of the panniculus

carnosus in animals, a fibromuscular layer enabling the skin to slide over underlying fascia [31]. In addition, ES are a valid alternate to *in vitro* 2D-monolayer cultures of human cells because of the lack of complex cell-cell and cell-ECM interactions [32]. Most tissue-engineered skin is created by expanding specially keratinocytes in the laboratory (at a rate much greater than in vivo happened) and using them to restore barrier function (the primary objective for burns patients) or to initiate wound healing (for chronic non-healing ulcers) or to study skin disease development (such as in melanoma evolution) [27] [33] (Fig. 3). Other uses include accelerating healing, reducing pain and correcting conditions in which healing has been suboptimal (for example, in scars or pigmentary defects), investigate malignant differentiation of epithelial cells and the *in vitro* use as screening platform for emerging drugs testing [34] [27]. Keratinocytes were first reliably cultured in the laboratory about 40 years ago [35]. This developed into the production of small sheets of cells three or four layers thick [36] (known as cultured epithelial autografts, CEAs). Keratinocytes are an ideal alternative treatment for large burns, instead of skin grafting. Since then, numerous clinical trials have demonstrated the efficacious application of cultured keratinocytes during wound repair process [37] [2]. However, due to lack of dermal structures, simple keratinocyte coverage is fragile and the take rate varies depending on the condition of the defected area. To improve an increase of survival [38] and proliferation [10] rate of keratinocytes, fibroblasts were used [2]. Fibroblasts are the second class of cells using by skin tissue engineering, are dermal cells plays an important role in the wound healing process by producing extracellular matrix (ECM) proteins and cytokines [39] [25]. Fibroblasts behaviour was investigated by introduction of artificial dermis or exogenous collagen and they have been incorporated into a three-dimensional scaffold, where these cells could secrete and organize an extracellular matrix [40] [41]. In this perspective it must be consider three factors for the development of tissue-engineered materials: the safety of the patient, clinical efficacy and economic convenience of use [42] [43]. Any cultured cell material, as the use of bovine or rat-tail collagen, carries the risk of transmitting viral or bacterial infection, and may also have a disease risk [33]. There must be clear evidence that tissue-engineered materials provide benefit to the patient and disease risk must be eradicated. In the light of that, significant progress has been made over the last years in the development of in vitro-engineered substitutes that mimic human skin, either to be used – without infection risk – as grafts for the replacement of

lost skin or for the establishment of human-based in vitro skin models. Moreover, tissue-engineered human skin equivalents (HSEs) have contributed significantly to the understanding of biological processes and skin diseases [44–46] This human tissue model recapitulates the morphology of skin to a large degree and has facilitated further clarification of different cellular roles for a normal epidermal/dermal morphogenesis. Moreover these optimally-engineered human tissues has been adapted to study a variety of human disease processes that simulate events that occur in human skin and other stratified squamous epithelia. As examples is how SE cultures have been used to characterize the response of human skin-like tissues following wounding and during early cancer development in a premalignant tissue [8 47]. Indeed the presence of a 3D-structure involves interactions between cancer cells and their microenvironment and create a context that promotes tumour growth and consequently, a good context were study cancer progression and related mechanism [48 27 49 14].

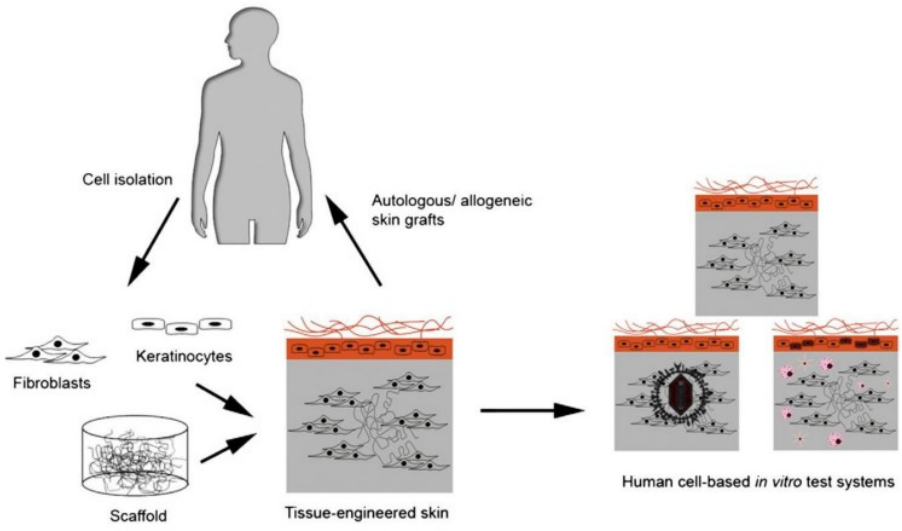

Fig. 3: Schematic illustration of principles of skin tissue engineering. Primary keratinocytes and fibroblasts are isolated from human donor tissues, which are then in vitro expanded prior seeding onto suitable scaffold materials/matrices. For a full-thickness skin equivalent, the fibroblasts and the matrix are initially used to establish the dermal part. The keratinocytes are seeded afterwards on the top of the dermis to ultimately form the epidermal part of the skin substitute. The in vitro-engineered skin can serve as skin graft or can be used as human-cell based in vitro test system.

1.2.1 Human skin: epidermis

The outermost layer of the skin is the epidermis. It forms a protective barrier over the body's surface which prevents pathogens from entering. It is also responsible of skin turgor, body temperature regulation and for nutrients absorption. The epidermal barrier layer is relatively thin (0.1–0.2 mm in depth) and securely attached to the underlying dermis by a specialized basement membrane zone [50] (Fig.4). The major cellular population are keratinocytes. These cells consist of 95% of all epidermal cell population. These cells progressively differentiate from cells in the basal layer, which is located on the basement membrane and gives rise to daughter keratinocytes, to cells without nuclei which are pushed upwards and product sheet of keratin. These upper keratinized epidermal layers provide the barrier layer, which resists bacterial entry and prevents fluid and electrolyte loss. This cell behaviour provides epithelium stratification [51]. Indeed, the epidermis can be subdivided into five layers: stratum basale (composed mainly of proliferative keratinocytes attach to the basement membrane); stratum spinosum; stratum granulosum (in this layer keratinocytes lose their nuclei and their cytoplasm appears granular); stratum lucidum; stratum corneum (this layer is full of keratin proteins). During development of epidermal layers, keratinocytes became anucleate, change shape and become highly organized, forming cellular junctions (desmosomes) between each other and secreting keratin proteins that aid in protection from external factors [522].

Melanocytes other non-epithelial epidermal cells and that provide skin pigmentation. Melanocytes are dendritic cells only found in the deepest layer of the epidermis. The basic features of these cells are the ability to melanin production. These cells form the epidermal melanin units as a result of the relationship between one melanocyte and 30-35 associated keratinocytes [53]. The ratio of melanocytes to keratinocytes is 1: 10 in the epidermal basal layer. Melanocytes origin from neural crest cells (melanoblasts) and the life cycle of these cells consists of several steps including migration and proliferation of melanoblasts, differentiation of melanoblasts into melanocytes, maturation of melanocytes and subsequent melanin production [49]. The embryonic development of melanocytes gives an opportunity to better understand the various skin diseases, for example melanoma and its heterogeneity. The precise mechanisms that control the organization and number of melanocytes in the epidermis are unknown [54 49].

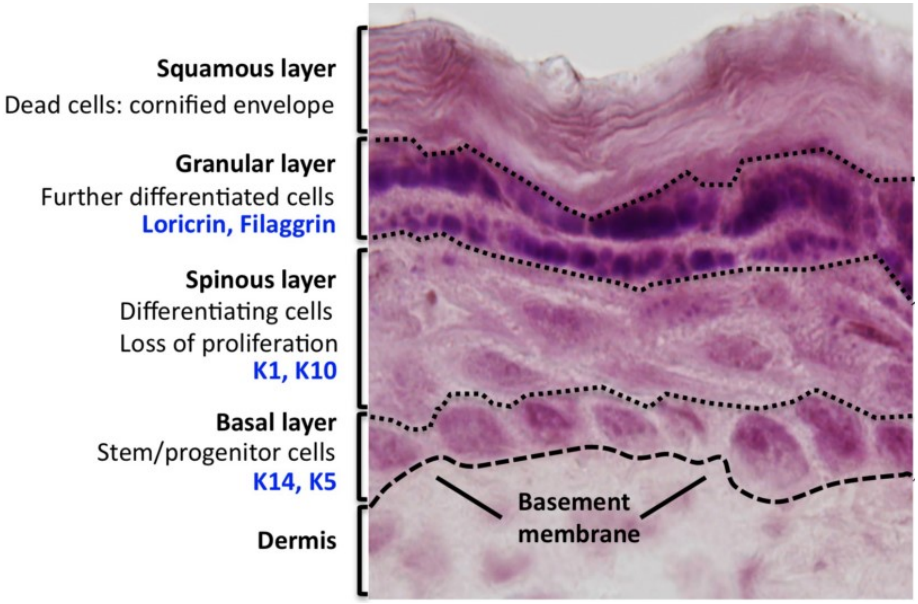

Fig. 4: The structure of epidermis. The epidermal barrier layer is relatively thin and composed of four different layers. Epidermis attached to the underlying dermis by a specialized basement membrane zone

1.2.2 Human skin: dermis and related components

The dermis is the second layer of skin and varies in thickness depending on the location of the skin. It is 0.3 mm on the eyelid and 3.0 mm on the back. The dermis specially composed of a cellular component and extra-cellular component (ECM) with a specific 3D-structure and architecture (Fig.5). The ECM exists in several biochemical and structural forms and is secreted and assembled by cooperative activity of numerous cell types for the formation of stroma [55]. The major cell population are fibroblasts. The ECM 3D-structure and its different components can signal specific information to fibroblasts and modulate cell migration into and within inflamed tissue, cell activation, proliferation and differentiation. Apart from these cells, the dermis is also composed of matrix components such as collagen (which provides strength), proteins, proteoglycans and glycosaminoglycans (GAGs), elastin and extrafibrillar matrix. This extra-cellular matrix (ECM) has a relevant role into dermis and each single component of ECM impart specific signal to cell that modulate basic function such as regeneration and maintenance of tissues and organs [56]. Presence both cells than extra-cellular components cause a relevant environment composed by an intricate 3D network of fibrillar proteins, proteoglycans and glycosaminoglycans (GAGs) (Fig). The major component

of ECM is collagen: it is the main component of connective tissue. Currently are identified more than 20 genetically different types of collagen [5758] [59]. Collagen molecules consist of three polypeptide A chains, each of them containing at least one repeating Gly-X-Y sequence, where X and Y are usually proline and hydroxyproline, respectively [58] [55]. All hydroxylation and glycosylation are post-translational modifications. The three chains are supercoiled around a central axis in a right-handed manner to form a triple helix. By a crosslinking mechanism, collagen molecules self-assemble into collagen fibrils to generate large amount of collagen fibers and consequently, collagen bundles. Depending on their structure and supra-molecular organization, collagens can be classified into fibrillar (accounting for 90% of all collagens) and non-fibrillar collagens; these two collagen components involve in different characteristics to connective tissue. For example, fibrillar collagens provide torsional stability and tensile strength. In contrast, basement membrane collagens such as collagen type IV are more flexible, giving the basement membrane its typical characteristics [60]. In general, collagens are mainly seen as structural proteins although they contain small sequences responsible for binding to cellular receptors. Other extra-cellular skin components are fibronectin (it is the second most abundant protein in ECM) witch are responsible for cell adhesion; elastin witch give to skin the ability of transiently stretching; GAGs witch are responsible for increase in tissue stiffness as they act as water pumps under mechanical loads; and laminin as first component of basal membrane [57]. Moreover ECM plays a critical role in successful tissue engineering as well [61].

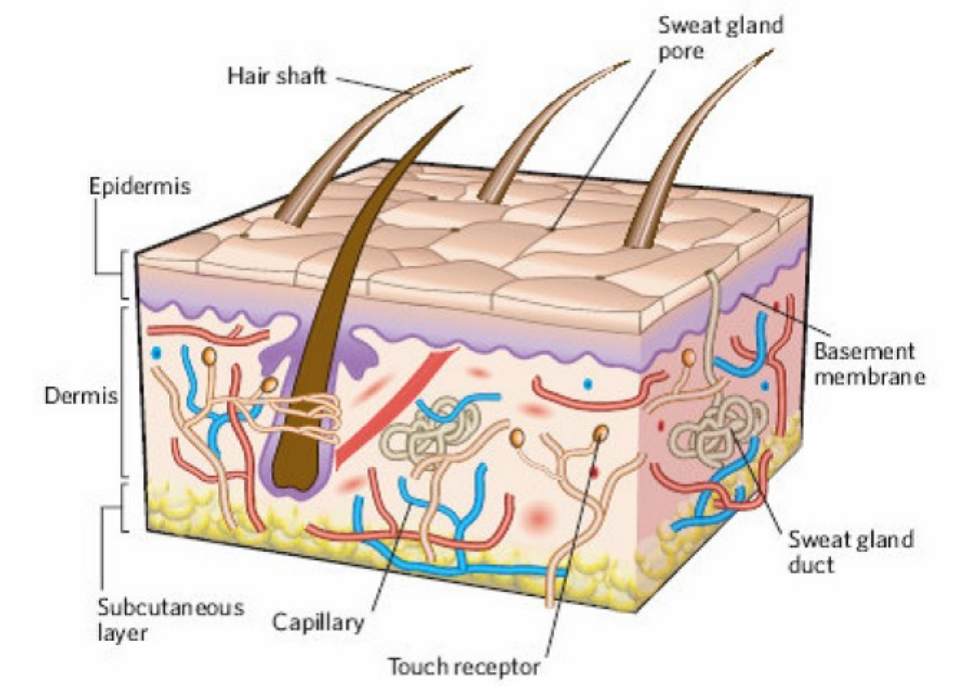

Fig. 5: The structure of human dermis. Dermis consists of several different types of collagen fibre, which attach cells securely to the underlying dermis, and is visible at the electron-microscope level. The dermis varies in thickness depending on its site in the body and is composed primarily of collagen I, with dermal inclusions of hair shafts and sweat glands, which are lined with epidermal keratinocytes. The dermis is well vascularized and also contains receptors for touch, temperature and pain.

1.3 *In vivo* applications

Necessity to use engineered skin in clinical applications born when physiological *in vivo* process doesn't restore normal physiognomy of tissue. There are numerous reasons for skin damage including genetic disorders, intense trauma, chronic wounds, inadequate immune-response or surgical interventions [26] [62] One of the most common causes for major skin injury is thermal trauma specially when the affected area of skin is too large and therefore cannot be successfully treated with conventional techniques with consequently death of the patient or a chronic ulcer formation [63]. Although autologous skin grafts remain the first option in the current standard of care for burn patients, there are clinical circumstances where using the donor's own skin might not be optimal above all because problems associated to the quantity of tissue damaged. For this reason tissue engineering is even more relevant in this context. Skin substitutes are artificial skin replacement constructs that provide the protective barrier of the skin when placed over acute burn injuries or other chronic skin wounds such as cutaneous ulcers and congenital anomalies [64] [65]. Their first objective is to work as skin

equivalents, facilitate repair, and restore the functional loose properties of skin. Indeed, the production and the use of skin substitutes have led to dramatic improvements in the odds of survival for severely burned patients, and in the cases of chronic wounds. Several reviews on many different products have appeared in the scientific press over the last few years and an extensive body of literature exists on the experimental and clinical use of epidermal/dermal replacements [63] [34] [26] [62]. These skin substitutes can have different roles indeed they can act both as temporary wound covers than permanent skin replacements, depending on their design and composition. The main advantage of using engineered skin constructs is that they reduce or eliminate the need for donor site area, which is required for autologous split-thickness grafts. Nowadays more than 20 products have actually commercially available for clinical trials and use as adequate grafts [66]. According to literature, skin substitutes can be divided by using several criteria: dermal versus full skin substitutes, biological and synthetic scaffold, acellular or cellular materials and substitutes based on allogeneic or autologous cells. At moment, many current products do not contain any living cells and vary in their capacity to harness the innate capacity of the body to heal itself [62] [67] [64]. Only recent engineered grafts include living cells with allogeneic or autologous origin, and are often referred to as 'cellular therapy' or 'tissue-engineered' products. The most commonly products that are being used at moment, for wound treatment are: Epicel® and Epidex® as epidermal platform; Biobrane™, Integra™, Alloderm™ Oasis® and TransCyte™ (in different conservation techniques) as acellular dermal platform, Dermagraft®, Apligraf® and Hyalograft® as cellular dermal substitutes and Apligraft™ and Orcel™ as available full-thickness constructs. Manly engineered construct are reported in table 1. All principles and characteristics of various skin substitution and relevant materials have been described already some decades ago in different reviews [67] [26] [63] [34]. In general, the majority of researches focus on the ability to allow epidermal coverage to restore barrier function of the skin and the presence or influx of cells that will function as dermal cells and produce dermal tissue rather than scar tissue. At present day, dermal substitutes function as an optimized wound bed to support outgrowth of keratinocytes, or from an epidermal component such as a skin graft or an artificial epidermal component containing autologous or allogeneic keratinocytes [40]. Despite developments in available skin substitutes, there are several limitations and various aspects witch involve

several problems in the clinical therapeutic collection such as reduced vascularization [36], scarring [62], failure to integrate, poor mechanical integrity [34] and immune rejection [1]. Indeed, a perfect graft should be easily available, afflict no immune response, cover and protect the wound bed in sterile condition, enhance the healing process, lessen the pain of the patient and result in little or no scar formation [26]. Despite recent development, for example, proper wound bed preparation, including cleaning, debridement and attention to aseptic conditions, must be conducted in a meticulous and timely fashion in order to obtain the best possible clinical outcome and to minimize number of infections (but not for completely avoid them) [27]. Moreover, despite this evidence, a relevant limit is the inability to avoid scar formation after the use of epidermal/dermal substrate *in vivo* applications. In vivo, it was shown that the presence of fibroblasts in the dermal matrix appears to inhibit migration of other mesenchymal cells but may also control fibroblast migration into the wound bed also evidence proves that a fibroblast-seeded matrix improves scar contraction in a cell number-dependent fashion in porcine full-thickness wounds [31] [30] [68] [69]. Moreover, it has been reported that wound contraction and scar formation in an *in vivo* model could be prevented with a responsive substitute dermal matrix seeded with skin cells. Fundamental research into wound healing and scar-free regeneration raises the hope that we will eventually be able to restore almost completely the appearance and function of skin after a grafting [70].

Skin subtitues	Composition	Comments
Integra™	Dermal analogbovine collagen and chondroitin-6- sulfate GAG; epidermal analog—silicone polymer	Silicone layer is removed upon vascularization of dermis, and replaced by a thin layer of autograft
Alloderm™	Human allograft skin that has been screened for transmissible pathogens, with all epidermal components and dermal cells removed	Grafted like dermal autograft and covered with a thin autograft
TransCyte™	Nylon mesh seeded with neonatal human foreskin fibroblasts that are destroyed before grafting	Temporary wound dressing upon which autografts are placed
Dermagraft™	Bioabsorbable polygalactin mesh matrix seeded with human neonatal fibroblasts and cryopreserved	Matrix facilitates re-epithelialization by the patient's own keratinocytes
OrCel™	Type I collagen matrix seeded with neonatal foreskin fibroblasts and keratinocytes	Wound dressing with two different cell types
Epicel™	Sheets of autologous keratinocytes attached to petrolatum gauze support	Wound dressing with autologous cells
Biobrane™	Outer epidermal analog—ultrathin silicone film; inner dermal analog—3D nylon filament with type I collagen peptides	Temporary wound dressing that is removed when wound is healed or when autograft skin is available
StrataGraft™	Full thickness skin substitute with dermal and fully differentiated epidermal layers	Made with naturally immortalized NIKS® keratinocyte cell line; contains two different cell types
Apligraf™	Bovine collagen gel seeded with neonatal foreskin fibroblasts and keratinocytes	Wound dressing with two different cell types
Permaderm™	Autologous tissue engineered skin consisting of epidermal and dermal cells	Contains two different cell types
denovoDerm ™	Autologous dermal substitute denovoSkin™	To be used in combination with split-thickness skin grafts
denovoSkin™	Autologous full thickness substitute consisting of dermal and epidermal layers	Contains two different cell types
Epidex™	Confluent autologous keratinocytes from hair follicles outer root sheath on silicone membrane	To be used for treat full- and partial-thickness burns and chronic ulcers
Laserskin™	Subconfluent autologous keratinocytes seeded on esterified laser-perforated hyaluronic acid matrix	To be used for treat full- and partial-thickness burns and chronic ulcers
Hyalograft 3D™	Esterified hyaluronic acid matrix seeded with autologous fibroblasts	Treat full- and partial-thickness wounds
ICX-SKN™	Allogeneic fibroblasts set in a natural human collagen matrix	Phase II trial pending
Matriderm™	Acellular scaffold made with bovine collagen types I, III, V and elastin	Treat partial- or full-thickness burns
Tiscover™ (A-Skin)	Autologous full thickness cultured skin for healing of chronic, therapy resistant wounds	Contains two different cell types

Table 1: commercially available *in vivo* epidermal and full-thickness skin substitutes

1.4 *In vitro* applications

During the last decade, human *in vitro* skin models has been developed as valid alternative to current study models and to mimic human skin,. At moment use patients and animal models are two defective alternatives to recapitulate disease processes and test innovative drugs. The possibilities to use patient as in vivo models are limited, due to obvious ethical considerations [71]. Current and common alternative is the use of animal models [31]. Despite the large number of studies describing mice, pigs, rabbits, rats and other animals as models to investigate various phenomena – such as cellular behavior, tissue contraction, evaluation of drugs absorption, reepithelialization process during wound healing, UV treatments, scar and hypertrophic scarring phenomena –, these processes presents significant differences in these species and it is extremely difficult compared with human tissue specially because of lack of specific biomarkers, differences in skin structure and physiology [72] [73] [74]. Moreover, with increasing pressure from the EU (Directive 2010/63/EU) and the introduction of 3R-principles "replace, reduce and refine" for the use of animal models, there is an urgent need to develop a physiologically relevant and responsive in vitro human wound model to investigate the skin response and the pathogenesis of tissue [75]. In skin TE, various biological and synthetic materials are combined with *in vitro*-cultured cells to generate functional tissues. For several years, two dimensional (2D) in vitro monolayer cultures of human cells were use but these platforms are low relevance due to the lack of complex cell–cell and cell–ECM interactions [76]. For example it must be kept in mind that the actual wound environment is infinitely more complex than the environment inside a Petri dish. In this way, novel *in vitro* ES are enables not only the investigation of fundamental processes in the skin, but also the hazard assessment of various chemical compounds that are topically applied on the skin. Presence of a 3D physiological environment, allows the interaction of the different cell types with one another and the surrounding matrix. This peculiarity, also help to elucidate fundamental processes in the skin such as the stimuli that lead to the formation of the epidermis [26] [77], the molecular cross-talk between different cell types both in normal than pathological conditions [16] [78], the process of wound repair [79], the maintenance of the stem cells [80], and the infection with different kinds of toxins and microorganisms [67]. Moreover the cellular composition is

completely controllable by the researcher in these conditions. First developed models focus on reepithelialization phenomena and allow possibility to study pathologies and drugs effect only at epidermal level [81]. Keratinocytes behaviour can be investigated followed by UV radiation or physical damage [82]. The rapid reestablishment of the epidermal barrier function after a skin defect is vital for preventing wound infection and restoring homeostasis to the wound area. Natural biological scaffolds often retain the natural basement membrane and can therefore produce a valid and full differentiated epidermis when cultured with keratinocytes [83] [84]. A fundamental aspect that can be evaluated is the differentiation of keratinocytes into a complete stratified epidermis with all the different strata found in native epidermis. In this perspective care should be taken in selecting the source of the keratinocytes [85]. Regarding skin irritation tests, presence of a 3D microenvironement is also important for the measurement of cytotoxicity, and for metabolic reactions such as cytokines and enzyme release. In response to physical or chemical stresses, keratinocytes release various substances such as different interleukin (IL-1 α, IL-8, IL-6, IL-7, IL-15, TNF-α) [86]. Employing in vitro skin substitutes, a dose dependent release of the cytosolic enzyme lactate dehydrogenase (LDH) and IL-α was observed in response to the application of various drugs and cosmetics [26]. However many drugs and cosmetics are applied to the skin, but the amount of the substances that reach the targeted site remains often unclear. Fibroblasts are another important cell type evaluated during skin alterations [78]. These cells have only recently begun to receive more attention. At moment, the engineering of skin substitutes can allow for the fabrication of biological constructs for various pathologic conditions like disease evolution with stroma alterations, burns or cutaneous ulcers [26] [48]. The importance of dermal components and mesenchymal cell to the SE is increasingly being recognized. Recent developments showed that a dermal component can accelerate the reepithelialization process and that greatly improve the outcome of the pathological process in an *in vitro* SE [34]. Moreover, recent studies have been demonstrated that the addition of a dermal matrix can also improve scar contraction in a dose-dependent fashion when applied to full-thickness wounds [87]. The currents SE are cultured at an air-liquid interface a synthetic or on a collagen matrix that could be acellular or populated with dermal fibroblasts. Porous membranes seeded with fibroblasts or coated with extracellular matrix proteins (as hyaluronic acid or fibrin) have also

been used to generate skin-like organotypic cultures [88] [76]. A few investigation and optimization were carried out to fabricate and maintain a stratified epithelium that demonstrates *in vivo*-like features of epidermal morphology, growth and differentiation, in 3D-cultures. To induce all of that, three components were developed: presence of keratinocyte stem cells with high proliferative potential, viable dermal fibroblasts and structured basement membrane [89]. For keratinocytes question, different cellular lineage has a relevant influence about a good epithelium development. Dermal fibroblasts are required to promote stratification and it was demonstrated that fibroblasts play a crucial role in the natural epidermal histogenesis [90]. Indeed keratinocytes/fibroblasts interactions are crucial to improve formation of a valid epithelium and co-culture studies with keratinocytes reveal that post-mitotic fibroblasts stimulate keratinocyte proliferation, increase the resistances of keratinocytes to toxic chemicals and induce a higher secretion of keratinocyte growth factor (KGF) [91] [44]. Interestingly, keratinocytes have also a positive effect on the proliferation of fibroblasts due a biochemical processes. Indeed it was hypothesized that this interaction of epidermal and dermal cells is due to a double-paracrine mechanism that regulates the growth of keratinocytes and fibroblasts [92] [93]. According to this hypothesis, keratinocytes secrete IL-1 that stimulates the skin fibroblasts to secret KGF and granulocyte-monocyte colony-stimulating factor (GM-CSF), consequently higher keratinocytes proliferation results [33]. Third, the presence of pre-existing basement membrane components was required to initiate and promote the rapid assembly of structured assembly BM in 3D-cultures and optimize epithelial architecture [94]. To date, many types of skin substitutes – with or without a dermal component – have been developed and commercially available by different groups [95] [26] [96].The main competitors in this market sector are Skinethic™ RHE, Episkin™ (SkinEthic/ L'Oreal corporation, France), Epiderm™, Epiderm FT™ (MatTek Corporation, USA), EST-1000, and AST-2000 (Cell-Sytems corporation, Germany). In table 2 shows the main characteristics of these SE. At moment, optimally-engineered human tissues can be adapted to study a variety of human disease processes that simulate events that occur in human skin. Typical applications are: studies on human disease [97], investigation of hypertrophic scar and keloids formation [30], characterization of human skin-like tissues response following wounding [98] or during early cancer development in a premalignant tissue [12]. It has been demonstrated that

presence of 3D- architecture is crucial to development of adequate microenvironement that mimic *in vivo* situation. Indeed, preliminary studies – that have utilized these 3-D tissues – have demonstrated the critical role of tissue architecture and cell–cell interactions during: the earliest stages in the development of cancer in stratified squamous epithelium [99]. Moreover, the importance of these 3D-structures was confirmed by studies on reepithelialization process of wounded human skin – from the initiation of keratinocyte activation until restoration of epithelial integrity. [2] At least these SE models have a higher responsivity to cells behaviour after wounding, in terms of growth, migration, differentiation, and growth-factor production. Thus, all these studies and applications demonstrate the benefits of these engineered skins in the study of skin alterations. Despite the big innovation in SE realization and studies, relevant problems are already detected. The extensive cell culture procedures imply that development of tissue engineered skin is time consuming. Indeed procedures usually require two or three weeks to obtain full-thickness *in vitro* models. This results in an increased turn over period for production of tissue engineered skin, which is a constraint for its regular use, and could be overcome, with technical advances in cell and tissue culture protocols [100] [101]. Moreover to data, tissue engineered skin aren't a circulatory system and contain only two or three cell types as fibroblasts, keratinocytes and melanocytes or cancer cells: Langerhans cells, adipose tissue, monocytes, leukocytes and nerve supply are absent [102] [2]. Hence, these substitutes are unable to provide immune regulation, adequate temperature control, insulation and pressure sensation [34].

Brand name	Scaffold materials	Cells source	Dermis
Episkin™/L'Oreal Nice, France	Collagen	Mammary/abdominal keratinocytes	No
Skinethict™ RHE/L'Oreal, Nice, France	Polycarbonate membrane	Neonatal and adult keratinocytes	No
EpiDermFT™/Mat Tek Corporation, Ashland MA, USA	Collagen	Neonatal and adult breast keratinocytes	Yes
EST-1000/CellSystem, Troisdorf, Germany	Polycarbonate membrane	Neonatal keratinocytes	No
EST-2000/CellSystem, Troisdorf, Germany	Collagen	Adult keratinocytes	Yes

Table 2: commercially available in vitro epidermal and full-thickness skin substitutes

1.5 Disease skin models

1.5.1 *In vitro* wound healing models

The human skin functions as a protective physical barrier against the outside and any break in it must be rapidly and efficiently repaired. In case of physical skin damage – and consequently an interruption in tissue continuity – a complex series of events involved to restore the gap [65]. Wound healing is a highly organized series of processes resulting in tissue integrity and function of the damaged tissue witch chemotaxis [103], cell division [104], granulation tissue formation [105], reepithelialization process [106], neovascularization [107], synthesis of new

extracellular matrix [108], formation and remodelling of the scar tissue are involved [109 110]. This process needs a complex microenvironement to be studied. Thus, to study the wound healing process in detail, the development of *in vitro* wound model systems is important. To date, most of 3D-engineered constructs were focus on repair mechanism investigations and all *in vitro* alternatives can easily be manipulated and are cost-effective compared to in vivo systems [67 27 30]. Of course, an ex-vivo skin cultures and monolayer cell culture assay are already widely studied but ethical problems and complexity of process – that cannot be reduced merely to cell migration – respectively, limit their use [111 112 83]. A 3D architecture is necessary to better understand repair mechanisms. Typical examples of 2D in vitro models involve use of a scratch assay, in which a confluent cell-monolayer is scratched with a tool such as a pipette cone or a razor blade, so as to mechanically remove a ‘‘strip of cells’’ from the monolayer [10385,103,113–116]. This method is based on the observation that, upon creation of a new artificial gap, or ‘‘scratch’’, the cells on the edge of the wound will move toward the opening to close the ‘‘scratch’’ until new cell–cell contacts are established again. Time-Lapse analyses – at the beginning and at regular intervals during cell migration – are crucial to follow closure phenomena and to determine the rate of cell migration [113–115]. These methods largely used to mimic *in vivo* migration of different cell types. An example are wound model assays were scratch of endothelial monolayer induces migration of endothelial cells (ECs) into the denuded area to close the wound [85]. Furthermore, the patterns of migration either as loosely connected population (e.g., fibroblasts) or as sheets of cells (e.g., epithelial and HaCat) also mimic the behavior of these cells during migration *in vivo*. Moreover, these *in vitro* scratch assays allow possibility to evaluate regulation of cell migration by cell interaction and cell contraction [116 117 118] . Recently have been demonstrated that for cells adhering to their substrate, and despite the presence of a contractile peripheral actomyosin cable at the free edge, the final stages of closure of wounds larger than a typical cell size result mostly from protrusive lamellipodial activity at the border. In that case, the function of the actin cable appears to be primarily to prevent the onset of migration fingers led by leader cells [114,116] at the free edge. Thus by using 2D *in vitro* scratch assay, mechanical basis such as measure cellular forces during epithelial gap closure was been studied. These studies revealed one class of closure that involves covering a bare surface in which leading cells in an advancing epithelial

monolayer migrate across the surface in an adhesion-dependent manner [85,115,116]. Across non-adhesive gaps, epithelial cells employ a different mechanism by generating traction forces parallel to the wound margin through the contraction of a multicellular actin purse string to close the wound [116]. Despite these mechanisms explain many aspects of reepithelialization, it is unclear how these findings relate to repair of fibrous tissues wherein mesenchymal cells ensconced in a fibrillar matrix restore the the 3D architecture of the tissue. Furthermore evaluation of epithelial differentiation and stratification, cell-cell and cell-matrix interaction, formation of provisional matrix and collagen behaviour can't be evaluated [19,119]. In this perspective only 3D wound-healing models can systematically and quantitatively characterized allowing the investigation of responses induced by different stimuli. There are several approaches of inducing a physical damage including burning, freezing, scratching, abrading or punching the epithelium [2779] The most commonly used instruments to induce injury are scalpels, biopsy punches, lasers, liquid nitrogen or burn injury at 150° C [79 120 79]. All these methods allow reproducible wound gap and can produce wounds of exactly dimensions and depth. A reproducible wound method is crucial for determining in vitro re-epithelialization and evaluate epidermal closure-times; in details, this is precisely the central question debated in the literature during wound healing process [46,67,68,81,83,109,121–124]. Figure 6 reported principal examples of *in vitro* 2D and 3D platform to study wound healing. It has been proved that 3D wound models simulates the chronology of events that occur during reepithelialization in human skin and currents studies evaluated the mechanism of the creation and extension of the epidermal tongue. To data, two reepithelialization mechanisms were postulated: the first is the leap-frog or rolling mechanism in which migrating suprabasal cells roll over leading basal cells and dedifferentiate ; the second is the tractor-tread or sliding mechanism postulates that layered keratinocytes move forward in a block [81]. Usui et al. (2005) proposed a variant of the sliding mechanism in which suprabasal cells migrate out of the wound, thereby outnumbering the basal cells [125]. It has up till now been unclear whether one of these mechanisms is correct and how such a mechanism is functionally embedded in the environment of the wound.

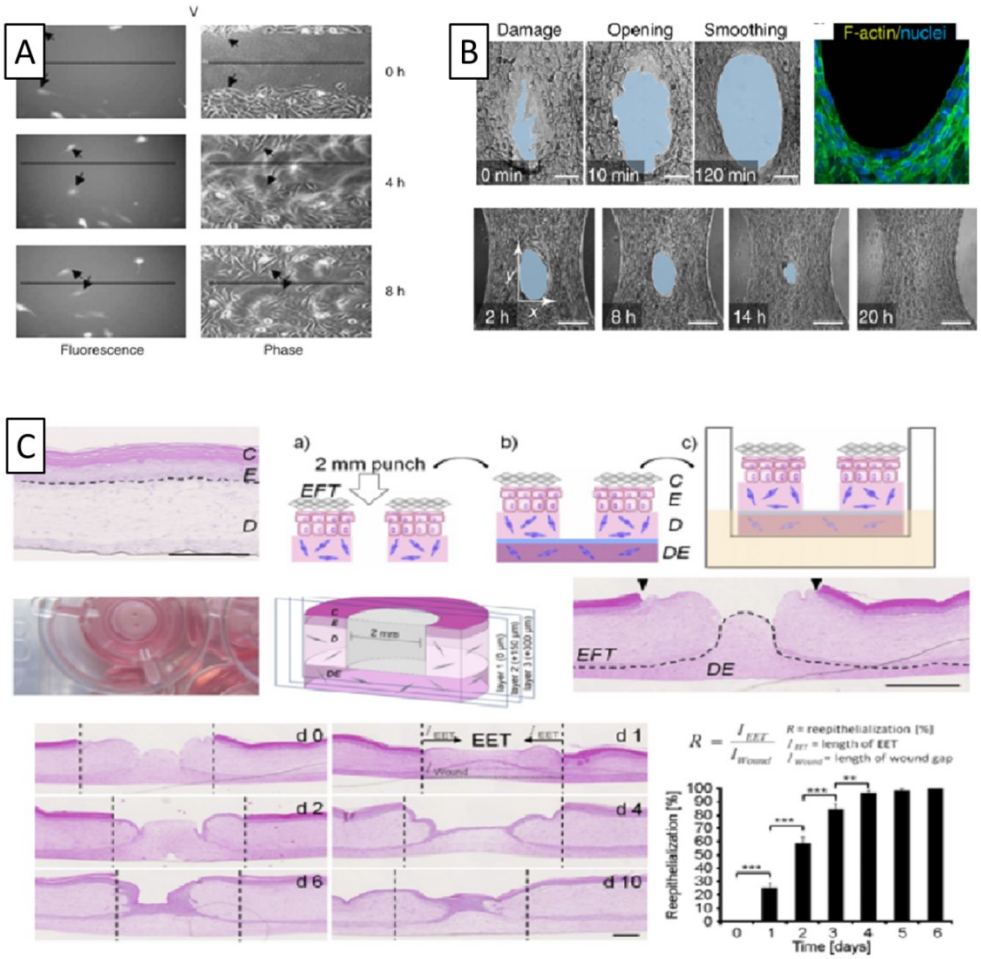

Fig. 6: Schematic example of typical 2D and 3D in vitro model to study wound healing: in A reported typical 2D scratch assay to evaluate epithelial gap closure [115]; in B reported a schematic microtissue device to study fibroblasts behaviour during repair [124], in C reported classical 3D in vitro model to study reepithelialization process [126]

As well as in vivo applications and substitutes, in vitro 3D models can be divided into different groups. At the beginning there was 3D wound models with only epidermal components, full-thickness in vitro models are born in the last years. All in vitro skin models induces a multilayered differentiated epidermis similar to native skin, expressing all the morphologic markers of epithelial differentiation 7. Indeed, these models constitutively express the keratin (K) markers such as K10, K14, K5, K19 and also differentiation markers as Involucrin and Filaggrin and p53 [127] [128] [129]. The presence of fibroblasts in these skin models have been shown an epidermal architecture more closely resembles to *in vivo* tissue due to production of ECM proteins and TNF-α and KGF expression [26,130] [26]. Human mesenchymal stem cells (MSCs) are another cell population that improve wound healing. MSCs derived from the stroma of the

bone marrow, are progenitor cells that give rise to many mesenchymal-derived tissues/cells both *in vivo* than *in vitro* and have been implicated in wound healing making them a potential candidate for cell-based bioengineered products for injured tissue. In vitro, these pluripotent cells have been shown to contribute towards cutaneous wound repair both in acute and chronic wounds [80,122,131]. One in vitro study using co-culture conditions demonstrated that MSCs contributed to reepithelialization by both transdifferentiation and fusion, indicating that they may not be mutually exclusive events [80]. It has been hypothesize that the use of human MSCs in the place of fibroblasts may also contribute to wound healing and provide an effective method for wound closure [80,83]. Another important parameter evaluated during wound healing studies is cellular contraction and fibroblasts behaviour after an injury. During an *in vivo* repair process fibrin clot serving as scaffold to induce fibroblasts migration and differentiation to induce tissue contraction and gap closure [132–134]. Indeed, the development of mechanical stress by injury, stimulates fibroblasts to develop stress fibres so they acquire the proto-myofibroblast phenotype that secrete transforming growth factor $\beta 1$ (TGF-$\beta 1$) and in a feedback loop, proto-myofibroblasts become differentiated myofibroblasts by synthesizing α-smooth muscle actin and generating increased contractile force in a process of remodelling results in shortening of the collagen matrix with wound closure [87,135–137]. The role of myofibroblasts in tissue contraction and ECM production and reorganization is an example showing the crosstalk between ECM and cells [137]. Recently, Christopher Chan (2015) demonstrated that fibroblasts close the open gap through the coordinated action of force-dependent contraction of the whole tissue, circumferential cell migration around the wound edge and assembly of fibronectin scaffolding [124]. These kinds of studies understand how the role of stroma is relevant to correctly evaluate cells migration, matrix contraction and ECM remodelling during a wound healing process. Thus, combination both epidermal than dermal component are the only valid models to better understand repair process. Dermal components are mainly based on chemical analogues of extracellular matrix (ECM) such as exogenous collagen, or hyaluronic acid, or fibrin matrix [2,106,133,134,138–142]. The main difference into full-thickness 3D wound model is matrix and scaffold used as dermal platform. These exogenous matrices can be acellular or may be cultured in vitro with fibroblasts [102,143]. Examples of dermal *in vitro* platforms are: de-epidermized dermis (DED) [80], epidermis

reconstructed on de-epidermized dermis (RE-DED) [84], collagen lattices contracted with dermal fibroblasts [144], microperforated hyaluronic acid scaffold (Hyalograft®) [26], bovine collagen gel seeded with human hypertrophic and keloids fibroblasts [31,145], provisional cellularized matrix of fibrin (ICX-SKN™) [95], fibroblasts/ keratinocytes/ monocytes/ mesenchymal stem cells in a 3D fibrin construct [146], 3T3 fibroblasts embedded in a type I collagen matrix [124], hypertrophic and keloids cells into a sponge-like collagen-elastin- matrix (Matriderm™) [147]. Strong example of full-thickness organotypic cultures is Apligraf™. This 3D wound model composed of allogeneic neonatal fibroblasts and keratinocytes grown on a collagen lattice and study many wound processes such as epidermal proliferation and differentiation, epithelial/mesenchymal interactions, and basement membrane production [80,143,148]. Recent new platforms are emerging to evaluate a further process occurred during repair: scar and abnormal scar formation. Scarring occurs after trauma, injury or surgery to any tissue or organ in the body; abnormal scar represent a form of pathologic wound healing and due to an abnormal inflammatory component of the wound healing process [40,66,149,149]. Currently, a few 3D tissue-engineered models exist to study scar and all of that avoid the main questions referring to why an adverse scar forms instead of a normotrophic scar and what causes a hypertrophic scar to form rather than a keloid scar [69,70,109,150]. Also, it was investigated if there is a genetic predisposition of the individual and if the immune system is involved. This information is essential if we are to identify new drug targets and develop optimal strategies in the future to prevent adverse scar formation. Current 3D skin equivalent models have been described using hypertrophic or keloid fibroblasts in combination with normal skin-derived keratinocytes. Using a similar method, a fully differentiated epidermis constructed from keratinocytes isolated from abnormal scars on a fibroblast (healthy)-populated dermal matrix was able to exhibit a few characteristics of an adverse scar (e.g. dermal thickness, epidermal thickness, collagen I) and illustrated the role of keratinocytes in hypertrophic scar formation [30,36,44,144,147,151–154].

1.5.2 *In vitro* melanoma models

Malignant melanoma is the most aggressive and most prominent cancer in the human population. Malignant melanoma develops in a multistep process starting in melanocytes in the epidermis [26]. In this process, melanocytes loose contact to the surrounding keratinocytes and enter a radial growth phase. This radial growth phase (RGP) is followed by a vertical growth phase (VGP) Radial growth phase (RGP) melanoma cells proliferate and form nests in the epidermis, but do not invade the dermis. In this phase, cancer cells are incapable biologically of generating metastatic events. Conversely, VGP cells cross the basement membrane, invade and proliferate in the dermis. Subsequent step is metastatic (met) melanoma formation that rapidly invades deep into the dermal compartment until arriving into organs [155,156]. Most studies of melanoma cell biology and anti-melanoma drug activity have come from work done with 2D adherent cell culture assays. Typical examples of 2D in vitro melanoma models involve use of cancer monocultures on plastic tissue culture plates [157,158]. In the past has contributed significantly to increasing our knowledge of cancer biology and to stimulating research into the field of anticancer drug discovery and development [157–159]. The principal advantages of such models are simplicity, convenience, and cost that they are pure and free from contaminating cells important for protein, RNA or DNA extraction [54]. Usually 2D-models can be use in pre-clinical research to delineate molecular mechanisms that drive melanoma growth and progression or to determine inefficacy of novel drugs indeed it is often the case that drugs that do not work in 2D cell culture have no effect in more realistic models too [4,147,160]. However, cytotoxicity assays based on 2D cell cultures show important limitations, in particular, conventional 2D models are not capable of mimicking the complexity and heterogeneity of melanoma. Indeed these models do not take into consideration that melanoma cells do not grow in isolation [76,161–163]. Instead they are oriented in a three-dimensional space, establishing continuous dynamic interaction with the stroma, i.e., extracellular matrix and other cell types such as fibroblasts, endothelial cells or immune cells. This is often referred to as the 'tumor organ' [12 54]. Consequently, numerous signals that govern different cellular processes are lost when cells are grown in 2D plastic substrata. 3D models represent an acceptable compromise between the lack of microenvironment and of complexity of melanoma in 2D cell culture and the great complexity of the *in vivo* animal

models [54]. 3D cell culture methods confer a high degree of clinical and biological relevance to *in vitro* models. Tumor spheroids are one of the most common and versatile scaffold-free methods for 3D cell culture and provide an environment that more closely resembles the physiology of human malignant melanoma than previously available systems [11,158,164]. Spheroid cultures are small aggregate of cells that grows free of foreign materials. In spheroid cultures, cells secrete the extracellular matrix (ECM) in which they reside, and they can interact with cells from their original microenvironment [12,160]. The value of spheroid cultures is increasing quickly due to novel microfabricated platforms amenable to high-throughput screening and advances in cell culture. Depending on the researcher's needs and on the method used, it is possible to obtain spheroids of any dimension. In particular, spheroids larger then 400–600 μm in diameter are with characterized by an external proliferating zone and an internal necrotic zone core [165]. This is likely due to the limited O^2 [11] and nutrient and metabolites availability [165]. Melanoma spheroids are usually implanted into a collagen gel matrix to simulate vertical growth phase and to closely mimic *in vivo* architecture and complex microenvironment [86]. Indeed, exploiting presence of spheroid's proliferative and necrotic zone, these 3D-models recreates the oxygen/nutrient gradient with a hypoxic zone and a central necrosis as well as *in vivo* happened between melanoma cells and their stroma [54]. In this way more realistic study of melanoma growth, invasion and drug response can be carried out. An advantage to use collagen gel is that can be easily manipulated to alter elasticity and stiffness. Typical 3D tumor spheroids derived from cell lines of early stage melanoma progression were poorly invasive, whereas the cell line derived from a metastatic stage rapidly colonized the entire collagen gel. The major applications of tumor spheroids models are in testing chemotherapeutic agents, in particular testing novel drug delivery systems [11,37], and mapping response to treatment evaluating reduction in melanoma nests [35], induction of apoptosis in tumor cells [164], percentage of cells in G0/G1 or cell cycle analysis [86]. For example several BRAF inhibitors are currently being studied and tested such as the BRAF inhibitors RAF-265 (Novartis)[166], PLX4032 (Plexxikon/Roche) and GSK2118436 (GSK) [166]. These drugs were evaluated as targeting oncogenic BRAF with PLX4720 or PLX4032 resulted in inhibition of growth and invasion of 3D spheroids and caused tumor regression of melanoma xenografts [167–169]. The last class of in vitro melanoma models are diseased 3D engineered human tissues.

Combination both epidermal than dermal component are new reality to study melanoma development and tumoral infiltration. To obtain an in vitro melanoma engineered skin, artificial skin is rebuilt from isolated cell populations and composed of a stratified, terminally differentiated epidermal compartment of keratinocytes and melanoma cells, a dermal compartment, and a well established basement membrane deposited by skin cells (Figure 7) [86,160]. Coculture of epidermal keratinocytes and melanoma cells can be plated on dermal substitutes mainly consists of deepidermized acellular cadaveric human skin, Matrigel, or fibroblasts embedded in a matrix containing type I collagen of rat tail tendon [156,170–172]; these dermal platforms can be enhanced with chitosan, chondroitin sulfate, hyaluronic acid or elastin [173]. Figure 7 recapitulated principal examples of *in vitro* 2D and 3D platform to study melanoma process.

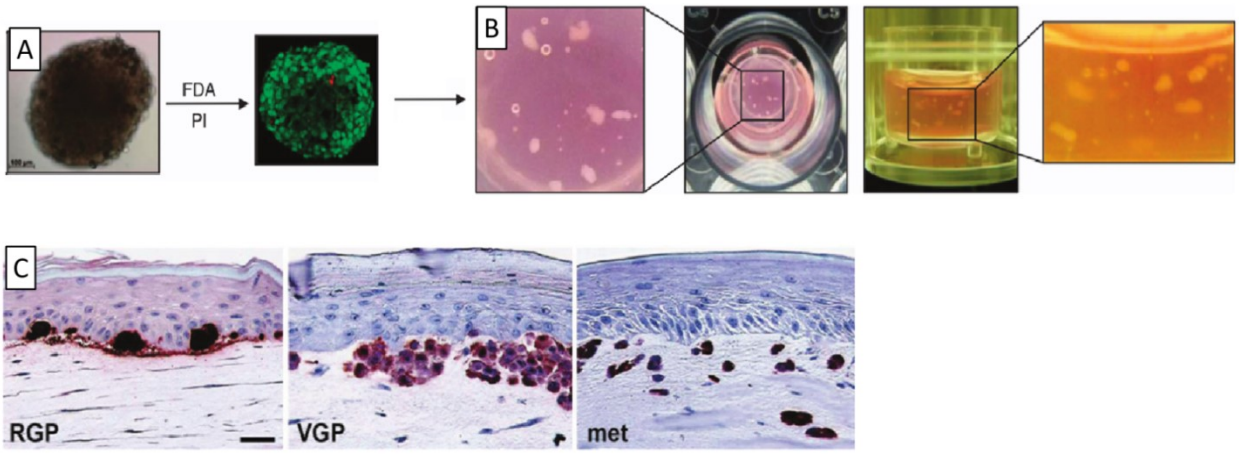

Fig. 7: Schematic example of typical 2D and 3D in vitro model to study melanoma: in A reported typical aspect of spheroid and in B spheroids implanted into a collagen gel matrix to mimic VGP melanoma phase [86]. In C reported 3D engineered melanoma models [156]

To test whether these skin equivalents are useful to study malignant melanoma in a 3D environment, several studies has been inserted cell lines representing different progression stages. In human skin reconstructs, melanoma cells from different stages of progression have the same properties as in the patients' skin, i.e., cells derived from a melanoma in situ/RGP are unable to invade the dermis from the epidermis, whereas advanced primary (VGP) and

metastatic melanoma cells readily invade the dermis [89,171,172,174,175]. For examples, it was proven, by S-100 protein stain, that VGP primary melanoma cells WM793 and WM115 formed nests and clusters at the epidermal-dermal junction, and exhibited invasive growth into the dermis. Whereas WM793 VGP melanoma cells invaded the dermis in clusters with only a few individual cells preceding the cluster, WM115 cell invaded the dermis more individually [156]. Thus, when metastatic melanoma cells were incorporated into skin reconstructs, they displayed rapid proliferation and aggressive invasive growth deep into the dermis [156,176,177]. Accordingly, reconstructed skin more closely resembles histologically human skin in architecture and composition, with all major cell types represented in physiologically relevant ratios and with a true relation between malignancy nature of melanoma cells and their *in vitro* tissue infiltration. (Figure 3C) [54]. A number of recent studies proved that the use of tissue-engineered skin as a 3D model of the invasion of malignant melanoma in vitro has great potential for further studying the biological characteristics of malignant melanoma and evaluating the efficacy of drugs. It has been demonstrated that vemurafenib, PLX4720 and roscovitine are capable of decreasing proliferation [167,168,173], inducing apoptosis in mutant BRAF melanomas [178,179] and in A375 melanoma cells [180] respectively Also, it has been reported reported that combinations of MAPK and AKT inhibitors completely suppressed invasive tumor growth of melanoma cells in a similar [169,179]. Melanoma engineered skins has unique properties to create a complex in vitro tumor model which could be useful to study melanoma biology and progression, and to identify new pharmacological targets.

1.6 The role of ECM-cells cross talking in pathological events: wound healing and melanoma

In the skin, the interaction of keratinocytes, fibroblasts and melanocytes is tightly controlled by various factors and cascades [127]. The microenvironment of each organ and tissue develops to specifically support the function of those cells: the ECM provides the structural scaffolding for these cells, as well as contextual information [2,55,162,181]. Under normal conditions, there is a

balance between cell types via cell–cell contact and ECM. The normal extracellular matrix in the dermis mainly consists of type I and type III collagen, proteoglycans, fibronectin and elastin. In particular, collagen fibrils are important for the strength and resilience of skin, and alterations in their number and structure are thought to be responsible for wrinkle formation [65,78,182]. The disruption of these equilibria can result in an uncontrolled stroma degeneration (as involved in scarring)[66,110] or uncontrolled proliferation of epithelial cells (as in malignant melanoma) [183,184]. Wound healing is a highly organized series of processes resulting in tissue integrity and function of the damaged tissue; this process needs a complex microenvironement to be studied [47,185,186]. Carcinogenesis is defined as complex, adaptive processes which are controlled by intricate communications between the host and the tissue microenvironment [48,187,188]. Therefore it shows that the microenvironment and the stroma play an important part both in wound healing process than in tumour development and progression. Various examples of cell-ECM interaction are studied. The role of myofibroblast in ECM production and reorganization in wound contraction is an example showing the crosstalk between ECM and cells. Indeed, it has been demonstrated that during skin wound healing, a fibrin clot is formed in the wound bed serving as a scaffold, allowing migration and proliferation of dermal fibroblasts [107,185]. The development of mechanical stress stimulates fibroblasts to develop stress fibres and to produce collagen, so they acquire the proto-myofibroblast phenotype that secrete transforming growth factor $\beta 1$ (TGF-$\beta 1$) and in a feedback loop, proto-myofibroblasts become differentiated myofibroblasts by synthesizing α-smooth muscle actin and generating increased contractile force in a process of remodelling results in shortening of the collagen matrix with wound closure [87,136,189]. Another example is the role of N-cadherins in metastasis. N-Cadherin mediated homotypic aggregation among melanoma cells as well as heterotypic adhesion of melanoma cells to dermal fibroblasts and vascular endothelial cells in ECM to improve melanoma infiltration in malignant melanoma. Indeed malignant melanoma is characterized by alterations to the dermal connective tissue and relates underline stroma [190–192]. The ECM represents a fundamental component of the skin, participating in the transport of biologically active substances needed for the communication between different cellular components and participating in the main important process occurring in skin disease. Consequently presence of ECM and appropriate studies

are necessary to better understand physiological and pathological processes occurring in human skin.

1.7 References

1. O'Brien FJ. Biomaterials & scaffolds for tissue engineering. *Mater Today*. 2011;14(3):88-95. doi:10.1016/S1369-7021(11)70058-X.

2. Bi H, Jin Y. Current progress of skin tissue engineering: Seed cells, bioscaffolds, and construction strategies. *Burn Trauma*. 2013;1(2):63-72. doi:10.4103/2321-3868.118928.

3. Williams D. Benefit and risk in tissue engineering. *Mater Today*. 2004;7(5):24-29. doi:10.1016/S1369-7021(04)00232-9.

4. Nyga A, Cheema U, Loizidou M. 3D tumour models: Novel in vitro approaches to cancer studies. *J Cell Commun Signal*. 2011;5(3):239-248. doi:10.1007/s12079-011-0132-4.

5. Nichol JW, Khademhosseini A. Modular tissue engineering: Engineering biological tissues from the bottom up. *Soft Matters*. 2010;5(7):1312-1319. doi:10.1039/b814285h.Modular.

6. Palmiero C, Imparato G, Urciuolo F, Netti P. Engineered dermal equivalent tissue in vitro by assembly of microtissue precursors. *Acta Biomater*. 2010;6(7):2548-2553. doi:10.1016/j.actbio.2010.01.026.

7. Yang J, Yamato M, Kohno C, et al. Cell sheet engineering: Recreating tissues without biodegradable scaffolds. *Biomaterials*. 2005;26(33):6415-6422. doi:10.1016/j.biomaterials.2005.04.061.

8. Langer R, Vacanti JP. Tissue Engineering. *Science (80-).* 1993;260:920-926. doi:10.1126/science.8493529.

9. Gooch KJ, Blunk T, Courter DL, Sieminski AL, Vunjak-Novakovic G, Freed LE. Bone morphogenetic proteins-2, -12, and -13 modulate in vitro development of engineered cartilage. *Tissue Eng*. 2002;8(4):591-601. doi:10.1089/107632702760240517.

10. Mironov V, Kasyanov V, Markwald RR, Prestwich GD. Bioreactor-free tissue engineering: directed tissue assembly by centrifugal casting. *Expert Opin Biol Ther*. 2008;8(2):143-152. doi:10.1517/14712598.8.2.143.

11. Friedrich J, Ebner R, Kunz-Schughart LA. Experimental anti-tumor therapy in 3-D: Spheroids – old hat or new challenge? *Int J Radiat Biol*. 2007;83(11-12):849-871.

doi:10.1080/09553000701727531.

12. Hickman JA, Graeser R, de Hoogt R, et al. Three-dimensional models of cancer for pharmacology and cancer cell biology: Capturing tumor complexity in vitro/ex vivo. *Biotechnol J*. 2014;9(9):1115-1128. doi:10.1002/biot.201300492.

13. Dhandayuthapani B, Yoshida Y, Maekawa T, Kumar DS. Polymeric scaffolds in tissue engineering application: A review. *Int J Polym Sci*. 2011;2011(ii). doi:10.1155/2011/290602.

14. Urciuolo F, Imparato G, Totaro A, Netti P a. Building a Tissue In Vitro from the Bottom Up: Implications in Regenerative Medicine. *Methodist Debakey Cardiovasc J*. 2013;9(4):213-217. http://www.pubmedcentral.nih.gov/articlerender.fcgi?artid=3846076&tool=pmcentrez&rendertype=abstract.

15. Khademhosseini A, Bong GC. Microscale technologies for tissue engineering. *2009 IEEE/NIH Life Sci Syst Appl Work LiSSA 2009*. 2009;103(8):56-57. doi:10.1109/LISSA.2009.4906708.

16. McGuigan AP, Sefton M V. Vascularized organoid engineered by modular assembly enables blood perfusion. *Proc Natl Acad Sci U S A*. 2006;103(31):11461-11466. doi:10.1073/pnas.0602740103.

17. Sodunke TR, Turner KK, Caldwell SA, McBride KW, Reginato MJ, Noh HM. Micropatterns of Matrigel for three-dimensional epithelial cultures. *Biomaterials*. 2007;28(27):4006-4016. doi:10.1016/j.biomaterials.2007.05.021.

18. Nakazawa K, Izumi Y, Fukuda J, Yasuda T. Hepatocyte spheroid culture on a polydimethylsiloxane chip having microcavities. *J Biomater Sci Polym Ed*. 2006;17(8):859-873. doi:10.1163/156856206777996853.

19. Gottwald E, Giselbrecht S, Augspurger C, et al. A chip-based platform for the in vitro generation of tissues in three-dimensional organization. *Lab Chip*. 2007;7(6):777-785. doi:10.1039/b618488j.

20. Torisawa Y suke, Takagi A, Nashimoto Y, Yasukawa T, Shiku H, Matsue T. A multicellular spheroid array to realize spheroid formation, culture, and viability assay on a chip. *Biomaterials*. 2007;28(3):559-566. doi:10.1016/j.biomaterials.2006.08.054.

21. Fennema E, Rivron N, Rouwkema J, van Blitterswijk C, De Boer J. Spheroid culture as a tool for creating 3D complex tissues. *Trends Biotechnol*. 2013;31(2):108-115. doi:10.1016/j.tibtech.2012.12.003.

22. Kelm JM, Djonov V, Ittner LM, et al. Design of custom-shaped vascularized tissues using microtissue spheroids as minimal building units. *Tissue Eng*. 2006;12(8):2151-2160. doi:10.1089/ten.2006.12.ft-129.

23. Wu MH, Huang S Bin, Cui Z, Cui Z, Lee G Bin. A high throughput perfusion-based microbioreactor platform integrated with pneumatic micropumps for three-dimensional cell culture. *Biomed Microdevices*. 2008;10(2):309-319. doi:10.1007/s10544-007-9138-3.

24. Lecuit T, Le Goff L. Orchestrating size and shape during morphogenesis. *Nature*. 2007;450(7167):189-192. doi:10.1038/nature06304.

25. Nelson CM, Bissell MJ, Division LS, et al. Of Extracellular Matrix, Scaffolds, and Signaling: Tissue Architecture Regulates Development, Homeostasis, and Cancer Celeste. *J Phys (main title)*. 2010;22(19):16-19. doi:10.1146/annurev.cellbio.22.010305.104315.Of.

26. Groeber, Florian, Holeiter, Monika, Hampel, Martina, Hinderer, Svenja, Schenke-Layland, Katja. Skin tissue engineering — In vivo and in vitro applications. *Adv Drug Deliv Rev*. 2011;63(4-5):352-366. doi:10.1016/j.addr.2011.01.005.

27. Auger FA, Lacroix D, Germain L. Skin substitutes and wound healing. *Skin Pharmacol Physiol*. 2009;22(2):94-102. doi:10.1159/000178868.

28. MacNeil S. Progress and opportunities for tissue-engineered skin. *Nature*. 2007;445(7130):874-880. doi:10.1038/nature05664.

29. Ramalingam M, Vallittu P, Ripamonti U, Li W-J. Tissue Engineering and Regenerative Medicine. 2012;7(1). doi:10.1201/b13049.

30. Broek LJ Van Den, Limandjaja GC, Niessen FB, Gibbs S. Human hypertrophic and keloid scar models : principles , limitations and future challenges from a tissue engineering perspective. *Exp Dermatol*. 2014:382-386. doi:10.1111/exd.12419.

31. Seo BF, Lee JY, Jung SN. Models of abnormal scarring. *Biomed Res Int*. 2013;2013. doi:10.1155/2013/423147.

32. Pizzimenti S, Daga M, Ciamporcero E, et al. Improved Anti-Tumoral Therapeutic Efficacy of 4-Hydroxynonenal Incorporated in Novel Lipid Nanocapsules in 2D and 3D Models. *J Biomed Nanotechnol*. 2015;11(12):2169-2185. doi:10.1166/jbn.2015.2131.

33. Pastar I, Stojadinovic O, Yin NC, et al. Epithelialization in Wound Healing: A Comprehensive Review. *Adv Wound Care (New Rochelle)*. 2014;3(7):445-464. doi:10.1089/wound.2013.0473.

34. Varkey M, Ding J, Tredget E. Advances in Skin Substitutes—Potential of Tissue Engineered Skin for Facilitating Anti-Fibrotic Healing. *J Funct Biomater*. 2015;6(3):547-563. doi:10.3390/jfb6030547.

35. Vörsmann H, Groeber F, Walles H, et al. Development of a human three-dimensional organotypic skin-melanoma spheroid model for in vitro drug testing. *Cell Death Dis*. 2013;4:e719. doi:10.1038/cddis.2013.249.

36. Vincent C., Martijn B A, Michiel C E. MMW, Middelkoop E. Biological background of dermal substitutes. *Burns*. 2010;36(3):305-321. doi:10.1016/j.burns.2009.07.012.

37. Currie LJ, Sharpe JR, Martin R. The use of fibrin glue in skin grafts and tissue-engineered skin replacements: a review. *Plast Reconstr Surg*. 2001;108(6):1713-1726. doi:10.1097/00006534-200111000-00045.

38. Sun T, Jackson S, Haycock JW, MacNeil S. Culture of skin cells in 3D rather than 2D improves their ability to survive exposure to cytotoxic agents. *J Biotechnol*. 2006;122(3):372-381. doi:10.1016/j.jbiotec.2005.12.021.

39. Tiedtke J, Marks O, Morel J. Stimulation of Collagen Production in Human Fibroblasts. *Citeseer*. 2007:15-18. http://citeseerx.ist.psu.edu/viewdoc/download?doi=10.1.1.119.3834&rep=rep1&type=pdf.

40. Middelkoop E, Bogaerdt AJ Van Den, Ulrich MM, Meeting S. Artificial dermis and cellular aspects of scar formation. 2006;(2):1-14.

41. Clark R a F, Ghosh K, Tonnesen MG. Tissue engineering for cutaneous wounds. *J Invest Dermatol*. 2007;127(5):1018-1029. doi:10.1038/sj.jid.5700715.

42. Langer R. Biomaterials in drug delivery and tissue engineering: One laboratory's experience. *Acc Chem Res*. 2000;33(2):94-101. doi:10.1021/ar9800993.

43. Mayet N, Choonara YE, Kumar P, et al. A Comprehensive Review of Advanced Biopolymeric Wound Healing Systems. *J Pharm Sci*. 2014;103(8):2211-2230. doi:10.1002/jps.24068.

44. Harrison CA, Ph D, Gossiel F, et al. Use of an in Vitro Model of Tissue-Engineered Skin to Investigate the Mechanism of Skin Graft Contraction. 2006;12(11).

45. Eves P, Katerinaki E, Simpson C, et al. Melanoma invasion in reconstructed human skin is influenced by skin cells--investigation of the role of proteolytic enzymes. *Clin Exp Metastasis*. 2003;20(8):685-700. http://www.ncbi.nlm.nih.gov/pubmed/14713103.

46. Van Kilsdonk JWJ, Van Den Bogaard EH, Jansen P a M, Bos C, Bergers M, Schalkwijk J. An in vitro wound healing model for evaluation of dermal substitutes. *Wound Repair Regen*. 2013;21(6):890-896. doi:10.1111/wrr.12086.

47. Gurtner GC, Werner S, Barrandon Y, Longaker MT. Wound repair and regeneration. *Nature*. 2008;453(7193):314-321. doi:10.1038/nature07039.

48. Bissel MJ, Radisky D. Putting tumors in context. *Nat Rev Cancer*. 2001;1(1):46-54. doi:10.1038/35094059.PUTTING.

49. Cichorek M, Wachulska M, Stasiewicz A, Tymińska A. Skin melanocytes: Biology and development. *Postep Dermatologii i Alergol*. 2013;30(1):30-41. doi:10.5114/pdia.2013.33376.

50. Sabolinski ML, Parenteau NL, Auletta M, Mulderss G. Cultured skin as a " smart material " for healing wounds : experience in venous ulcers. 1996;17(3):311-320.

51. Mcheik JN, Barrault C, Pedretti N, et al. Study of proliferation and 3D epidermal reconstruction from foreskin, auricular and trunk keratinocytes in children. *Burns*. 2014;(1879-1409 (Electronic)):1-7. doi:10.1016/j.burns.2014.07.003.

52. Fernandez TL, Van Lonkhuyzen DR, Dawson RA, Kimlin MG, Upton Z. Characterization of a human skin equivalent model to study the effects of ultraviolet B radiation on keratinocytes. *Tissue Eng Part C Methods*. 2014;20(7):588-598. doi:10.1089/ten.TEC.2013.0293.

53. Salazar-Onfray F, López M, Lundqvist a, et al. Tissue distribution and differential expression of melanocortin 1 receptor, a malignant melanoma marker. *Br J Cancer*. 2002;87(4):414-422. doi:10.1038/sj.bjc.6600441.

54. Beaumont KA, Mohana-Kumaran N, Haass NK. Modeling melanoma in vitro and in vivo. *Healthcare*. 2013;2(1):27-46. doi:10.3390/healthcare2010027.

55. Sorokin L. The impact of the extracellular matrix on inflammation. *Nat Rev Immunol*. 2010;10(10):712-723. doi:10.1038/nri2852.

56. Fernandes H, Moroni L, van Blitterswijk C, de Boer J. Extracellular matrix and tissue engineering applications. *J Mater Chem*. 2009;19:5474. doi:10.1039/b822177d.

57. Compton CC, Butler CE, Yannas I V., Warland G, Orgill DP. Organized skin structure is regenerated in vivo from collagen-GAG matrices seeded with autologous keratinocytes. *J Invest Dermatol*. 1998;110(6):908-916. doi:10.1046/j.1523-1747.1998.00200.x.

58. Myllyharju J, Kivirikko KI. Collagens, modifying enzymes and their mutations in humans, flies and worms. *Trends Genet*. 2004;20(1):33-43. doi:10.1016/j.tig.2003.11.004.

59. Kruger TE, Miller AH, Wang J. Collagen scaffolds in bone sialoprotein-mediated bone regeneration. *ScientificWorldJournal*. 2013;2013(I):812718. doi:10.1155/2013/812718.

60. Hudson BG, Reeders S, Tryggvason K. Type IV Collagen: Structure, Gene Organization, and Role in Human Diseases. *J Biol Chem*. 1993;238(35):26003-26036. doi:10.1097/01.ASN.0000141462.00630.76.

61. Wu P-C, Hsieh T-Y, Tsai Z-U, Liu T-M. In vivo quantification of the structural changes of collagens in a melanoma microenvironment with second and third harmonic generation microscopy. *Sci Rep*. 2015;5:8879. doi:10.1038/srep08879.

62. Balasubramani M, Kumar TR, Babu M. Skin substitutes : a review. 2001;27:534-544.

63. Shevchenko R V, James SL, James SE. A review of tissue-engineered skin bioconstructs available for skin reconstruction. *J R Soc Interface*. 2010;7(43):229-258. doi:10.1098/rsif.2009.0403.

64. Jones I, Currie L, Martin R. A guide to biological skin substitutes. *Br J Plast Surg*. 2002;55(3):185-193. doi:10.1054/hips.2002.3800.

65. Iii JTS, Tompkins RG, Burke JF. Artificial skin. *Rev Med*. 2000;(3):231-244.

66. Hari G. Garg MTL. *Scarless in Wound Healing*. Vol 133.; 2000. doi:10.1016/B978-0-444-62644-8.00008-X.

67. Debels H, Hamdi M, Abberton K, Morrison W. Dermal matrices and bioengineered skin substitutes: a critical review of current options. *Plast Reconstr surgery Glob open*. 2015;3(1):e284. doi:10.1097/GOX.0000000000000219.

68. I.F.K. Muir Control. Control of fibroblast activity in scars : a review. 1998;(February 1997):1-7.

69. Thomas JR, Somenek M. Scar Revision Review. *Arch Facial Plast Surg*. 2012;14(3):162-174.

70. Cecelia C. Y, Patricia H, Alan W. Skin Wound Healing and Scarring: Fetal Wounds and Regenerative Restitution. 2012;96(4):325-333. doi:10.1002/bdrc.21024.Skin.

71. Longaker MT, Whitby DJ, Ferguson MW, Lorenz HP, Harrison MR, Adzick NS. Adult skin wounds in the fetal environment heal with scar formation. *Ann Surg*. 1994;219(1):65-72. doi:10.1097/00000658-199401000-00011.

72. Lin RY, Sullivan KM, Argenta PA, Meuli M, Lorenz HP, Adzick NS. Exogenous transforming growth factor-beta amplifies its own expression and induces scar formation in a model of human fetal skin repair. *Ann Surg*. 1995;222(2):146-154. doi:10.1097/00000658-199508000-00006.

73. Klinge U, Klosterhalfen B, Birkenhauer V, Junge K, Conze J, Schumpelick V. Impact of polymer pore size on the interface scar formation in a rat model. *J Surg Res*. 2002;103(2):208-214. doi:10.1006/jsre.2002.6358.

74. Kloeters O, Tandara A, Mustoe TA. Hypertrophic scar model in the rabbit ear: A reproducible model for studying scar tissue behavior with new observations on silicone gel sheeting for scar reduction. *Wound Repair Regen*. 2007;15(SUPPL. 1):40-45. doi:10.1111/j.1524-475X.2007.00224.x.

75. Nowacki M, Pietkun K, Pokrywczyńska M, et al. Filling effects, persistence, and safety of dermal fillers formulated with stem cells in an animal model. *Aesthet Surg J*. 2014;34(8):1261-1269. doi:10.1177/1090820X14548212.

76. Song H-HG, Park KM, Gerecht S. Hydrogels to model 3D in vitro microenvironment of tumor vascularization. *Adv Drug Deliv Rev*. 2014;79-80:19-29. doi:10.1016/j.addr.2014.06.002.

77. Ojeh NO, Navsaria HA. An in vitro skin model to study the effect of mesenchymal stem

cells in wound healing and epidermal regeneration. *J Biomed Mater Res - Part A*. 2014;102(8):2785-2792. doi:10.1002/jbm.a.34950.

78. El-Ghalbzouri A, Gibbs S, Lamme E, Van Blitterswijk CA, Ponec M. Effect of fibroblasts on epidermal regeneration. *Br J Dermatol*. 2002;147(2):230-243. doi:10.1046/j.1365-2133.2002.04871.x.

79. Richards S, Ph D, Leavesley DI, Ph D, Upton Z, Ph D. Development of a Three-Dimensional Human Skin Novel Wound Healing Therapies. 2010;16(5).

80. Ojeh NO, Navsaria H a. An in vitro skin model to study the effect of mesenchymal stem cells in wound healing and epidermal regeneration. *J Biomed Mater Res - Part A*. 2014;102(8):2785-2792. doi:10.1002/jbm.a.34950.

81. Safferling K, S??tterlin T, Westphal K, et al. Wound healing revised: A novel reepithelialization mechanism revealed by in vitro and in silico models. *J Cell Biol*. 2013;203(4):691-709. doi:10.1083/jcb.201212020.

82. Sugawara T, Gallucci RM, Simeonova PP, Luster MI. Regulation and Role of Interleukin 6 in Wounded Human Epithelial Keratinocytes. *Cytokine*. 2001;15(6):328-336. doi:10.1006/cyto.2001.0946.

83. Lin YC, Grahovac T, Oh SJ, Ieraci M, Rubin JP, Marra KG. Evaluation of a multi-layer adipose-derived stem cell sheet in a full-thickness wound healing model. *Acta Biomater*. 2013;9(2):5243-5250. doi:10.1016/j.actbio.2012.09.028.

84. Lee D, Ahn H, Cho K. A new skin equivalent model : dermal substrate that combines de-epidermized dermis with fibroblast-populated collagen matrix. 2000;23:132-137.

85. Vedula SRK, Peyret G, Cheddadi I, et al. Mechanics of epithelial closure over non-adherent environments. *Nat Commun*. 2015;6:6111. doi:10.1038/ncomms7111.

86. Kimlin LC, Casagrande G, Virador VM. In vitro three-dimensional (3D) models in cancer research: An update. *Mol Carcinog*. 2013;52(3):167-182. doi:10.1002/mc.21844.

87. Yang L, Hashimoto K, Tohyama M, et al. Interactions between myofibroblast differentiation and epidermogenesis in.pdf. *J Dermatol Sci*. 2012;65:50-57.

88. Grinnell F, B. Rocha L, Iucu C, Rhee S, Jiang H. Nested collagen matrices: A new model to study migration of human fibroblast populations in three dimensions. *Exp Cell Res*.

2006;312:86-94. doi:10.1016/j.yexcr.2005.10.001.

89. Gibot L, Galbraith T, Huot J, Auger FA. Development of a tridimensional microvascularized human skin substitute to study melanoma biology. *Clin Exp Metastasis*. 2013;30(1):83-90. doi:10.1007/s10585-012-9511-3.

90. Yang L, Hashimoto K, Tohyama M, et al. Interactions between myofibroblast differentiation and epidermogenesis in constructing human living skin equivalents. *J Dermatol Sci*. 2012;65(1):50-57. doi:10.1016/j.jdermsci.2011.10.008.

91. El Ghalbzouri A, Hensbergen P, Gibbs S, Kempenaar J, Schors R van der, Ponec M. Fibroblasts facilitate re-epithelialization in wounded human skin equivalents. *Lab Investig*. 2004;84(1):102-112. doi:10.1038/labinvest.3700014.

92. Werner S, Krieg T, Smola H. Keratinocyte–Fibroblast Interactions in Wound Healing. *J Invest Dermatol*. 2007;127(5):998-1008. doi:10.1038/sj.jid.5700786.

93. Shamis Y, J. Hewitt K, Bear SE, et al. IPSC-derived fibroblasts demonstrate augmented production and assembly of extracellular matrix proteins. *Vitr Cell Dev Biol - Anim*. 2012;48(2):112-122. doi:10.1007/s11626-011-9478-4.

94. Ridky TW, Chow JM, Wong DJ, Khavari P a. Invasive three-dimensional organotypic neoplasia from multiple normal human epithelia. *Nat Med*. 2010;16(12):1450-1455. doi:10.1038/nm.2265.

95. Berning M, Prätzel-Wunder S, Bickenbach JR, Boukamp P. Three-Dimensional In Vitro Skin and Skin Cancer Models Based on Human Fibroblast-Derived Matrix. *Tissue Eng Part C Methods*. 2015;00(00):1-13. doi:10.1089/ten.TEC.2014.0698.

96. Hayden PJ, Bachelor M, Ayehunie S, et al. Application of MatTek *In Vitro* Reconstructed Human Skin Models for Safety, Efficacy Screening, and Basic Preclinical Research. *Appl Vitr Toxicol*. 2015;1(3):226-233. doi:10.1089/aivt.2015.0012.

97. Mertsching H, Weimer M, Kersen S, Brunner H. Human skin equivalent as an alternative to animal testing. *GMS Krankenhhyg Interdiszip*. 2008;3(1):Doc11.

98. Flasza Marzena KP et al. Development and manufacture of an investigational human living dermal equivalent (ICX-SKN). 2007:2(6), 903-918.

99. Garlick JA. Engineering Skin to Study Human Disease – Tissue Models for Cancer

Biology and Wound Repair. 2006;(January):207-239.

100. Ahlfors JEW, Billiar KL. Biomechanical and biochemical characteristics of a human fibroblast-produced and remodeled matrix. *Biomaterials*. 2007;28(13):2183-2191. doi:10.1016/j.biomaterials.2006.12.030.

101. Grellner W. Time-dependent immunohistochemical detection of proin ¯ ammatory cytokines (IL-1 b , IL-6 , TNF- a) in human skin wounds. 2002;130:90-96.

102. Metcalfe AD, Ferguson MWJ. Bioengineering skin using mechanisms of regeneration and repair. *Biomaterials*. 2007;28(34):5100-5113. doi:10.1016/j.biomaterials.2007.07.031.

103. Liang C, Park AY, Guan J. In vitro scratch assay : a convenient and inexpensive method for analysis of cell migration in vitro. 2007;2(2):329-333. doi:10.1038/nprot.2007.30.

104. Kim W-S, Park B-S, Sung J-H, et al. Wound healing effect of adipose-derived stem cells: A critical role of secretory factors on human dermal fibroblasts. *J Dermatol Sci*. 2007;48(1):15-24. doi:10.1016/j.jdermsci.2007.05.018.

105. Lillian A. Repesh, Thomas J. Fitzgerald LTF. Fibronentin involvement in granulation tissue and wound healing in rabbits. 1981;LXV.

106. Clark RAF, Lanigan JM, DellaPelle P, Manseau E, Dvorak HF, Colvin RB. Fibronectin and fibrin provide a provisional matrix for epidermal cell migration during wound reepithelialization. *J Invest Dermatol*. 1982;79(5):264-269. doi:10.1111/1523-1747.ep12500075.

107. Baum CL, Arpey CJ. Normal cutaneous wound healing: clinical correlation with cellular and molecular events. *Dermatol Surg*. 2005;31(6):674-686; discussion 686. http://www.ncbi.nlm.nih.gov/entrez/query.fcgi?cmd=Retrieve&db=PubMed&dopt=Citation&list_uids=15996419.

108. Burkhardt MA, Waser J, Milleret V, et al. Synergistic interactions of blood-borne immune cells, fibroblasts and extracellular matrix drive repair in an in vitro peri-implant wound healing model. *Sci Rep*. 2016;6(February):21071. doi:10.1038/srep21071.

109. Coolen NA, Schouten KCWM, Boekema BKHL, Middelkoop E, Ulrich MMW. Wound healing in a fetal, adult, and scar tissue model: A comparative study. *Wound Repair Regen*. 2010;18(3):291-301. doi:10.1111/j.1524-475X.2010.00585.x.

110. Enoch S, Leaper DJ. Basic science of wound healing. *Surg*. 2008;26(2):31-37. doi:10.1016/j.mpsur.2007.11.005.

111. Hulkower KI, Herber RL. Cell migration and invasion assays as tools for drug discovery. *Pharmaceutics*. 2011;3(1):107-124. doi:10.3390/pharmaceutics3010107.

112. Studies B. Acute wounds: clinical and basic studies 001. *Wound Repair Regen*. 2005;(April):4-48.

113. Poujade M, Grasland-Mongrain E, Hertzog A, et al. Collective migration of an epithelial monolayer in response to a model wound. *Proc Natl Acad Sci U S A*. 2007;104(41):15988-15993. doi:10.1073/pnas.0705062104.

114. Cochet-Escartin O, Ranft J, Silberzan P, Marcq P. Border forces and friction control epithelial closure dynamics. *Biophys J*. 2014;106(1):65-73. doi:10.1016/j.bpj.2013.11.015.

115. Anon E, Serra-Picamal X, Hersen P, et al. Cell crawling mediates collective cell migration to close undamaged epithelial gaps. *Proc Natl Acad Sci U S A*. 2012;109(27):10891-10896. doi:10.1073/pnas.1117814109.

116. Nier V, Deforet M, Duclos G, et al. Tissue fusion over nonadhering surfaces. *Proc Natl Acad Sci*. 2015;112(31):9546-9551. doi:10.1073/pnas.1501278112.

117. Ravasio A, Cheddadi I, Chen T, et al. Gap geometry dictates epithelial closure efficiency. *Nat Commun*. 2015;6:7683. doi:10.1038/ncomms8683.

118. Jonkman JEN, Cathcart JA, Xu F, et al. An introduction to the wound healing assay using live-cell microscopy. *Cell Adhes Migr*. 2014;8(5):440-451. doi:10.4161/cam.36224.

119. Figallo E, Cannizzaro C, Gerecht S, et al. Micro-bioreactor array for controlling cellular microenvironments. *Lab Chip*. 2007;7(6):710-719. doi:10.1039/b700063d.

120. Lavoie A, Fugère C, Beauparlant A, et al. Human epithelial stem cells persist within tissue-engineered skin produced by the self-assembly approach. *Tissue Eng Part A*. 2013;19(7-8):1023-1038. doi:10.1089/ten.TEA.2012.0117.

121. Kairuz E, Upton Z, Dawson R a, Malda J. Hyperbaric oxygen stimulates epidermal reconstruction in human skin equivalents. *Wound Repair Regen*. 2007;15(2):266-274.

doi:10.1111/j.1524-475X.2007.00215.x.

122. Micallef L, Vedrenne N, Billet F, Coulomb B, Darby I a, Desmoulière A. The myofibroblast, multiple origins for major roles in normal and pathological tissue repair. *Fibrogenesis Tissue Repair*. 2012;5 Suppl 1(Suppl 1):S5. doi:10.1186/1755-1536-5-S1-S5.

123. Geer DJ, Andreadis ST. A Novel Role of Fibrin in Epidermal Healing: Plasminogen-Mediated Migration and Selective Detachment of Differentiated Keratinocytes. *J Invest Dermatol*. 2003;121(5):1210-1216. doi:10.1046/j.1523-1747.2003.12512.x.

124. Selman Sakar M, Eyckmans J, Pieters R, Eberli D, Nelson BJ, Chen CS. Cellular forces and matrix assembly coordinate fibrous tissue repair. *Nat Commun*. 2016;7:1-8. doi:10.1038/ncomms11036.

125. Usui ML, Underwood RA, Mansbridge JN, Muffley LA, Carter WG, Olerud JE. Morphological evidence for the role of suprabasal keratinocytes in wound reepithelialization. *Wound Repair Regen*. 2005;13(5):468-479. doi:10.1111/j.1067-1927.2005.00067.x.

126. Safferling K, Sutterlin T, Westphal K, et al. Wound healing revised: A novel reepithelialization mechanism revealed by in vitro and in silico models. *J Cell Biol*. 2013;203(4):691-709. doi:10.1083/jcb.201212020.

127. Fuchs E. Keratins and the skin. *Annu Rev Cell Dev Biol*. 1995;11:123-153. doi:10.1146/annurev.cb.11.110195.001011.

128. Niderla-Bielińska J, Moskalewski S. Involucrin, but not filaggrin and Kdap mRNA, expression is downregulated in 3-D cultures of intact rat hair bulbs after calcium stimulation. *Folia Histochem Cytobiol*. 2011;49(2):335-343.

129. Truong AB, Kretz M, Ridky TW, Kimmel R, Khavari PA. P63 Regulates Proliferation and Differentiation of Developmentally Mature Keratinocytes. *Genes Dev*. 2016;20(22):3185-3197. doi:10.1101/gad.1463206.

130. Lázár-Molnár E, Hegyesi H, Tóth S, Falus A. Autocrine and Paracrine Regulation By Cytokines and Growth Factors in Melanoma. *Cytokine*. 2000;12(6):547-554. doi:10.1006/cyto.1999.0614.

131. Tan GK, Dinnes DLM, Cooper-White JJ. Modulation of collagen II fiber formation in 3-D

porous scaffold environments. *Acta Biomater*. 2011;7(7):2804-2816. doi:10.1016/j.actbio.2011.03.022.

132. Soffer E, Ouhayoun JP, Anagnostou F. Fibrin sealants and platelet preparations in bone and periodontal healing. *Oral Surg Oral Med Oral Pathol Oral Radiol Endod*. 2003;95(5):521-528. doi:10.1067/moe.2003.152.

133. Brown LF, Lanir N, McDonagh J, Tognazzi K, Dvorak AM, Dvorak HF. Fibroblast migration in fibrin gel matrices. *Am J Pathol*. 1993;142(1):273-283. http://www.pubmedcentral.nih.gov/articlerender.fcgi?artid=1886838&tool=pmcentrez&rendertype=abstract.

134. Greiling D, Clark R a. Fibronectin provides a conduit for fibroblast transmigration from collagenous stroma into fibrin clot provisional matrix. *J Cell Sci*. 1997;110 (Pt 7:861-870.

135. Alpha-smooth muscle actin is transiently expressed by myofibroblasts during experimental wound healing. 2015.

136. Tomasek JJ, Gabbiani G, Hinz B, Chaponnier C, Brown R a. Myofibroblasts and mechano-regulation of connective tissue remodelling. *Nat Rev Mol Cell Biol*. 2002;3(5):349-363. doi:10.1038/nrm809.

137. Darby IA, Hewitson TD. Fibroblast Differentiation in Wound Healing and Fibrosis. *Int Rev Cytol*. 2007;257:143-179. doi:10.1016/S0074-7696(07)57004-X.

138. Leary RO, Wood EJ. A novel in vitro dermal wound- healing model incorporating a response to mechanical wounding and repopulation of a fibrin provisional matrix. 2003;(June):204-207.

139. Wang F, Garza LA, Kang S, et al. In Vivo Stimulation of De Novo Collagen Production Caused by Cross-linked Hyaluronic Acid Dermal Filler Injections in Photodamaged Human Skin. 2007;143.

140. Lanir N, Ciano PS, Van de Water L, McDonagh J, Dvorak a M, Dvorak HF. Macrophage migration in fibrin gel matrices. II. Effects of clotting factor XIII, fibronectin, and glycosaminoglycan content on cell migration. *J Immunol*. 1988;140(7):2340-2349.

141. Monteiro IP, Gabriel D, Timko BP, et al. A two-component pre-seeded dermal-epidermal scaffold. *Acta Biomater*. 2014;10(12):4928-4938.

doi:10.1016/j.actbio.2014.08.029.

142. Bhardwaj N, Sow WT, Devi D, Ng KW, Mandal BB, Cho N-J. Silk fibroin–keratin based 3D scaffolds as a dermal substitute for skin tissue engineering. *Integr Biol*. 2015;7(1):53-63. doi:10.1039/C4IB00208C.

143. Falanga V, Isaacs C, Paquette D, et al. Wounding of bioengineered skin: cellular and molecular aspects after injury. *J Invest Dermatol*. 2002;119(3):653-660. doi:10.1046/j.1523-1747.2002.01865.x.

144. Harrison C a, Gossiel F, Layton CM, et al. Use of an in Vitro Model of Tissue-Engineered Skin to Investigate the Mechanism of Skin Graft Contraction. *Tissue Eng*. 2006;12(11):061004065151003. doi:10.1089/ten.2006.12.ft-241.

145. Torkian BA, Yeh AT, Engel R, Sun C. Modeling Aberrant Wound Healing Using Tissue-Engineered Skin Constructs and Multiphoton Microscopy. *Arch Facial Plast Surg*. 2016;6(June 2004):180-187.

146. Lui PPY, Wong OT, Lee YW. Transplantation of tendon-derived stem cells pre-treated with connective tissue growth factor and ascorbic acid in vitro promoted better tendon repair in a patellar tendon window injury rat model. *Cytotherapy*. 2016;18(1):99-112. doi:10.1016/j.jcyt.2015.10.005.

147. van den Broek LJ, Niessen FB, Scheper RJ, Gibbs S. Development, validation and testing of a human tissue engineered hypertrophic scar model. *ALTEX*. 2012;29(4):389-402. doi:10.14573/altex.2012.4.389.

148. Ananta M, Brown RA, Mudera V. A Rapid Fabricated Living Dermal Equivalent for Skin Tissue Engineering: an In-Vivo Evaluation in an Acute Wound Model. *Tissue Eng Part A*. 2012;18(3-4):353-361. doi:10.1089/ten.TEA.2011.0208.

149. Knapp TR, Daniels RJ, Kaplan EN. Pathologic scar formation. Morphologic and biochemical correlates. *Ajpa*. 1977;86(1):47-70. http://eutils.ncbi.nlm.nih.gov/entrez/eutils/elink.fcgi?dbfrom=pubmed&id=12661&retmode=ref&cmd=prlinks¥npapers3://publication/uuid/8419C8FD-1832-4BE8-9726-57F1C380C523.

150. In vitro human Models SCAR Models In SCAR SKIN Tissue Engineering Research. 2006.

151. Chen G, Chen J, Zhuo S, et al. Nonlinear spectral imaging of human hypertrophic scar based on two-photon excited fluorescence and second-harmonic generation. *Br J Dermatol*. 2009;161:48-55. doi:10.1111/j.1365-2133.2009.09094.x.

152. Ehrlich HP, Desmoulière A, Diegelmann RF, et al. Morphological and immunochemical differences between keloid and hypertrophic scar. *Am J Pathol*. 1994;145(1):105-113. http://www.pubmedcentral.nih.gov/articlerender.fcgi?artid=1887298&tool=pmcentrez&rendertype=abstract.

153. Gabbiani G. The myofibroblast in wound healing and fibrocontractive diseases. *J Pathol*. 2003;200(4):500-503. doi:10.1002/path.1427.

154. Thomas JR, Somenek M. Scar Revision Review. 2015;14(3):162-174.

155. Ruiter D, Bogenrieder T, Elder D, Herlyn M. Melanoma – stroma interactions : structural and functional aspects. :35-43.

156. Meier F, Nesbit M, Hsu MY, et al. Human melanoma progression in skin reconstructs : biological significance of bFGF. *Am J Pathol*. 2000;156(1):193-200. doi:10.1016/S0002-9440(10)64719-0.

157. Smalley KSM, Lioni M, Noma K, Haass NK, Herlyn M. In vitro three-dimensional tumor microenvironment models for anticancer drug discovery. 2008:1-10.

158. Beaumont KA, Mohana-Kumaran N, Haass NK. Modeling melanoma in vitro and in vivo. *Healthcare*. 2013;2(1):27-46. doi:10.3390/healthcare2010027.

159. Friedrich J, Ebner R, Kunz-Schughart L a. Experimental anti-tumor therapy in 3-D: spheroids--old hat or new challenge? *Int J Radiat Biol*. 2007;83(11-12):849-871. doi:10.1080/09553000701727531.

160. Marrero B, Heller R. The use of an invitro 3D melanoma model to predict invivo plasmid transfection using electroporation. *Biomaterials*. 2012;33(10):3036-3046. doi:10.1016/j.biomaterials.2011.12.049.

161. Kuo C-T, Chiang C-L, Yun-Ju Huang R, Lee H, Wo AM. Configurable 2D and 3D spheroid tissue cultures on bioengineered surfaces with acquisition of epithelial–mesenchymal transition characteristics. *NPG Asia Mater*. 2012;4(9):e27. doi:10.1038/am.2012.50.

162. Blehm BH, Jiang N, Kotobuki Y, Tanner K. Deconstructing the role of the ECM microenvironment on drug efficacy targeting MAPK signaling in a pre-clinical platform for cutaneous melanoma. *Biomaterials*. 2015;56:129-139. doi:10.1016/j.biomaterials.2015.03.041.

163. Blehm BH, Jiang N, Kotobuki Y, Tanner K. Deconstructing the role of the ECM microenvironment on drug efficacy targeting MAPK signaling in a pre-clinical platform for cutaneous melanoma. *Biomaterials*. 2015;56:129-139. doi:10.1016/j.biomaterials.2015.03.041.

164. Kelm JM, Timmins NE, Brown CJ, Fussenegger M, Nielsen LK. Method for generation of homogeneous multicellular tumor spheroids applicable to a wide variety of cell types. *Biotechnol Bioeng*. 2003;83(2):173-180. doi:10.1002/bit.10655.

165. Zanoni M, Piccinini F, Arienti C, et al. 3D tumor spheroid models for in vitro therapeutic screening: a systematic approach to enhance the biological relevance of data obtained. *Sci Rep*. 2016;6(August 2015):19103. doi:10.1038/srep19103.

166. Villanueva J, Vultur A, Lee JT, et al. Acquired Resistance to BRAF Inhibitors Mediated by a RAF Kinase Switch in Melanoma Can Be Overcome by Cotargeting MEK and IGF-1R/PI3K. *Cancer Cell*. 2010;18(6):683-695. doi:10.1016/j.ccr.2010.11.023.

167. Tokuda EY, Leight JL, Anseth KS. Modulation of matrix elasticity with PEG hydrogels to study melanoma drug responsiveness. *Biomaterials*. 2014;35(14):4310-4318. doi:10.1016/j.biomaterials.2014.01.063.

168. Leight JL, Tokuda EY, Jones CE, Lin AJ, Anseth KS. Multifunctional bioscaffolds for 3D culture of melanoma cells reveal increased MMP activity and migration with BRAF kinase inhibition. *Proc Natl Acad Sci U S A*. 2015;112(17):5366-5371. doi:10.1073/pnas.1505662112.

169. Perna D, Karreth FA, Rust AG, et al. BRAF inhibitor resistance mediated by the AKT pathway in an oncogenic BRAF mouse melanoma model. *Proc Natl Acad Sci*. 2015;112(6):201418163. doi:10.1073/pnas.1418163112.

170. Mcheik JN, Barrault C, Pedretti N, et al. Study of proliferation and 3D epidermal reconstruction from foreskin, auricular and trunk keratinocytes in children. *Burns*. 2014;(1879-1409 (Electronic)):1-7. doi:10.1016/j.burns.2014.07.003.

171. Van Kilsdon, Bergers M, Van Kempen, Schalkwijk J, GW. S. Keratinocytes drive melanoma invasion in a reconstructed skin model. *Melanoma Res*. 2010;20(5):372-380.

172. Woodward JKL, Nichols CE, Rennie IG, Parsons MA, Murray AK, Sisley K. An in vitro assay to assess uveal melanoma invasion across endothelial and basement membrane barriers. *Investig Ophthalmol Vis Sci*. 2002;43(6):1708-1714.

173. Zhou L, Lu Y, Wu J, Yang G, Yang T. Cinnamic aldehyde inhibits proliferation and invasion in a well-defined 3-dimensional culture of human cutaneous melanoma cells in tissue engineered-skin. 2013;7(2):145-153. doi:10.5372/1905-7415.0702.162.

174. Coulombe PA, Kopan R, Fuchs E. Expression of keratin K14 in the epidermis and hair-follicle: Insights into complex programs of differentiation. *J Cell Biol*. 1989;109(5):2295-2312. doi:10.1083/jcb.109.5.2295.

175. Alonso SR, Tracey L, Ortiz P, et al. A high-throughput study in melanoma identifies epithelial-mesenchymal transition as a major determinant of metastasis. *Cancer Res*. 2007;67(7):3450-3460. doi:10.1158/0008-5472.CAN-06-3481.

176. Satyamoorthy K, Meier F, Hsu MY, Berking C, Herlyn M. Human xenografts, human skin and skin reconstructs for studies in melanoma development and progression. *Cancer Metastasis Rev*. 1999;18(3):401-405. doi:10.1023/A:1006333627271.

177. Meier F, Nesbit M, Hsu M, et al. Human Melanoma Progression in Skin Reconstructs Biological Significance of bFGF. 2000;156(1):193-200.

178. Paraiso KHT, Xiang Y, Rebecca VW, et al. PTEN Loss Confers BRAF Inhibitor Resistance to Melanoma Cells through the Suppression of BIM Expression. *Cancer Res*. 2011;71(7):2750-2760. doi:10.1158/0008-5472.CAN-10-2954.

179. Jiang CC, Lai F, Thorne RF, et al. MEK-independent survival of B-RAFV600E melanoma cells selected for resistance to apoptosis induced by the RAF inhibitor PLX4720. *Clin Cancer Res*. 2011;17(4):721-730. doi:10.1158/1078-0432.CCR-10-2225.

180. Mohapatra S, Coppola D, Riker AI, Pledger WJ. Roscovitine inhibits differentiation and invasion in a three-dimensional skin reconstruction model of metastatic melanoma. *Mol Cancer Res*. 2007;5(2):145-151. doi:10.1158/1541-7786.MCR-06-0300.

181. Yang J, Yamato M, Shimizu T, et al. Reconstruction of functional tissues with cell sheet engineering. *Biomaterials*. 2007;28(34):5033-5043.

doi:10.1016/j.biomaterials.2007.07.052.

182. Siu MKY, Cheng CY. Dynamic cross-talk between cells and the extracellular matrix in the testis. *BioEssays*. 2004;26(9):978-992. doi:10.1002/bies.20099.

183. Elder D, Elder D. Melanoma Progression. 2016;(2015):1-8. doi:10.1016/j.pathol.2015.12.002.

184. Mandalà M, Massi D. Tissue prognostic biomarkers in primary cutaneous melanoma. *Virchows Arch*. 2014;464(3):265-281. doi:10.1007/s00428-013-1526-x.

185. Adam J. Singer RAFC. Cutaneous wound healing. 1999.

186. Martin P. Wound healing--aiming for perfect skin regeneration. *Science*. 1997;276(5309):75-81. doi:10.1126/science.276.5309.75.

187. Gatenby RA, Vincent TL, Gatenby RA, Vincent TL. An Evolutionary Model Of Carcinogenesis. 2003:6212-6220.

188. Yamada KM, Cukierman E. Modeling Tissue Morphogenesis and Cancer in 3D. *Cell*. 2007;130(4):601-610. doi:10.1016/j.cell.2007.08.006.

189. Hinz B, Phan SH, Thannickal VJ, et al. Recent Developments in Myofibroblast Biology. *Am J Pathol*. 2012;180(4):1340-1355. doi:10.1016/j.ajpath.2012.02.004.

190. Hazan RB, Phillips GR, Qiao RF, Norton L, Aaronson SA. Exogenous Expression of N-Cadherin in Breast Cancer Cells Induces Cell Migration , Invasion , and Metastasis. 2000;148(4):779-790.

191. The Catenin/Cadherin Adhesion System Is Localized in Synaptic Junctions Bordering Transmitter Release Zones. 1996;135(3):767-779.

192. Wei CJ, Francis R, Xu X, Lo CW. Connexin43 associated with an N-cadherin-containing multiprotein complex is required for gap junction formation in NIH3T3 cells. *J Biol Chem*. 2005;280(20):19925-19936. doi:10.1074/jbc.M412921200.

2 Engineered 3D human dermis model to study tissue repair *in vitro*: experimental set-up comparison

2.1 Introduction

2.1.1 *In vivo* wound healing process

The SKIN functions as a protective physical barrier against the outside [1]. Any break in it must be rapidly and efficiently mend: any perturbation of skin integrity can induce a number of pathologic conditions. In case of physical skin damage, a complex series of events involves to restore the barrier function of the skin. This efficient and complete process, named wound healing, include chemotaxis [2], cell division [3], granulation tissue formation [4], neovascularization [5], synthesis of new extracellular matrix [6], formation and remodelling of the scar tissue [7] [8]. This dynamic and interactive process is classically divided into four overlapping but distinct stages: hemostasis (or early phase), inflammation, proliferation, and remodeling. Figure 1 recapitulates first wound healing aspects.

- Hemostasis The early phase is an immediate phenomenon, indeed it begins minutes after skin injury and manifested with tissue blanching and formation of a clot. The clot represents a viable, dynamic matrix of proteins and cells that not only contribute to hemostasis but also serve as a provisional lattice for incoming inflammatory cells, fibroblasts, and growth factors [6]. It consists of platelets embedded in a mesh of crosslinked fibrin fibers derived by thrombin cleavage of fibrinogen, together with smaller amounts of plasma fibronectin, vitronectin, and thrombospondin [9]. At the cellular level, the most important mediators of hemostasis are fibrin, platelets, and blood vessels [5].

- Inflammatory Immediately after formation of clot, inflammation starts. Components of the coagulation cascade, inflammatory pathways and immune system are needed to prevent ongoing blood and fluid losses, to remove dead and devitalized (dying) tissues and to prevent infection [10]. Inflammation can be divided into early and late phases depending on the time and duration of response and the type of inflammatory cell involve. Early inflammatory phase (days 1–2): inflammation begins with the activation of the classical and alternative pathways of the complement cascade [11]. This leads to infiltration of the wound with neutrophil granulocytes (polymorphonuclear leukocytes) that are attracted to the wound site within 24–48 hours of injury by a number of chemoattractants [12]. Late inflammatory phase (days 2–3): on arriving at the wound site, blood monocytes undergo a phenotypic change to become tissue macrophages [13]. Macrophages are thought to be crucial for coordinating later events in the response to injury, but the importance of neutrophils and macrophages in wound repair is incompletely understood [6]. Recent data suggest, however, that a deficiency in either cell type can be compensated for by the redundancy in the inflammatory response [14].
- Proliferative phase The third stage of wound repair — the proliferative phase with formation of a new tissue — splits into other four phases: granulation tissue formation and fibroplasia, angiogenesis, epithelialization and contraction [6]. Proliferative phase starts at about day 3 and lasts for 2–4 weeks after wounding and is characterized by fibroblast migration, deposition of the extracellular matrix and formation of granulation tissue [15,16]. With progression of the proliferative phase, the provisional fibrin/fibronectin matrix is replaced by the newly formed granulation tissue. Epithelialization of the wound represents the final stage of the proliferative phase [12]. Approximately 4 days after injury, fibroblasts are attracted to the wound by a number of factors, including platelet-derived growth factor and transforming growth

factor-β [12], in this conditions they migrate, proliferate and produce the matrix proteins: fibronectin, hyaluronic acid, collagen and proteoglycans [5,17–19]. Migration induces generation of a rudimentary tissue witch takes name granulation tissue. It appears in the wound already during the inflammatory phase and continues growing until the wound bed is covered [6]. The granulation tissue consists of new blood vessels, inflammatory cells, fibroblasts, myofibroblasts, endothelial cells and the component of a new provisional matrix [12]. This provisional ECM is different in composition from normal ECM and its components originate from fibroblasts. Such components include fibronectin, collagen, glycosaminoglycans, elastin, glycoproteins and proteoglycans. In details, fibronectin and hyaluronan are the main components witch create a really hydrated matrix and facilitate cell migration [9] [20,21]. This provisional matrix is then replaced with an ECM more closely resembles to non-injured tissue. This morphologic change, attributed primarily to the invading capillaries that underlie the granular appearance, also represents at the cellular level the arrival of the permanent residents of the repaired dermis. Macrophages, fibroblasts, and blood vessels move into the wound space at the same time [22]. The macrophages provide a continuing source of growth factors necessary to stimulate fibroplasia and angiogenesis; the fibroblasts – the most important mesenchymal cells involved in wound healing [23] – produce the ECM necessary to support cell ingrowth and help reapproximate wound edges through their contractile properties; and blood vessels carry oxygen and nutrients necessary to sustain cell metabolism [24–26] [27]. During this phase, it observes production of collagen III with a peak at three weeks and continues until the later phase of process, in which it is replaced by the stronger type I collagen [14].

The formation of new blood vessels is necessary to sustain the newly formed granulation tissue. Angiogenesis, also called neovascularization, is a complex process by which damaged blood vessels are replaced by “sprouts” from intact capillaries in the local vicinity of the wound [6]. Local changes in the tissue environment, such as, decreased pH, the inadequate tissue perfusion secondary to damaged capillaries, increased lactate and low oxygen tension stimulate angiogenesis [5]. In addition, several growth factors and cytokines like VEGF, FGF, angiopoietin, and TGF, stimulate and regulate angiogenesis [28]. Others angiogenesis inductors are proteoglycans, MMPs, and the arrangement of the ECM [29] [28]. Angiogenesis is imperative for other stages in wound healing.

The formation of granulation tissue is an open wound allows the reepithelialization phase to take place. Keratinocytes migration can starts within hours after injury and initially, a single layer of epidermal cells migrates from the wound edges to form a delicate covering over the exposed raw area [5]. Once the denuded wound surface has been covered by a monolayer of keratinocytes, epidermal migration ceases and a new stratified epidermis with underlying basal lamina is re-established from the margins of the wound inward [19]. The migration of keratinocytes preferably takes place over an intact basement membrane. More commonly, however, wounds breach the basement membrane and keratinocytes must migrate across the provisional matrix of collagens I and V, fibronectin, vitronectin, and tenascin [5]. Fibrin not only serves in a supportive or guidance role but also stimulates keratinocyte migration directly by disrupting cellular adhesions and indirectly by exposing keratinocytes to plasminogen, a stimulator of migration [30]. Analogous to the migration of fibroblasts through the provisional ECM, keratinocytes also express a number of enzymes that facilitate the degradation of ECM and thereby clear a path for the migrating cells [5].

Proliferative phase runs out with contraction, a key phase of wound healing process. Differentiations of fibroblasts in myofibroblast phenotype - characterized by large bundles of actin-contain microfilaments disposed along the cytoplasmic face of the plasma membrane of the cells and by cell–cell and cell–matrix linkages [20] – induces beginning of contraction (approximately 1 week after injury) witch continues even after the wound is completely reepithelialized [14]. Interaction between fibroblasts and myofibroblasts produce new extracellular matrix, mainly in the form of collagen, which ultimately forms the bulk of the mature scar [31] [32].

- Tissue Remodelling When levels of collagen production and degradation equalize, the maturation phase of tissue repair starts [22], there is a continuous synthesis and breakdown of collagen as the extracellular matrix during this phase. In this phase, type III collagen, witch prevails during proliferation, is gradually degraded and the stronger type I collagen is laid down in its place [33] [34]. In normal wound healing, there is a steady state about 21 days after wounding. Originally disorganized collagen fibers are rearranged, cross-linked and aligned along tension lines [10]. The onset of the maturation phase may vary extensively, depending on the size of the wound and whether it was initially closed or left open [35], ranging from approximately 3 days 33 to 3 weeks [36]. The maturation phase can last for a year or longer, similarly depending on wound type [6].

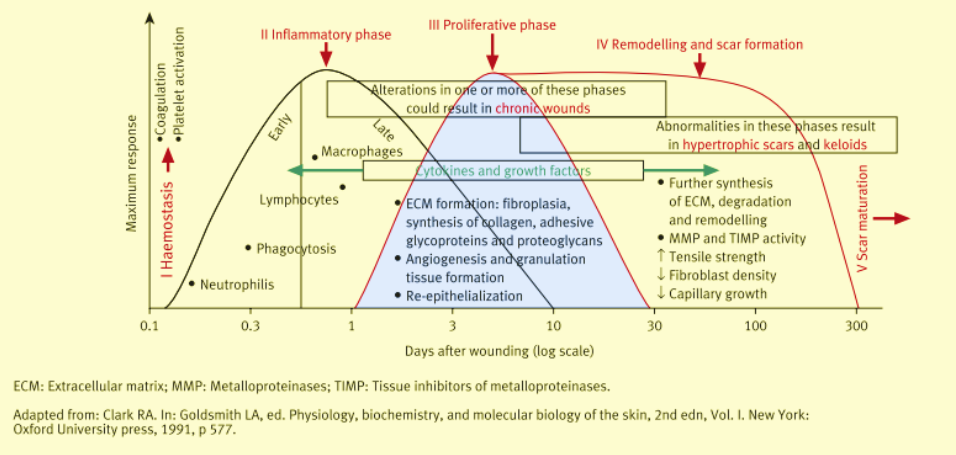

Fig. 1: Phases of repair in acute wound healing

2.1.2 Engineered wound healing models

Wounds represent a significant and increasing burden on healthcare systems globally and new therapies and wound management approaches are urgently required. Numerous difficulties are associated to use of small animal models [37], for this reason *in vitro* wound models using human cells in two- and three-dimensional (2D and 3D) [38–42] environments have been developed to delineate the molecular mechanisms of cellular repair. Typical examples of 2D in vitro models involve use of a scratch assay, in which a confluent cell-monolayer is scratched with a tool such as a pipette cone or a razor blade, so as to mechanically remove a "strip of cells" from the monolayer [43]. This method is based on the observation that, upon creation of a new artificial gap, or "scratch", the cells on the edge of the newly created gap will move toward the opening to close the "scratch" until new cell–cell contacts are established again [44] [38]. These in vitro scratch assays allow possibility to evaluate regulation of cell migration by cell interaction and cell contraction. Recently have been demonstrated that, for cells adhering to their substrate, and despite the presence of a contractile peripheral actomyosin cable at the free edge, the final stages of closure of wounds larger than a typical cell size result mostly from protrusive lamellipodial activity at the border. In that case, the

function of the actin cable appears to be primarily to prevent the onset of migration fingers led by leader cells at the free edge [45]. Thus by using 2D in vitro scratch assay, mechanical basis such as measure cellular forces during epithelial gap closure was been studied. These studies revealed one class of closure that involves covering a bare surface in which leading cells in an advancing epithelial monolayer migrate across the surface in an adhesion-dependent manner [39]. Across non-adhesive gaps, epithelial cells employ a different mechanism by generating traction forces parallel to the wound margin through the contraction of a multicellular actin purse string to close the wound [46]. Despite these mechanisms explain many aspects of reepithelialization, it is unclear how these findings relate to repair of fibrous tissues wherein mesenchymal cells ensconced in a fibrillar matrix restore the the 3D architecture of the tissue. Skin equivalents have already been developed to investigate *in vitro* wound healing. Although these studies extensively described the re-epithelialization process [42], and the state of keratinocyte's differentiation during healing, to the best of our knowledge a few of information on dermal healing and on cell-matrix interaction are reported in literature [47 4849]. In order to provide a model more closely resembles the *in vivo* system, here we introduce a 3D organotypic construct to study the fibroblasts behavior and to describe the dermal wound healing process and the related ECM response. In this perspective, a new 3D human dermal equivalent (3D-HDE) [50] – based on endogenous ECM – was used as wound model. Dermal full-thickness injury was tested on wound platform testing by two different experimental set up. We demonstrate the relationship between cell migration, differentiation marker and ECM production during the wound healing process and self-repair capability in our 3D wound dermal platform.

2.2 Fabrication 3D dermal equivalent model: materials and methods

2.2.1 Porous scaffold fabrication

Microporous scaffolds were made by gelatin type B (Sigma Aldrich Chemical Company, Bloom 225, Mw=l 76654 Dalton) and it resulted by microporous microbeads with a diameter of 50-200 mm. Microbeads (GPMs) have been prepared according to a modified double emulsion technique (O/W/O) [13]. Gelatin was dissolved into 10 ml of water containing TWEEN 85 (6% w/v) (Sigma Aldrich Chemical Company). The solution was kept at 60° C. Toluene containing SPAN 85 (3% w/v) (Sigma Aldrich Chemical Company) was continuously added to the aqueous gelatin solution (8 % w/v) to obtain primary oil in water emulsion. The added toluene formed droplets in the gelatin solution until saturation. Beads of gelatin containing droplets of toluene were produced through the addition of excess toluene (30 ml). The overload of toluene allowed the obtaining of a double emulsion (O/W/O). After cooling below 5° C, 20 ml of ethanol was added to extract toluene and stabilize GPMs. The resulting microspheres were filtered and washed with acetone and then dried at room temperature. Microspheres were separated selectively by using commercial sieves (Sieves IG/3EXP, Retsch, Germany). GPMs with 75-150 mm size range were recovered and further processed. Microbeads morphology has been examined by means of Scanning Electron Microscopy (SEM). Once obtained scaffold, GPMs have been stabilized by means of chemical treatment with glyceraldehyde (GAL), in order to make them stable in aqueous environment at body temperature. In particular, 3.8% and 4% have been used of the crosslinking agent. Process involves the use of acetone/water solution containing the amount of GAL and mixed at 4° C for 24 h. The crosslinked microspheres were washed with acetone and then dried at room temperature. GPM were sterilized by absolute ethanol sub-immersion for 24 h before use.

2.2.2 Cells isolation and culture

Primary human foreskin fibroblasts were isolated from human breast (45 years old) obtained from routine surgical excisions of normal ski as described previously [51]. Briefly, the harvested tissue was divided into pieces witch were incubated overnight in 1.8 U/ml Dispase in PBS (Sigma, St. Louis, MO, USA) at 4° C. After dispase digestion, dermal sheets were separated from epidermis with forceps. For isolation of human dermal fibroblasts (HDF), dermal piece were scraped and put in 30 ml collagenase A solution (ROCHE) at concentration of 2mg/ml for 40 minutes at 37° C. After stop the collagenase solution, piece were resuspended in a little volume of Eagle's BSS Minimum Essential Medium supplemented with 10% fetal bovine serum, 100 mg/mL L-glutamine, 100 U/ml penicillin/streptomycin, and 0, 1 mM Non Essential Amino Acids. Cells were maintained at 37° C in humidified atmosphere containing 5% CO2. HDF were propagated in monolayer culture onto 150 mm Petri dishes in culture medium (Eagle's BSS Minimum Essential Medium containing 20% fetal bovine serum, 100 mg/mL L-glutamine, 100 U/mL penicillin/streptomycin, and 0,1 mM Non Essential Amino Acids) with a cell population of 3.5 x103 cells cm-2. HDF were maintained at same conditions and 5-9 passages cells were used.

2.2.3 Tissue precursor fabrication and human dermis equivalent assembling

HDF of 7 passage and GPM differently crosslinked have been used to start µ-tissue precursor fabrication. GPM were sterilized by absolute ethanol and successively they washed in calcium-free and magnesium-free phosphate buffered saline (PBS) in order to completely

remove ethanol. PBS was removed and replaced 30 minutes with the culture medium before cell seeding. Once GPM acclimatized, HDF were inoculated with scaffold at initial concentration of 11 cell/beads. To seed cells into micro-scaffolds, two medium spinner flasks were loaded with 13 x 10^6 HDF and 231 mg of microbeads. The culture suspension was stirred intermittently at 30 rpm (5 min stirring and 30 min static incubation) for the first 6h post-inoculation for cell adhesion, and then continuously agitated at 30 rpm. The growth medium was replenished on the first day and every 2 days until the end of experiments (7 days in total). From the day 2^{th} 50 µg/ml of ascorbic acid was added. HD µTP samples were taken for assay at day 1, 3 and 6.

2.2.4 Tissue assembling and biohybrid fabrication

To obtain a single and compact macro-tissue of the desired shape and thickness, the µTP suspension was withdrawn from the spinner flask and transferred and cultured in an assembling chamber (Fig. 1B). The assembling chamber has a sandwich-like structure (Fig. 1Ba), in the middle of which is a silicon mould with four empty spaces (1 mm in thickness, dimensions 6x12 mm, Fig. 1Bb), where the µTPs assembly takes place. The silicon mould is delimited on both the top and bottom sides by two stainless steel rigid grids (Fig. 1Bc) characterized by a porous mesh (18 lm) that is able to retain the µTPs. Two polytetrafluoroethylene (PTFE) rings (Fig. 1Bd) are placed on the grids on both sides of the system and are fastened to each other by means of stainless steel screws, which close the system and ensure that the µTPs are retained. The system is autoclavable in each part. The µTP suspension was transferred from the spinner flask to a 50 ml Falcon centrifuge tube and, after settling, transferred by pipetting into the empty spaces of the silicon mould of the

assembling chamber (Fig. 1B) to allow the assembly. Each opening was filled with approximately 13 mg of the μTPs. Furthermore, the assembling chamber was placed on the bottom of a spinner flask (Bellco biotechnology code 1967- 00050) and completely surrounded by culture medium. The spinner was operated at 60 rpm and the medium was exchanged every 2 days. After 2 weeks of culture the assembling chamber was opened and the biohybrids were collected and used as wound healing platform.

2.3 First experimental set-up

2.3.1 Materials and Methods

3D-Wound healing model: full-thickness damage

Maturation chambers were opened and organotypic dermis constructs were transferred into petri dish. One type of wound was randomly made using a stainless-steel sterile scalpel (Brown No. 11; Feather Safety Razor, Osaka, Japan) in the middle of tissue. Different tissues were used in order to study healing process at different time. Each incision was 1 mm in length and was performed to the surface of a silicon layer to apply the correct pressure and obtain a full-thickness injury. Damaged 3D-HDE was clamped and overlain with an o-ring and a silicon layer and was placed in a petri-dish. Manufactured wound tissues were carried out in static conditions, at 37° C, 5% CO2 and humidity 90%. Medium and ascorbic acid were replenished every 2 days. The wound healing process and its effects were evaluated in time-lapse for 20 days.

Time-Lapse analysis and wound remodelling

The wound healing assay carried out on a microscope that combines automated image capture, point visiting and incubation, so that multi-position measurements can be carried out over time under the same conditions (Olympus IX 50 op). Time-Lapse microscope were: equipped with image acquisition software and a scientific-grade digital CoolSnap camera (Photometrics), environmental chamber, motorized stage (PRIOR) for multi-position acquisition, and motorized focus with autofocus capability to minimize focal drift over time [52]. An automated system relies on software for triggering image acquisition using a digital camera at regular time intervals of 30 min over 24-hour period were used. Moreover, the environmental chamber replicates an incubator on the microscope by controlling temperature, pH and humidity [53]40; it allows samples to remain on the microscope rather than being repeatedly taken in and out of an incubator, thus avoiding any compromises in cell physiology arising from fluctuations in these parameters. A 10x objective using a standard CCD camera was used.

Cellular response

Morphological analyses were performed on histological section at 14, 17 and 20 days after damage. All tissues were fixed in 4% paraformaldehyde for 30 min followed by overnight incubation in 2 M sucrose for cryopreserved sections. Samples were embedded in Tissue Tek (Killik, Bio Optica, Milano, Italy), submerged in liquid nitrogen vapors for 1 min and then stored at -80 ° C. After embedding in OCT, 7-mm sections were prepared from across the middle of each wound, by using Criomicrotome (Leica CM 1850, Milano, Italy). Tissue

samples were consecutively cut until the wound was microscopically visible. The dermis healing process was monitored after wound. Monitoring was carried out by analyzing data from the full extension of the wound in different days post-wounding. Tissue morphology and self-repair tissue capability were assessed by performing histological analysis on transverse sections of biohybrid, along the peace of the sheet thickness. Samples were stained using Hematoxylin-Eosin (HE) (Bio Optica) solutions for frozen section, following standard procedure and analysed by an optical microscope (BX53; Olympus Tokyo, Japan).

For immunofluorescence same slices were used for the anti-Alpha smooth muscle detection. The cut was oriented so as to view the cross section of the samples in order to visualize cut section. Frozen thick slices were immunostained with specific antibodies for 3 hours followed by incubation with the appropriate secondary antibody. The primary monoclonal antibodies used in this work is anti-Alpha smooth muscle actin monoclonal antibody blue (diluted 1:100, Abcam, Cambridge, UK). The secondary antibodies used were: Alexa Fluor (Life Techologies, Milano, Italy) 594 goat anti-mouse with dilution of 1:500 in PBS/BSA 3%. Nucleus detections were assessed by using Sytox Green staining (Invitrogen, Life). Markers expression were evaluated at 14, 17 and 20 days after damage.

Extracellular matrix response

To better characterize the increased matrix in the wounded tissue, further targets for selective histochemical localization of components of the extracellular ground substance were evaluated. These were stained by histochemical reaction, either as an overall reaction covering all proteoglycans and glycoproteins. Although the base reaction (PAS reaction) alone couples the chromogen to all GAGs and glycoproteins more or less extensively, a combination

of this staining with the Alcian Blue stain, allow a distinction between acidic (Alcian Blue-positive) and neutral/alkaline (PAS-positive) proteoglycans and GAGs. The Alcian Blue stain reacts strongly blue, and the PAS reaction provides a pink stain. The combination of the Alcian Blue and the PA stain (Bio Optica) were used as a means of distinguishing neutral mucins from acid mucins. 7 µm of frozen sections were stained with the standard Alcian Blue (pH 2.5) method followed by the PAS technique.

Microscopy studies, on our damage human equivalent dermis, were performed on a versatile confocal microscopy Confocal Leica TCS SP5 II combined with a Multiphoton Microscope where the NIR femtosecond laser beam was derived from a tunable compact mode locked titanium: sapphire laser (Chamaleon Compact OPOVis, Coherent). The samples for nonlinear imaging were prepared by freezing them and by cutting them in a compact routine cryostat. Two-photon excited fluorescence was used to induce Second-harmonic generation (SHG) and obtain high-resolution images of unstained collagen structures around and into edge of the wound during 20 days of healing. SHG imaging can help reveal interactions between cells and ECM answer. Samples were observed by using λ_{ex} = 840 nm (two photons) and λ_{em}=415-425 nm. The SHG images, with a size of 200 x 200 µm, were acquired with a resolution of 12 bit, 1024 x 1024 pixels by using a 20X N.A. 1.25 objective.

2.3.2 Results and Discussions

Wound healing assays performed on a scaffold-free dermis equivalents model, realized by a bottom-up approach [50]. A cell-free gap can be created in 3D tissue by direct manipulation.

To examine the response of these microtissues to damage, we wounded them in the centre of the tissue with a scalpel and then observed how they evolved (Fig. 2a). Scalpels have been frequently used because their simplicity of applicability, accuracy and minimal damage to the surrounding tissue [54]. Nevertheless, because of cutting is created manually, it was difficult to generate reproducible wounds for all samples and experiments. It was important to angle the scalpel correctly as well as to apply consistent pressure to create a consistent gap [55]: applying too much pressure we could have damaging the extracellular matrix of tissue, which can affect migration rates [53] [56]. Consequently, to improve wound assay and apply the correct pressure, a silicon layer putted under tissue into a petri dish.

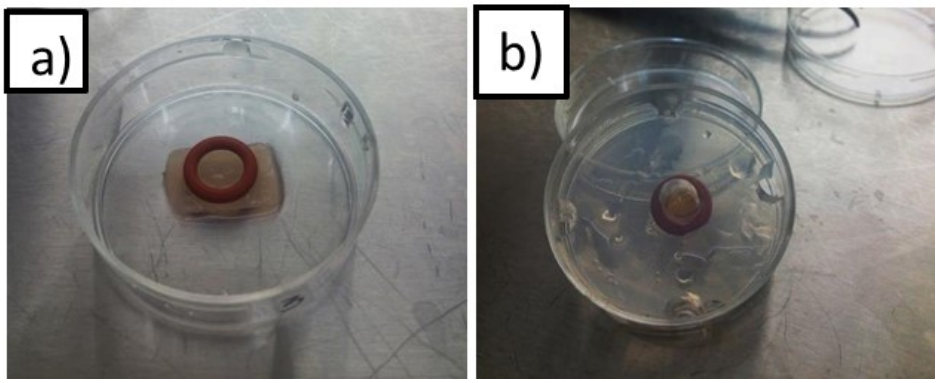

Fig. 2: Wounding and experimental set-up of 3D macrotissues. (a) 3-D dermis equivalent with o-ring in a Petri-dish; (b) silicone layer, o-ring, 3-D dermis equivalent in a Petri-dish.

Studies on migration of fibroblasts in 3D models largely depend on histological analysis, making it impossible to follow migration in real time. For this reason, to examine the response of these macrotissues to damage, we wounded 3D engineered constructs in the centre of the tissue with a sterile scalpel. Samples were mounted in a perfusion chamber and then

observed to evaluate damage closure (Fig. 3a). The open gap created by this “wound” was inspected microscopically over time as the cells move in and fill the damaged area by using transmitted-light techniques [57]. The wound healing assay were carried out on a microscope that combines automated image acquisition software and a scientific-grade digital camera, environmental chamber, motorized stage for multi-position acquisition, and motorized focus with autofocus capability to minimize focal drift over time [53]. The environmental chamber replicated an incubator on the microscope by controlling temperature, pH and humidity [53]. Process followed in time-lapse for 17 days and the exposure to the cell-free area induces the cells to migrate into the gap. We observed that within a few days after the full-thickness incision was made, the gap further widened (Fig. 3a, day 5). As the area of the gap stabilized over ten days (Fig. 3c), the rough wound edge smoothened to form an ellipse (Fig. 3a, day 14), a process associated with alignment and elongation of the cells along the circumferential boundary of the wound edge (Fig. 3b). Over the course of the next three days, the gap progressively closed, while maintaining its elliptical shape and keeping the centroid position of the wound stationary. From literature we know that in the presence of the extracellular matrix (ECM), cell crawling with lamellipodia protrusion [43,58,59] seems to be the predominant mechanism used to close the voided area, particularly when the gap is a large one as happened at 10 days after cut (Fig 3a,). Owing to the stochastic nature of lamellipodia formation, this closure mechanism is characterized by a ‘rough’ edge [60 61], as well as wounded 3D- HDE appears at 10 days after cutting (Fig. 3a). Often it has been observed that one cell takes the lead and drags the neighbouring cells along [59]. Moreover recently have been demonstrated that for cells adhering to their substrate, and despite the presence of a contractile peripheral actomyosin cable at the free edge, the final stages of closure of wounds

larger than a typical cell size result mostly from protrusive lamellipodial activity at the border. In that case, the function of the actin cable appears to be primarily to prevent the onset of migration fingers led by leader cells at the free edge [45]. Supracellular coordination of this motion induces the shape of the gap to become rounder and with 'smooth' edges as in this platform as well as happened in our organotypic model at 14 days [62 58 63]. This mechanism has been observed to be involved in closure of small gaps (Fig. 3a, day 14). As reveals figure 3c, measurements by planimetry of the surface area of the wound reveals that for the first 11 days, the surface area of wound wasn't really diminished. When wound surface achieve the shape of the gap to become rounder and have 'smooth' edges, we found that collective migration of cells in a wound model experiment was increased. Really, closure of gaps started immediately after the rounder-shape formation (Fig. 3b) and the area of the gap decreased in a near-linear manner irrespective of the initial shape (Fig. 3c).

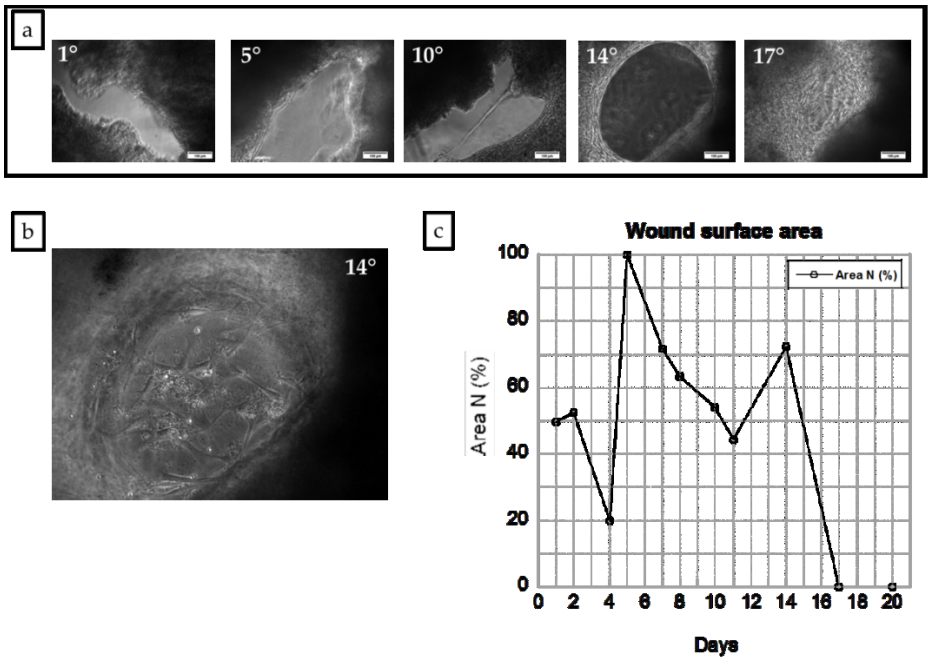

Fig. 3: Wounding and closure of 3D macrotissues. (a) Temporal sequence of wound area showing opening and smoothing of the wound edge (original magnification- 20 and scale bar, 100 µm). (b) Smoothing of the wound edge and cellular migration at 14 days after damage (original magnification- 20 and scale bar, 100 µm). (c) Visual representation of spatiotemporal dynamics of gap area during closure, graph showing gap area in function of time.

To detect possible differences, tissues were analyzed by histological staining and the complete repair verified. In the panel reported in figure 4, histological images of HE (Fig. 4a, b, c, d) concerning human dermis equivalent at three times of healing have been shown. 10 days after cut, HE staining revealed a partial remodeling of wound edge (Fig. 4a, 4b) as time-lapse analysis revealed. 17 days after cut, stains revealed a total closure of tissue in different sections: fibroblasts had completely closed the gap (Fig. 4c, 4d). It is possible to note that the fibroblasts are completely immersed in collagen matrix and the elongated nuclear morphology underlines the good condition of the cells in their own extracellular matrix. There was a weak HE staining (Fig. 4c) into new tissue suggesting that percentage neo extra-cellular matrix is really low. The biggest part of new tissue formed mostly by cells. It appears a different matrix concentration in wound area. It is interesting to highlight that in 20 days of healing the tissue is completely made-up of endogenous ECM. Stains revealed a total repair of tissue in different sections and along tissue edge (Fig. 4d). There was a uniform staining in all tissue suggesting that extra-cellular matrix completely re-established.

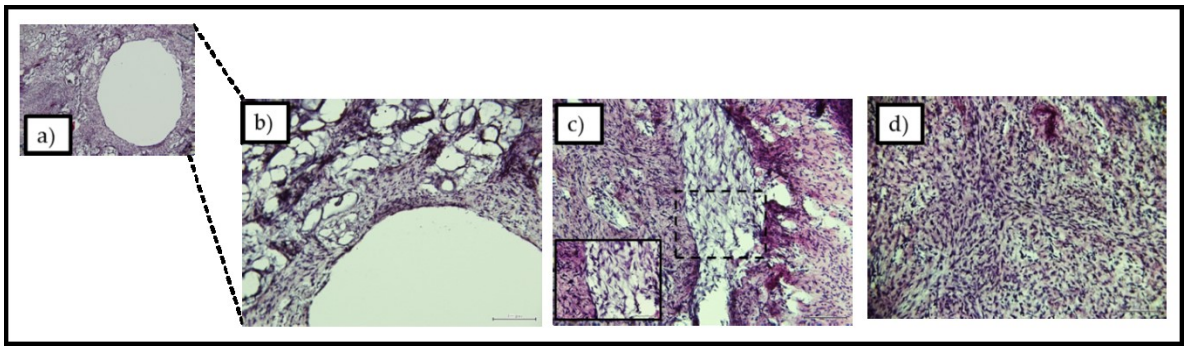

Fig .4: Hematoxylin and eosin staining and temporal sequence of micrographs showing closure progressive of wounded dermis after: (a) 10 days of healing low magnification (scale bar 200 µm); (b) 10 days of healing (scale bar 100 µm) ; (c) 17 days of healing (scale bar 100 µm); (d) 20 days of healing (scale bar 100 µm).

To better define cellular response and demonstrate the relationship between cell migration and differentiation during the wound healing process, we demonstrated that fibroblasts become activated and acquire a smooth muscle cell-like phenotype by evaluating levels expression of the smooth muscle specific protein α-smooth muscle actin (α-SMA) at 10, 17 and 20 days after cut. Myofibroblasts are mesenchymal cells, differentiated by fibroblasts, with features of both fibroblasts – like spindle shape, prominent cytoplasmic projections, abundant rough endoplasmic reticulum – and smooth muscle cells – like longitudinal cytoplasmic bundles of microfilaments and multiple nuclear membrane folds [24] [64]. Myofibroblasts have been observed in practically all fibrotic conditions involving retraction and reorganisation of extra-cellular matrix and have been the subject of several reviews [65] [66]. In addition to their involvement in skin wound healing [64]. The role of myofibroblasts has been extensively studied during this process and works confirm their role in the granulation tissue formation and wound contraction [66] [67]. Indeed, after 10 days by cutting, while time lapse analysis demonstrated starting of contraction and migration, at same times, immunofluorescence analysis detected high levels of SMA (Fig. 5, stain red): studies quantifying myofibroblasts in granulation tissue have shown that the number of myofibroblasts is proportional to the rate of wound contraction and surface remodelling [6624]. When healing and repair process progresses in our dermal platform, myofibroblasts begin to appear (Fig. 5a, red) and a gradually increase (fig. 5b). At 20 days after cut, when process is exhausted, α-SMA wasn't anymore detected (fig. 5c) as literature reports.

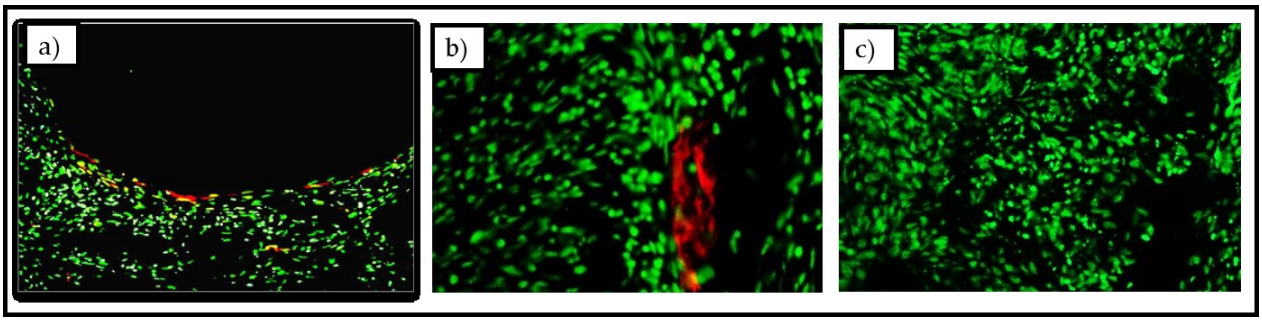

Fig .5 Immunofluorescence and temporal sequence of micrographs showing closure progressive of wounded dermis after: (a) 10 days of healing low magnification (scale bar 200 µm); (b) 10 days of healing (scale bar 100 µm) ; (c) 17 days of healing (scale bar 100 µm); (d) 20 days of healing (scale bar 100 µm). Frozen sections were immunostained for α -SMA and Sytox Green as nuclear stain

Studies demonstrate that myofibroblastic cells synthesize and deposit the extracellular matrix components which will replace the provisional matrix [67]. Thus, once demonstrated cellular response capability of the system and presence of myofibroblasts in damaged tissue, PAS/Alcian blue stain has been investigated to demonstrate synthesis of provisional extracellular matrix. The Alcian blue at a pH of 2.5 will stain all acid mucins (mostly Hyaluronic acid that stains with Alcian blue at pH 2.5.) deep blue but will not color the neutral mucins. The subsequent application of the PAS technique will stain the neutral mucins bright magenta. Tissues or cells that contain both neutral and acidic mucins may demonstrate a dark blue or purple coloration (Jain et al. 2014). In our study mucin histochemistry was an indirect evidence of provisional matrix full of HA as we found that acidic mucins are increased (Fig. 6). Indeed, edges of wound at 14 days and neo-formed matrix at 17 days showed strong Alcian blue staining intensity and a weak intensity of PAS (Fig. 6a, 6b, colour blue), thus highlighting the fact that acidic mucins were predominant in these variants – HA is the predominant GAG found in loose connective tissues [68]. Conversely, the ECM, 20 days after cutting, was strongly PAS positive with an increased amount of neutral mucin (Fig. 6c, colour magenta). The presence of this glycosaminoglycan in developing systems has been related to

cellular migration; its removal by hyaluronidase marks the onset of differentiation [68]. It is possible that a hyaluronic acid-rich environment promotes the migration of fibroblasts into the wound.

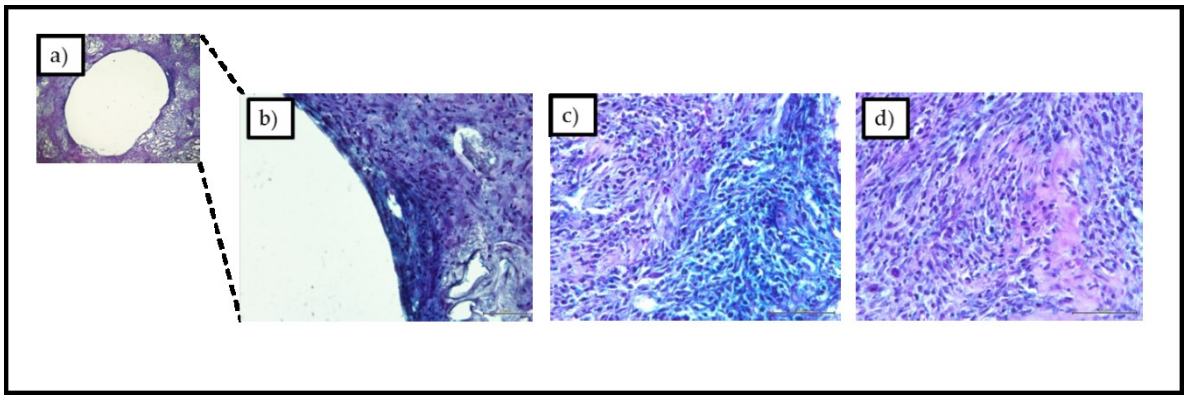

Fig .Pas/Alcian Blue stain and temporal sequence of micrographs showing closure progressive of wounded dermis after: (a) 10 days of healing low magnification (scale bar 200 µm); (b) 10 days of healing (scale bar 100 µm) ; (c) 17 days of healing (scale bar 100 µm); (d) 20 days of healing (scale bar 100 µm).

The last part of repair process is collagen production and remodelling. In order to demonstrate tissue capability to synthetize new collagen in neo-formed matrix we used second harmonic generation (SHG) analysis [69]. The structure of collagen fibrils was observed by MPM that allowed visualize unstained collagen structure. In this purpose SHG imaging was performed into the gap in order to highlight collagen timing production in wound edge. The figure 7a, 7b and 7c reported the SHG images of 14, 17 e 20 days after cutting respectively, the signal was strong only in last image: 20 days after wounding, a relevant quantity of collagen was detected into gap (Fig. 7c). After migrating into wounds, fibroblasts commence the synthesis of extracellular matrix, cells in the wound undergo apoptosis and the provisional extracellular matrix is gradually replaced with a collagenous matrix as in-vivo process [6].

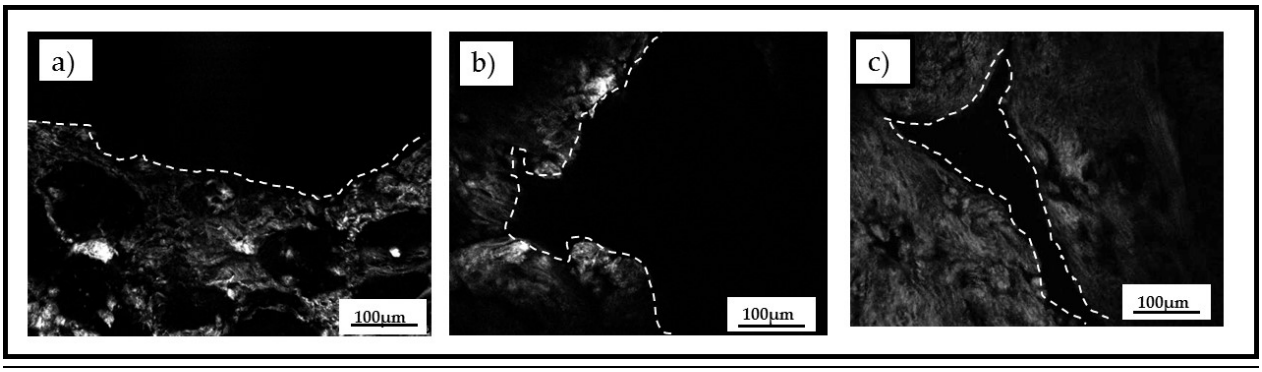

Fig .7 SHG and temporal sequence of micrographs showing closure progressive of wounded dermis after: (a) 10 days of healing; (b) 17 days of healing; (c) 20 days of healing. Frozen sections were immunostained for α collagen detection, scale bar 100 µm.

Christopher Chen (2015), in contrast to mechanisms previously described by planar in vitro models to evaluate gap closure, have already demonstrated that fibroblasts close the open gap through the coordinated action of force-dependent contraction of the whole tissue, circumferential cell migration around the wound edge and assembly of fibronectin scaffolding [47]. With this study they start understand the relevant role of stroma to correctly evaluate cells migration, matrix contraction and ECM remodelling (by the expression of fibronectin). Following the same path, we investigated the role of stroma during wound healing process evaluating tissue contraction and closure, fibroblasts migration and differentiation, proteoglycans and endogenous collagen production. Summarize we demonstrated that this 3D model lead to the possibility of studying in vitro some phases of wound-healing process about the effects of variations in human dermis of full- thickness dermal wounds, also we demonstrated the relationship between cell migration, differentiation marker and ECM production during the wound healing process.

2.4 Second experimental set-up

2.4.1 Materials and Methods

3D-Wound healing model: cut and assembleMaturation chambers were opened after four weeks of maturation and organotypic dermis constructs were transferred into petri dish. Porous gelatin microbeads at 3.8% of crosslink were used to obtain a scaffold-free model. Using a sterile scalpel (Brown 11), linear full thickness cuts have been made through each sample, simulating surgical wounds. 3D-HDE were separated in two parts and washed with 5 ml of the growth medium. Each parts of tissue were transferred into the empty spaces of the silicon mould of the assembling chamber by a shovel, in order to allow contact between the two separated edge and to induced healing process. This method it was carried out in order to mimic suture effect and process. Maturation chamber were also used as healing chamber. Manufactured wound tissues were carried out in dynamic conditions, operated at 60 rpm at 37° C, 5% CO2 and humidity 90%. Medium and ascorbic acid were replenished every 2 days. Repair process and its effects were evaluated at 1 and 2 weeks of healing.

3D-Wound healing model: morphological analysisMorphological analyzes were performed on histological section at 1 and 2 weeks after cut to evaluate microbeads degradation and repair process. Hematoxylin-Eosin (HE) (Bio Optica) Masson Trichrome (Bio Optica) and PAS-Alcian Blue (Bio Optica) stain were performed.

2.4.2 Results and discussions

Microscopic analysis and histological stain suggest 3D-HDE wasn't repaired at 1 week of healing (Fig. 8a), at 2 weeks tissue were repaired (Fig. 8b).

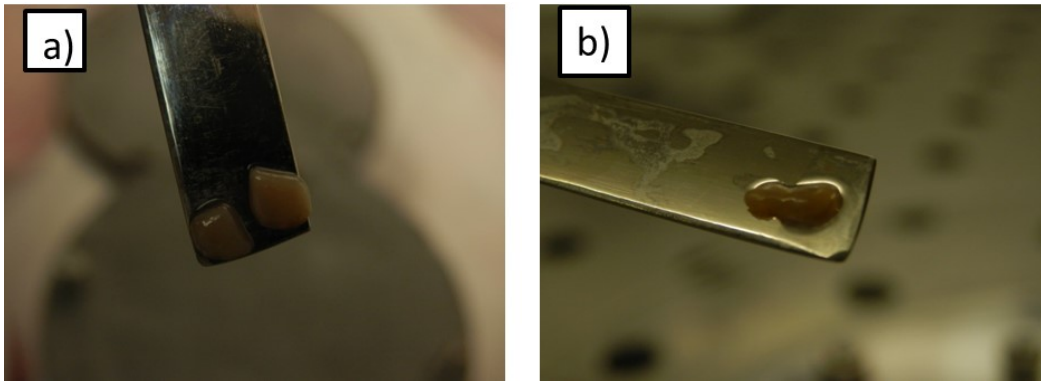

Fig. 8: Representative images of 3D dermis equivalent (a) soon after cut and (b) after healing.

In the panel reported in figure 9, histological images of HE (Fig. 9a), Masson Trichrome (Fig. 9b) and PAS-Alcian Blue concerning human dermis equivalent at two weeks after wounding have been shown. Stains revealed a complete closure of tissue in different sections: fibroblasts had completely covered wound area (Fig. 9) except to external border of repaired tissue. It is possible to note that the fibroblasts are completely immersed in collagen matrix and the elongated nuclear morphology underlines the physiological condition of the cells in their own extracellular matrix. There was an intense color both for HE (Fig. 9a) than Masson Trichrome staining (Fig. 9b) along new tissue suggesting relevant celluarization of tissue. Fig. 9c showed strong Alcian blue staining intensity and a weak intensity of PAS (colour blue), thus highlighting the fact that acidic mucins were predominant in these variants.

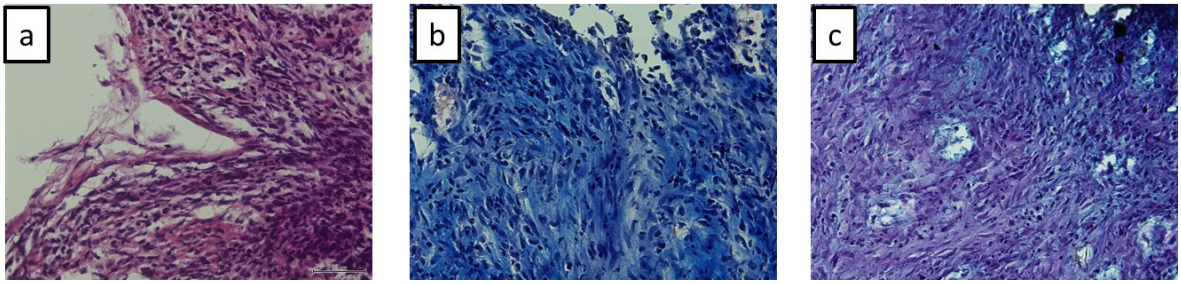

Fig .9: Hematoxylin and eosin staining and temporal sequence of micrographs showing closure progressive of wounded dermis after: (a) 1 weeks after cut; (b) 2 weeks after cut ; (c) 3 weeks after cut; (d). Scale bar 50 µm

Major problem of this platform is the impaired healing. During wound studies by using first experimental set-up, tissue repaired after 14 days too but gap was even more pronounced. We had suggested a shorter healing time by using this platform and we ascribe this delay to a strong tissue contraction for the duration of the culture. We observed a very high variation of 3D-tissue measurements (Fig. 10). At beginning we obtained a 3D-HDE with measurement 6x12 mm (Fig. 10a, 10b), immediately after cut 3D-tissue were significantly reduced (Fig. 10c). 2 weeks after cut (4 weeks of maturation in total) 3D-wounded tissue was even more contracted and smaller than 2 weeks of maturation (Fig. 10d). In fig. 10e-10f were reported measurements after 4 weeks of maturation (2 weeks after cut).

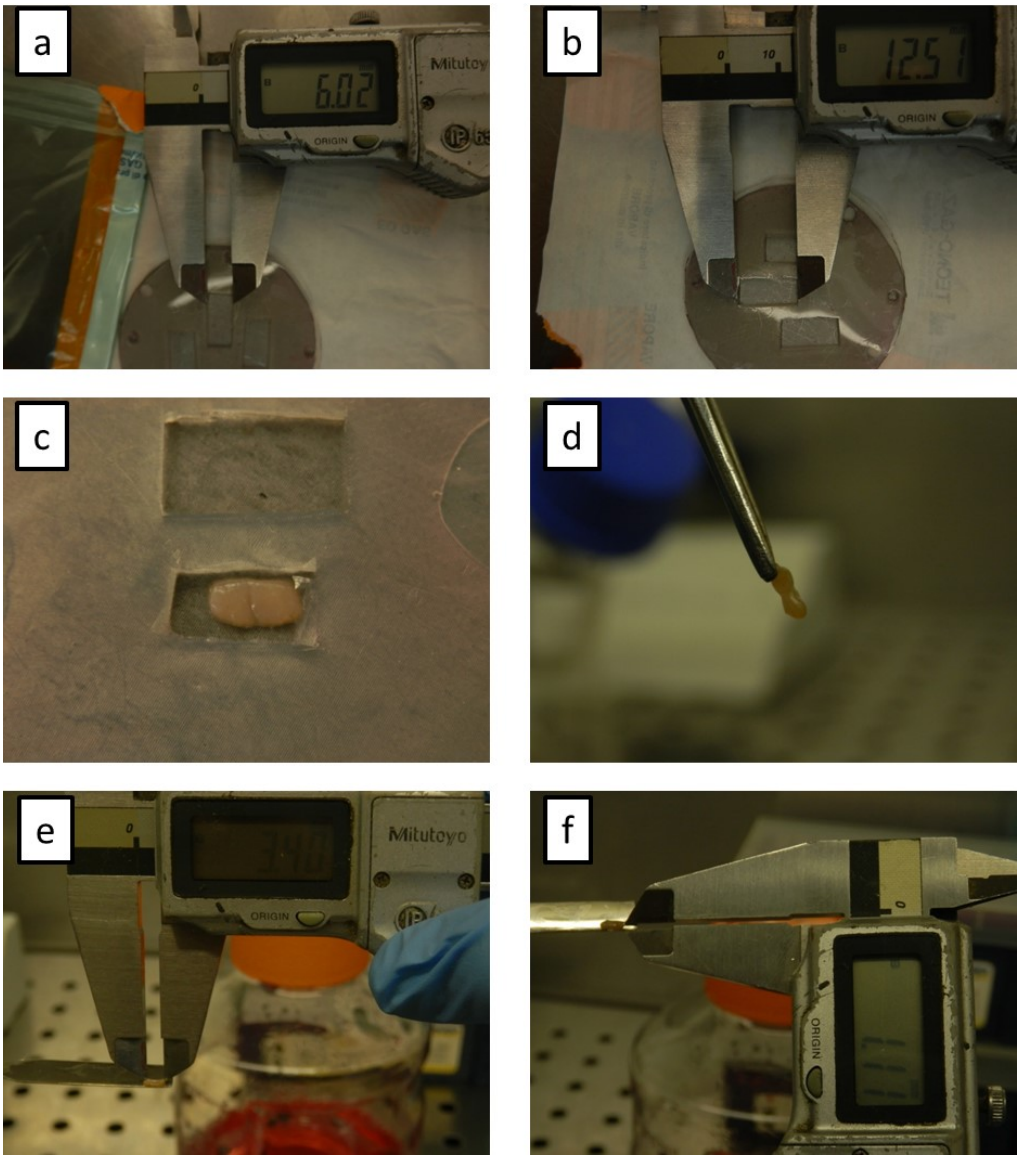

Fig .10: Representative panel to show tissue contraction. (a) and (b) measurements of initial mould, (c) and (d) macroscopic aspect of 3D dermis equivalent after 2 weeks of maturation and before cut,(e) and (f) measurements of dermis equivalent after 4 weeks of maturation (2 weeks after cut).

We calculated the change in measures and observed a very high degree of spontaneous contractions in 3D-HDE after 2 weeks of maturation (Fig. 11). Except for thickness, length and width decreased significantly (Fig. 11a). Measurements variations were strictly function of

percentage of contraction. After 2 weeks of maturation 3D-tissue lost about 40% of their length and 50% of their widht, after 2 weeks of healing (4 weeks of maturation) about 72% and 82% respectively (Fig. 11b).

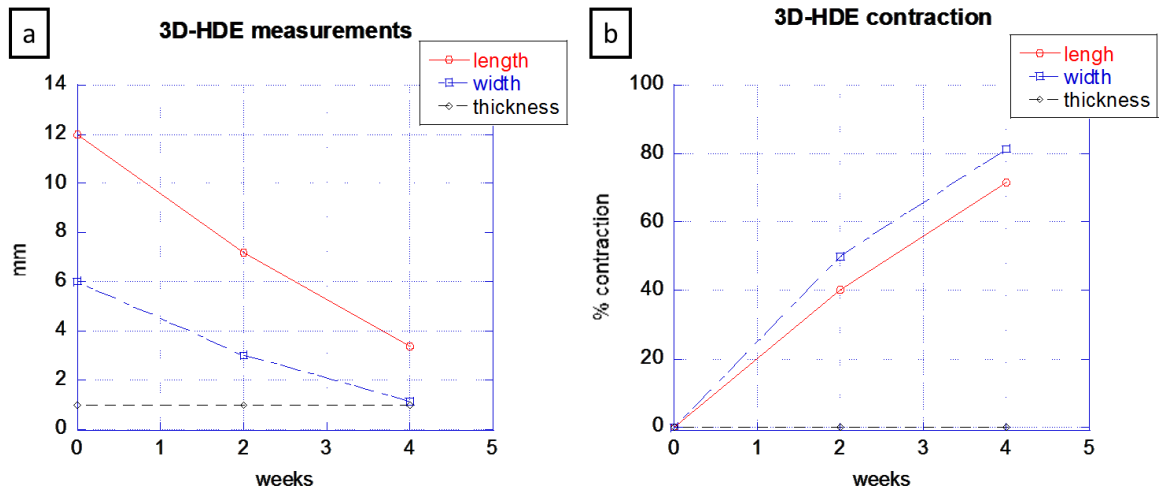

Fig .11: Quantitative analysis of tissue dimension variations (a) in terms of change in measures in nm, (b) in terms of contraction.

Recent studies demonstrated that cell behaviour can be quite diverse in response to a scaffold. Features such as surface chemistry, morphology and mechanics, can have an influence over cell fate [70]. Recent studies revealed that scaffold stiffness had elicit changes in focal adhesion structure, cytoskeleton assembly, morphology, migration and spreading of fibroblasts[71], and smooth-muscle cells [71]. Scaffold properties also affect cell growth, differentiation, and organization during tissue repair [3] . We hypnotize scaffold-influence in tissue repair at 1 week of healing specially. Imparato et al. [72] have investigated the role of

micro-scaffold mechanical properties and degradation rate on the composition, organization and maturation of de novo synthesized ECM in the 3D human dermal equivalent tissue used by wound model in this work. Their results indicate clearly that composition, organization and maturation of de novo synthesized ECM can be controlled by microscaffold properties. Indeed, the morphology of HD-µTPs was affected by the GPM's crosslinking density: 3% HD-mTPs exhibited a strong contraction due to the low mechanical properties of the 3% GPM compared to cell traction forces. The result biohybrid underwent consistent contraction of both shape and thickness even before 2 weeks of culture. Indeed presence of compliant and rapid degradable GPM does not support the process of production-degradation and maturation of collagen within the scaffold frame. During a repair process this turnover is even more pronounced, migration of myofibroblasts is really important for cell invasion and spreading of fibroblasts is necessary for formation of new tissue in wound edge. Thus, the scaffold itself should be sufficiently stable to allow new granulation tissue to mature, while the injured tissue is replaced by new collagen deposition. Second, the collagen matrix should not persist indefinitely, but be degradable within the time limits compatible with the healing process as well as is verified by Masci et al. [73]. For this reason, the strong contraction of tissue sample – before and after cut –doesn't promote repair but adversely affects wound healing, moreover strong contraction detaches the two wounded edges and prevents physical contact.

2.5 Conclusions

Wound healing is a dynamic, interactive process that passes in three phases and overlap in time: inflammation, tissue formation, and tissue remodelling. Studies, analyzing wound healing, use mainly mechanical methods for wound induction, which are laborious and difficult to standardize [14]. Hereby, we were able to set multiple standardized injuries with

defined dimensions in a human full-thickness 3D dermal equivalent, enabling the investigation of wound healing. In summary, the model proposed, due to its endogenous nature, could represent a valuable tool to study tissue status in vitro at both a cellular and an extra-cellular level. Our study paves the way to the development of a new class of in vitro wound-tissue models that correctly reproduce in composition and organization the extracellular space. Such models would lead to the possibility of studying in vitro some phases of wound-healing process about the effects of variations in human dermis of full- thickness dermal wounds, including fibroblast proliferation, migration, differentiation and proteoglycans expression. In conclusion with our 3D-HDE in vitro model we can demonstrate the relationship between cell migration, differentiation marker and ECM production during the wound healing process. We believe that our 3D-HDE wound model could be a starting point for a novel platform to test dermal wound therapies and could be further improved. Indeed, first experimental set-up allows possibility to evaluate how this 3D-HDE react to a physical damage and defines healing in-vitro timing and relate marker to follow. Only problem of this platform is reproducibility. Without standardization of experimental variables, it is difficult to make meaningful comparisons among different reports in the literature. Furthermore, to achieve a high level of accuracy and reproducibility, a well-defined procedure for the wound healing assay is crucial. Developing a standard approach for the wound healing assay promotes comparability between studies and could lead to a useful database containing collective migration data for a variety of cell lines. In this perspective, second experimental set-up work out this question. Anyway contraction phenomenon is a strong question to considerate: scaffold – and relate tissue – contraction, also affect tissue repair process by inhibiting or altering healing. We conclude that the *in vitro* model presented here is a good

approximation of the complex and dynamic composition and organization of the ECM in a human cutaneous wound and is potentially useful for studying biology of wound healing. This wound platform could provide as starting point to investigate the efficacy of potential anti-wound healing drugs. Significant future developments will include the continued development of artificial human dermal equivalent products under consensus efficacy standards and that uses cells embedded into an endogenous ECM without contraction phenomenon and that better recapitulate *in vivo* healing-timing. Summarize this bioengineered 3D model of wound closure may become a valuable tool to investigate the underlying mechanics of gap closure and ECM remodelling.

2.6 References

1. Iii JTS, Tompkins RG, Burke JF. Artificial skin. *Rev Med*. 2000;(3):231-244.

2. Gillitzer R, Goebeler M. Chemokines in cutaneous wound healing. *J Leukoc Biol*. 2001;69(4):513-521. http://www.ncbi.nlm.nih.gov/pubmed/11310836¥nhttp://www.jleukbio.org/content/69/4/513.full.pdf.

3. Ingber DE. Tensegrity II. How structural networks influence cellular information processing networks. *J Cell Sci*. 2003;116(Pt 8):1397-1408. doi:10.1242/jcs.00360.

4. Chen WYJ, Abatangelo G. Functions of hyaluronan in wound repair. *Wound Repair Regen*. 1999;7(2):79-89. doi:10.1046/j.1524-475X.1999.00079.x.

5. Baum CL, Arpey CJ. Normal cutaneous wound healing: clinical correlation with cellular and molecular events. *Dermatol Surg*. 2005;31(6):674-686; discussion 686. http://www.ncbi.nlm.nih.gov/entrez/query.fcgi?cmd=Retrieve&db=PubMed&dopt=Citation&list_uids=15996419.

6. Adam J. Singer RAFC. Cutaneous wound healing. 1999.

7. Hari G. Garg MTL. *Scarless in Wound Healing*. Vol 133.; 2000. doi:10.1016/B978-0-444-62644-8.00008-X.

8. Enoch S, Leaper DJ. Basic science of wound healing. *Surg*. 2008;26(2):31-37. doi:10.1016/j.mpsur.2007.11.005.

9. Clark RAF, Lanigan JM, DellaPelle P, Manseau E, Dvorak HF, Colvin RB. Fibronectin

and fibrin provide a provisional matrix for epidermal cell migration during wound reepithelialization. *J Invest Dermatol*. 1982;79(5):264-269. doi:10.1111/1523-1747.ep12500075.

10. Gurtner GC, Werner S, Barrandon Y, Longaker MT. Wound repair and regeneration. *Nature*. 2008;453(7193):314-321. doi:10.1038/nature07039.

11. Greaves NS, Ashcroft KJ, Baguneid M, Bayat A. Current understanding of molecular and cellular mechanisms in fibroplasia and angiogenesis during acute wound healing. *J Dermatol Sci*. 2013;72(3):206-217. doi:10.1016/j.jdermsci.2013.07.008.

12. Stuart Enoch DJL. Basic science of wound healing. *Surg*. 2010;28(9):409-412. doi:10.1016/j.mpsur.2010.05.007.

13. Metcalf D, Factors S. The Granulocyte-Macrophage Colony-Stimulating Factors. 229.

14. Bash E. Wound Healing. 2009;5.

15. Falanga V, Isaacs C, Paquette D, et al. Wounding of bioengineered skin: cellular and molecular aspects after injury. *J Invest Dermatol*. 2002;119(3):653-660. doi:10.1046/j.1523-1747.2002.01865.x.

16. Baum CL, Arpey CJ. Normal cutaneous wound healing: clinical correlation with cellular and molecular events. *Dermatol Surg*. 2005;31(6):674-686; discussion 686.

17. Desmoulibre A. Transforming Growth Factor-ill Induces u-Smooth Muscle Actin Expression in Granulation Tissue Myofibroblasts and in Quiescent and Growing Cultured Fibroblasts. 1993;122(1):103-111.

18. Cliff WJ, Chir B, Phil D, et al. Myofibroblasts in human granulation tissue. :55-67.

19. Martin P. Wound healing--aiming for perfect skin regeneration. *Science*. 1997;276(5309):75-81. doi:10.1126/science.276.5309.75.

20. Welch MP, Odland GF, Clark RAF. Temporal relationships of F-actin bundle formation, collagen and fibronectin matrix assembly, and fibronectin receptor expression to wound contraction. *J Cell Biol*. 1990;110(1):133-145. doi:10.1083/jcb.110.1.133.

21. Brown LF, Lanir N, McDonagh J, Tognazzi K, Dvorak AM, Dvorak HF. Fibroblast migration in fibrin gel matrices. *Am J Pathol*. 1993;142(1):273-283. http://www.pubmedcentral.nih.gov/articlerender.fcgi?artid=1886838&tool=pmcentrez&rendertype=abstract.

22. Clark R. *The Molecular and Cellular Biology of Wound Repair*. 2nd ed. New York: Plenum Press; 1996.

23. Lawrence WT. Physiology of the acute wound. *Clin Plast Surg*. 1998:25:321-340.

24. Tomasek JJ, Gabbiani G, Hinz B, Chaponnier C, Brown R a. Myofibroblasts and mechano-regulation of connective tissue remodelling. *Nat Rev Mol Cell Biol*. 2002;3(5):349-363. doi:10.1038/nrm809.

25. Strieter RM, Burdick MD, Mehrad B. The role of circulating mesenchymal progenitor cells, fibrocytes, in promoting pulmonary fibrosis. 2009;120:49-59.

26. El-Ghalbzouri A, Gibbs S, Lamme E, Van Blitterswijk CA, Ponec M. Effect of fibroblasts on epidermal regeneration. *Br J Dermatol*. 2002;147(2):230-243. doi:10.1046/j.1365-2133.2002.04871.x.

27. Heldin C-H WB. *The Molecular and Cellular Biology of Wound Repair*. (New York: Plenum Press, ed.).; 1996.

28. Li J, Zhang Y-P KR. Angiogenesis in wound repair: angiogenic growth factors and the extracellular matrix. *Microsc Res Tech*. 2003:60:107-114.

29. Raza SL CL. Matrix metalloproteinases: pro- and anti- angiogenic activities. *J Invest Dermatol Symp*. 2005:5:47-54.

30. Geer DJ, Andreadis ST. A Novel Role of Fibrin in Epidermal Healing: Plasminogen-Mediated Migration and Selective Detachment of Differentiated Keratinocytes. *J Invest Dermatol*. 2003;121(5):1210-1216. doi:10.1046/j.1523-1747.2003.12512.x.

31. Fomby P, Cherlin AJ. Controlled architectural and chemotactic studies of 3D cell migration. *Biomaterials*. 2012;32(10):2634-2641. doi:10.1038/nature13314.A.

32. Werner S, Krieg T, Smola H. Keratinocyte–Fibroblast Interactions in Wound Healing. *J Invest Dermatol*. 2007;127(5):998-1008. doi:10.1038/sj.jid.5700786.

33. Myllyharju J, Kivirikko KI. Collagens, modifying enzymes and their mutations in humans, flies and worms. *Trends Genet*. 2004;20(1):33-43. doi:10.1016/j.tig.2003.11.004.

34. Gabbiani G, Chaponnier C, Istvan HUITNER. Cytoplasmic filaments and gap junctions in epithelial cells and myofibroblasts during wound healing. 1978;76:561-568.

35. Gray a J, Bishop JE, Reeves JT, Laurent GJ. A alpha and B beta chains of fibrinogen stimulate proliferation of human fibroblasts. *J Cell Sci*. 1993;104 (Pt 2:409-413.

36. Folkman J. *Angiogenesis and Angiogenesis Inhibition: An Overview*.; 1997.

37. Nowacki M, Pietkun K, Pokrywczyńska M, et al. Filling effects, persistence, and safety of dermal fillers formulated with stem cells in an animal model. *Aesthet Surg J*. 2014;34(8):1261-1269. doi:10.1177/1090820X14548212.

38. Liang C, Park AY, Guan J. In vitro scratch assay : a convenient and inexpensive method for analysis of cell migration in vitro. 2007;2(2):329-333. doi:10.1038/nprot.2007.30.

39. Anon E, Serra-Picamal X, Hersen P, et al. Cell crawling mediates collective cell migration to close undamaged epithelial gaps. *Proc Natl Acad Sci U S A*. 2012;109(27):10891-10896. doi:10.1073/pnas.1117814109.

40. Young AA, Legrice IJ, Young MA, Smaill BH. Extended confocal microscopy of myocardial laminae and collagen network. *J Microsc*. 1998;192(2):139-150. doi:10.1046/j.1365-2818.1998.00414.x.

41. El Ghalbzouri A, Hensbergen P, Gibbs S, Kempenaar J, Schors R van der, Ponec M. Fibroblasts facilitate re-epithelialization in wounded human skin equivalents. *Lab Investig*. 2004;84(1):102-112. doi:10.1038/labinvest.3700014.

42. Safferling K, S??tterlin T, Westphal K, et al. Wound healing revised: A novel reepithelialization mechanism revealed by in vitro and in silico models. *J Cell Biol*. 2013;203(4):691-709. doi:10.1083/jcb.201212020.

43. Poujade M, Grasland-Mongrain E, Hertzog A, et al. Collective migration of an epithelial monolayer in response to a model wound. *Proc Natl Acad Sci U S A*. 2007;104(41):15988-15993. doi:10.1073/pnas.0705062104.

44. Cochet-Escartin O, Ranft J, Silberzan P, Marcq P. Border forces and friction control

epithelial closure dynamics. *Biophys J*. 2014;106(1):65-73. doi:10.1016/j.bpj.2013.11.015.

45. Vedula SRK, Peyret G, Cheddadi I, et al. Mechanics of epithelial closure over non-adherent environments. *Nat Commun*. 2015;6:6111. doi:10.1038/ncomms7111.

46. Nier V, Deforet M, Duclos G, et al. Tissue fusion over nonadhering surfaces. *Proc Natl Acad Sci*. 2015;112(31):9546-9551. doi:10.1073/pnas.1501278112.

47. Selman Sakar M, Eyckmans J, Pieters R, Eberli D, Nelson BJ, Chen CS. Cellular forces and matrix assembly coordinate fibrous tissue repair. *Nat Commun*. 2016;7:1-8. doi:10.1038/ncomms11036.

48. Boekema BKHL, Vlig M, Olde Damink L, et al. Effect of pore size and cross-linking of a novel collagen-elastin dermal substitute on wound healing. *J Mater Sci Mater Med*. 2014;25(2):423-433. doi:10.1007/s10856-013-5075-2.

49. Wojtowicz AM, Oliveira S, Carlson MW, Zawadzka A, Rousseau CF, Baksh D. The importance of both fibroblasts and keratinocytes in a bilayered living cellular construct used in wound healing. *Wound Repair Regen*. 2014;22:246-255. doi:10.1111/wrr.12154.

50. Palmiero C, Imparato G, Urciuolo F, Netti P. Engineered dermal equivalent tissue in vitro by assembly of microtissue precursors. *Acta Biomater*. 2010;6(7):2548-2553. doi:10.1016/j.actbio.2010.01.026.

51. Zwirner NW, Dole K, Stastny P. Differential surface expression of MICA by endothelial cells, fibroblasts, keratinocytes, and monocytes. *Hum Immunol*. 1999;60(4):323-330. doi:S0198885998001281 [pii].

52. Goldman R.D. SDL. *Live Cell Imaging : A Laboratory Manual*. 2° edition. (Cold Spring

Harbor NY. CSHLP, ed.).; 2005.

53. Jonkman JEN, Cathcart JA, Xu F, et al. An introduction to the wound healing assay using live-cell microscopy. *Cell Adhes Migr*. 2014;8(5):440-451. doi:10.4161/cam.36224.

54. Ryu S-W, Lee S-H, Yoon H-J. A comparative histological and immunohistochemical study of wound healing following incision with a scalpel, CO2 laser or Er,Cr:YSGG laser in the guinea pig oral mucosa. *Acta Odontol Scand*. 2012;70(6):448-454. doi:10.3109/00016357.2011.635598.

55. Straatman K. Wound healing assay. 2008:67-80.

56. Hulkower KI, Herber RL. Cell migration and invasion assays as tools for drug discovery. *Pharmaceutics*. 2011;3(1):107-124. doi:10.3390/pharmaceutics3010107.

57. De Rossi G, Whiteford JR. A novel role for syndecan-3 in angiogenesis. *F1000Research*. 2013;2:270. doi:10.12688/f1000research.2-270.v1.

58. Ravasio A, Cheddadi I, Chen T, et al. Gap geometry dictates epithelial closure efficiency. *Nat Commun*. 2015;6:7683. doi:10.1038/ncomms8683.

59. Reffay M, Parrini MC, Cochet-Escartin O, et al. Interplay of RhoA and mechanical forces in collective cell migration driven by leader cells. *Nat Cell Biol*. 2014;16(3):217-223. doi:10.1038/ncb2917.

60. Schnyder I, Katsaros C, Chiquet M. Accelerated Wound Closure In Vitro by Fibroblasts from a Subgroup of Cleft Lip / Palate Patients : Role of Transforming Growth Factor- a. 2014;9(10):1-15. doi:10.1371/journal.pone.0111752.

61. Kanazawa S, Fujiwara T, Matsuzaki S, Shingaki K, Taniguchi M. bFGF Regulates PI3-Kinase-Rac1-JNK Pathway and Promotes Fibroblast Migration in Wound Healing. 2010;5(8):1-12. doi:10.1371/journal.pone.0012228.

62. Bement WM, Forscher P, Mooseker MS. A novel cytoskeletal structure involved in purse string wound closure and cell polarity maintenance. *J Cell Biol*. 1993;121(3):565-578. doi:10.1083/jcb.121.3.565.

63. Jacinto A, Martinez-Arias A, Martin P. Mechanisms of epithelial fusion and repair. *Nat Cell Biol*. 2001;3(5):E117-E123. doi:10.1038/35074643.

64. Darby IA, Hewitson TD. Fibroblast Differentiation in Wound Healing and Fibrosis. *Int Rev Cytol*. 2007;257:143-179. doi:10.1016/S0074-7696(07)57004-X.

65. Desmoulière A, Darby I, Gabbiani G. Normal and pathologic soft tissue remodeling: role of the myofibroblast, with special emphasis on liver and kidney fibrosis. *Lab Invest*. 2003;83(12):1689-1707. doi:10.1097/01.LAB.0000101911.53973.90.

66. Schmitt-Gräff a, Desmoulière a, Gabbiani G. Heterogeneity of myofibroblast phenotypic features: an example of fibroblastic cell plasticity. *Virchows Arch*. 1994;425(1):3-24. doi:10.1007/BF00193944.

67. Micallef L, Vedrenne N, Billet F, Coulomb B, Darby I a, Desmoulière A. The myofibroblast, multiple origins for major roles in normal and pathological tissue repair. *Fibrogenesis Tissue Repair*. 2012;5 Suppl 1(Suppl 1):S5. doi:10.1186/1755-1536-5-S1-S5.

68. Radi ZA, Guzman RE, Bell RR. Increased connective tissue extracellular matrix in the op/op model of osteopetrosis. *Pathobiology*. 2009;76(4):199-203. doi:10.1159/000218336.

69. Raub CB, Suresh V, Krasieva T, et al. Noninvasive assessment of collagen gel microstructure and mechanics using multiphoton microscopy. *Biophys J*. 2007;92(6):2212-2222. doi:10.1529/biophysj.106.097998.

70. Ahmed M, Ramos TADS, Damanik F, et al. A combinatorial approach towards the design of nanofibrous scaffolds for chondrogenesis. *Sci Rep*. 2015;5:1-12. doi:10.1038/srep14804.

71. Ang YULIW. Cell locomotion and focal adhesions are regulated by. *Proc Natl Acad Sci*. 1997;94(December):13661-13665. doi:10.1073/pnas.95.20.13661.

72. Imparato G, Urciuolo F, Casale C, Netti PA. The role of microscaffold properties in controlling the collagen assembly in 3D dermis equivalent using modular tissue engineering. *Biomaterials*. 2013;34(32):7851-7861. doi:10.1016/j.biomaterials.2013.06.062.

73. Masci VL, Taddei AR, Gambellini G, Giorgi F, Fausto AM. Ultrastructural investigation on fibroblast interaction with collagen scaffold. *J Biomed Mater Res - Part A*. 2016;104(1):272-282. doi:10.1002/jbm.a.35563.

3 Engineered 3D human dermis model to study the scar formation: recapitulating cellular and extracellular machineries during dermal repair.

3.1 Introduction

Tissue-engineered human skin equivalents (HSEs) have contributed significantly to the understanding of biological processes and skin diseases [1] [2] [3]. Wound healing has been studied before in HSEs in which wounds were created by burning, freezing, or punching the epithelium [4] [5] : however to the best of our knowledge a few of information on dermal healing are reported in literature. Indeed, the central question debated in the literature in skin wound healing are often process and mechanism of the creation and extension of the epidermal tongue [6] [5–8]. Dermal substitutes function as an optimized wound bed to support outgrowth of keratinocytes from the wound margins, or from an epidermal component such as a skin graft, cultured skin or an artificial epidermal component containing autologous or allogeneic keratinocytes [9–11]. Following any injury,various intracellular and intercellular pathways must be activated and coordinated if tissue integrity need to be restored. Relevant processes regards dermal matrix [12]. In dermal wound healing, after a skin injury, several interacting events are initiated including inflammation, tissue formation, angiogenesis, tissue contraction and tissue remodeling [13]. Regarding the phase of tissue formation and contraction (third phase of wound healing process), the crosstalking between cells and extracellular matrix (ECM) is crucial. After the blood clot has formed, white blood cells invade the wound region by migrating through the ECM [14]. Fibroblasts subsequently differentiate into myofibroblasts and migrate

into the region and begin to replace the blood clot with provisional matrix [15,16]. The formation of this provisional matrix – granulation tissue – and regulation of collagen fibers and bundles formation by the fibroblasts, as well as the organization of these elements into an endogenous stroma after wounding, was the key issue of these two stages [17 18].

Regarding the last phase of a wound repair – remodeling – recent studies confirmed that the natural evolution of an adult wound healing process is scar formation. Scarring can be assessed clinically by using the Vancouver scar scale, or the Manchester scar proforma or the Visual Analogue Scale [19]. Scarring involves high collagen deposition in response to tissue injury, for this reason a variety of treatment modalities have been attempted. Moreover, with the introduction of new treatments for *in vivo* injury, as the development of skin replacement materials and grafting with autologous split thickness grafts, scar question is more and more relevant. In spite of dermal substitutes are important in treating full thickness skin defects, relevant problems associated to their use because usually severe scarring occurred after grafting [10,20,21]. For this reason in the last few years there was an increase of focusing on the mechanism of scar formation and progression. It is really important to *in vivo* track the wound status at the molecular, cellular and tissue levels, helping to understand the scarring response mechanisms and prevent it. Recent works have shown that molecular biology at the wound margin is important for scarring [22], and the advancing or receding of a wound margin may be potentially used for prevention [14]. Although several of the ECM–fibroblast interactions have been experimentally studied, this area remains poorly understood [23,24] [25]. This is partly because all interactions have not been found, but mainly because the processes involved interact in a complex manner. A major limitation in the progress of scar management is the lack of physiologically relevant human models to explore the pathogenesis of scar formation

and to test new therapeutics [26] [10]. Today, human models, animal models, and in vitro cell culture models are used to study skin scar formation. The possibilities to use patient as in vivo models are limited, due to obvious ethical considerations [27]. Current and common alternative is the use of animal models [28]. Despite the large number of studies describing mice, pigs, rabbits, rats and other animals as models to investigate scar and hypertrophic scarring, the wound healing process in these species presents significant differences and is extremely difficult compared with human tissue specially because of lack of specific biomarkers, differences in skin structure and physiology with consequently differences in scar formation, presence of aberrant scars formation [29] [30] [31]. Moreover, with increasing pressure from the EU (Directive 2010/63/EU) for the replacement, reduction, and refinement of the use of animal models, there is an urgent need to develop a physiologically relevant and responsive in vitro human wound model to investigate the matrix response and the pathogenesis of scar formation [32–34] [26]. In current in vitro models, is possible to study only cell migration, contraction and proliferation, cell–cell interaction and protein synthesis [35] [28] [26]. Accurate study it is not possible to evaluate granulation tissue and scar formation. Moreover it was seen that an *in vitro* model of burn wound healing in human skin did not induce the differentiation of myofibroblasts [36] [10]. This shows that a human skin equivalent model – with just a stratified and differentiated epithelium – isn't enough to correctly mimic *in vivo* situation. To date, no gold standard exists for the treatment of scar tissue.

In this perspective, the development of biologically relevant three-dimensional human dermal equivalent (3D-HDE) as *in vitro* model can emerge as new challenge in tissue engineering to evaluate dermal remodeling during healing process. The fabrication of an endogenous stroma that interact in a complex manner with cells population allows possibility to confirm the

relationship between cell migration, differentiation marker and ECM production during a wound healing process and also demonstrated the same *in vivo* timing into a highly responsive endogenous matrix. Also, the presence of a responsive dermis – that mimic *in vivo* response occurred during a repair that take place in the stroma – allows possibility to evaluate scar formation and to study and understand processes involved during scarring. This should be a great achievement considering difficulties to understand mechanism of scarring and the high request of new strategies for prevention.

3.2 Materials and methods

3.2.1 Tissue precursor fabrication and human dermis equivalent production

The 3D-HDE was prepared as reported by Palmiero et al. (2010). Briefly dermal microtissues were produced by seeding HDF passage seventh on biodegradable gelatin porous microcarries. Glyceraldehydes has been used as gelatin crosslinker at 4% w/w of the microbeads, only this percentage has been used in order to obtain a completely endogenous tissue without the presence of microbeads or contraction phenomenon. The microbeads / fibroblasts cultures were propagated in two spinner flasks for 7 days using a continuous stirring regime [9]. Each spinner flask was initially loaded with 6.5 x 10^6 HDF and 115 mg/ml of microbeads, corresponding to 11 cells/beads. From the day 2th, 50 µgr/ml of ascorbic acid were added. After 7 days, microtissues precursor transferred into maturation chamber in order to provide the assembly of microtissues and the fabrication of macrotissue by using a bottom up approach as previously described (Imparato et al. 2013). Maturation chamber was used to allow their molding in parallelepiped-shaped and obtained the 3D-HDE (thickness 1 mm,

dimensions 6x12 mm). Maturation of 3D-HDE was carried out in dynamic conditions by placing the chamber on the bottom of a spinner flask operated at 60 rpm at 37° C, 5% CO2 and humidity 90%. Maturation process was carried out for 4 weeks in order to provide a scaffold-free dermis construct. The medium was changed every 2 days and ascorbic acid was added at each medium change at a concentration of 50 μgr/ ml.

3.2.2 3D-Wound healing model

Maturation chambers were opened and organotypic dermis constructs were transferred into petri dish. Using a sterile scalpel (Brown 11), linear full thickness cuts have been made through each sample, simulating surgical wounds. HDE were separated in two parts and washed with 5 ml of the growth medium.

Critical step: it is important to cut in the middle of the tissue in order to obtain two similar dermis layers and minimize any possible variation caused by the difference of tissue dimension.

Each parts of tissue were transferred into the empty spaces of the silicon mould of the assembling chamber by a shovel, in order to allow contact between the two separated edge and to induced healing process. This method is based on the observation that, upon creation of a new artificial gap in our tissue, the cells on the edge of the newly created gap will move toward the opening to repair damage until new tissue-tissue contacts are established again. Assembling chamber is similar at the maturation chamber used to realize dermis. Manufactured wound tissues were carried out in dynamic conditions, operated at 60 rpm at 37° C, 5% CO2 and humidity 90%. Medium and ascorbic acid were replenished every 2 days.

The wound healing process and its effects were evaluated 1, 2 and 3 weeks after damage for all samples. The final 3D disk-shape wound- tissues were named as follows: cut 1 week after wounding, cut 2 weeks after wounding and cut 3 weeks after wounding respectively (with related controls).

3.2.3 Histological and immunofluorescence analysis to monitor wound healing process

Morphological analyzes were performed on histological section at 1, 2 and 3 weeks after damage. All tissues were fixed in 4% paraformaldehyde for 30 min followed by overnight incubation in 2 M sucrose for cryopreserved sections. Samples were embedded in Tissue Tek (Killik, Bio Optica, Milano, Italy), submerged in liquid nitrogen vapors for 1 min and then stored at -80 ° C. Samples were cut in slices 7 µm in thickness by using Criomicrotome (Leica CM 1850, Milano, Italy). The dermis healing process was monitored after wound. Monitoring was carried out by analyzing data from the full extension of the wound in different days post-wounding. ECM composition and tissue morphology were assessed by performing histological analysis on transverse sections of biohybrid, along the peace of the sheet thickness. Samples were stained using Hematoxylin-Eosin (H&E) and Masson's Trichrome (Bio Optica) solutions for frozen section, following standard procedure and analyzed by an optical microscope (BX53; Olympus Tokyo, Japan). Also, immunofluorescence staining were carried out, for this analysis wounded sample were oriented so as to view the cross section of the samples in order to visualize cut section. For immunofluorescences analyses, frozen thick slices were immunostained with specific antibodies for 3 hours followed by incubation with

the appropriate secondary antibody. The primary monoclonal antibodies used in this work include:

- anti-Alpha smooth muscle actin monoclonal antibody blue (diluted 1:100, Abcam, Cambridge,UK)
- anti-Hyaluronic acid polyclonal antibody red (diluted 1:50, Abcam).

The secondary antibodies used were: Alexa fluor (Life Techologies, Milano, Italy) 594 goat anti-mouse and 546 Rabbit Anti-Sheep IgG H&L (Abcam) respectively. Antibody monoclonal was produced in mouse and the polyclonal antibody was produced in rabbit, all secondary antibodies were diluted 1:500 in PBS/BSA 3%. Nucleus detections were assessed by using Sytox Green staining (Invitrogen, Life Technologies, Italy). The samples were investigated by using confocal microscopy (TCS SP5 II Leica, Milano, Italy). Hyaluronic acid production and alpha-smooth muscle actin expression were evaluated at 1, 2 and 3 weeks after damage.

3.2.4 Second harmonic generation (SHG) analysis

Microscopy studies, on our damage human equivalent dermis, were performed on a versatile confocal microscopy Confocal Leica TCS SP5 II combined with a Multiphoton Microscope where the NIR femtosecond laser beam was derived from a tunable compact mode locked titanium: sapphire laser (Chamaleon Compact OPOVis, Coherent). Our control were foreskin at 30 and 80' years old [37]. The samples for nonlinear imaging were prepared by freezing them and by cutting them in a compact routine cryostat. Before imaging, samples were unfrozen and closed with a microscope coverslide together with some PBS droplets in order to maintain the natural tissue osmolarity. Two-photon excited fluorescence was used to induce Second-harmonic generation (SHG) and obtain high-resolution images of unstained collagen

structures around edge of the wound during three weeks of healing. SHG imaging can help reveal interactions between cells and ECM answer. Samples were observed by using λ_{ex} = 840 nm (two photons) and λ_{em}=415-425 nm. The SHG images, with a size of 200 x 200 µm, were acquired with a resolution of 12 bit, 1024 x 1024 pixel by using a 20X N.A. 1.25 objective. Collagen production in wound area was evaluated at 1, 2 and 3 weeks after damage.

3.2.5 Scanning electron microscopy (SEM) analysis

To quantitatively assess the collagen-related changes from 1 to 3 weeks of healing, we characterized the morphologies of the collagen fibers by a scanning electron microscopy (SEM, FEG_Ultrapluss by ZEISS). Previously, to preserve sample morphology, a critical point drying (CPD-300 Leica) was used for drying samples slices 7 µm thick. Samples were then mounted on aluminum stubs and coated with 100 A ultrathin platinum layer (thickness 7 nm) in a glow-discharge coater to minimize charging and increase the conductivity of the biological material (sputter coater Cressington_HR 208). All data shown were taken on an environmental SEM with a field-emission electron gun at electron energy of 4.00 keV by using Inlens detector for high magnification and ESB detector for low magnification. The microscopy studies and fiber tracking were then performed on combining image acquisition by SEM and the ImageJ: we evaluated bundles diameter of each fiber extracted by ImageJ analysis software Image J®. Twenty images were evaluated for each time and related control, all images were acquired with same parameters and same magnification.

Furthermore, the microscopy studies and fiber tracking were then performed on combining image acquisition by SEM and the CT-FIRE algorithm. Fibers are then extracted using an

automated tracking algorithm called fiber extraction (FIRE). We evaluated diameter, length, angle and position of the automatically extracted fibers with those of manually extracted fibers in twenty-five SEM images of control and damaged matrix. We found that the curvelet-denoising filter followed by FIRE, a process we call CT-FIRE, was successfully applied to track collagen fiber shape changes over time. CT-FIRE is an automated tracking method that can extract the geometric structure of 3-D collagen images and is capable of generating information about the number, length, and curvature of the collagen fibers in an image. The first step of this method is to apply a threshold to form a binary image such that foreground pixels represent potential fibers and background pixels represent pixels where no fiber is present. Next, the distance transform on the binary image is performed to yield the distance from each fore-ground pixel to the nearest background pixel. Then, the maximal ridges of the smoothed image formed by the distance transform are searched to create a list of nucleation points. Branches are formed by extending the fiber from each nucleation point based on fiber trajectory. Short fiber branches are then pruned and closely associated fibers are finally linked based on the fiber length, fiber direction, and the distance between adjacent fibers. In the associated FIRE software [38], there are about 20 adjustable parameters initialized with default values. There are usually only a few parameters that need to be adjusted such as those impacting the binary image generation, the search for nucleation points, and fiber linkage. To our knowledge, the FIRE method has only been tested on confocal reflectance and confocal fluorescence images of in vitro collagen gels, but has not been applied to extract collagen fibers from SHG images of tissue. Each preprocessing technique described in this article was followed by nearly identical implementations of the FIRE algorithm. The only difference is in the threshold used for creating the initial binary image. This threshold was hand optimized to

produce the highest quality fiber extractions across all test cases for each algorithm [39]. To evaluate algorithm accuracy and compare tissues exposed to a physical damage or not, unwounded HDE matrix, at same maturation timing for each wounded HDE matrix, were used as control

3.2.6 Transmission electron microscopy (TEM)

Transmission electron microscopy (TEM - Tecnai $G^2$20_FEI Company) was performed to observe collagen bundles in the HDE three weeks after wounding. Orhanotypic tissue was first fixed with 2.5% glutaraldehyde (SigmaAldrich) in sodium cacodylate buffer 0.1 M (pH 7.2), washed with sodium cacodylate buffer and then fixed with 1% aqueous osmium tetroxide (Electron microscopy sciences, USA). Afterwards, the samples were dehydrated in a graded series of ethanol (SigmaAldrich), block contrasted with 1% uranyl acetate (Merck, Germany) and embedded in EMbed 812 (Electron microscopy sciences, USA). The prepared ultrathin sections (80 nm) were contrasted with 0.3% lead citrate (Merck, Germany) and imaged with a 2HS_EAGLE transmission electron microscope camera at an accelerating voltage of 120 kV and a time $_{exp}$ of 1 sec_ 2048 x 2048.

3.2.7 Stat Image analysis and statistics.

Images were analyzed with the in-house CT-FIRE software and ImageJ. Data analysis, statistics, graph plotting and fitting were performed using the MS Excel (Microsoft) and Kaleidagraph (GraphPad) software. Statistical analysis was performed by an ANOVA-Tukey HSD test. The significance threshold was set for the Tukey HSD test as $p_{valeau} < 0.001$. For all data sets, experiments were repeated in independent.

3.3 Results

3.3.1 Macroscopic view

In this study, a bottom-up approach was exploited to build up 3D tissue constructs *in vitro:* microtissues precursor were growth for 7 days and assembling and maturation process was carried out for four weeks. It was obtained a scaffold-free dermis equivalents perfectly modeling (Fig. 1a). As show in figure 1a human dermis equivalent appears ductile, flexible, strong and resistant to torsion stress and at the pull.

Once realized 3D-HDE constructs, wound healing studies are performed on dermis's endogenous matrix. Understanding how dermis and extra-cellular matrix are orchestrated in our full-thickness wound healing models requires the development of injury assays. In this purpose, a cut-induced directional wound healing assay systematically and quantitatively reproducible was used. Linear full thickness cuts have been made through each sample, simulating surgical wounds and separating HDE in two parts (Fig. 1b). Each parts of tissue were transferred into the empty spaces of the silicon mould of the assembling chamber (Fig. 1c), flaps are overlapped (Fig. 1d, 1e).

Tissues results repaired after 1 week (Fig. 2a). Macroscopic analysis confirmed this result at 2 and 3 weeks too (fig 2b, 2c). Indeed figure 2 reported the multichannel macroscopic images of 1 week after injury (Fig. 2a), 2 weeks after injury (Fig. 2b) and 3 weeks after injury (Fig. 2c). Still at 1 week tissue appeared repaired but edges aren't completely overlapped and tissue is not tight (look at the edge of tissue in Fig. 2a). Samples at 2 and 3 weeks results completely repaired and edge of tissues fused each other.

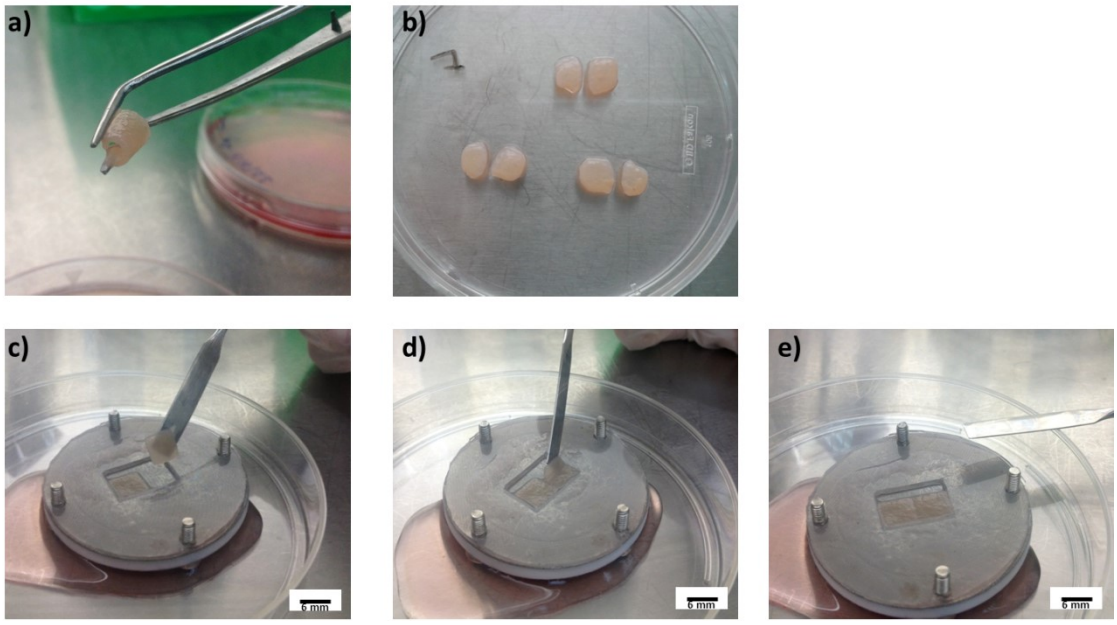

Fig. 1: Dermis equivalent fabrication and wounding and closure of 3D macrotissues. (a) 4% biohybrid at 4 weeks of culture. (b) Macrographs of macrotissues after damage. (c) Temporal sequence of wound maturation chamber. (d) Flaps approximation to mimic suture closure. (e) Final wound arrangement. Scale bar, 6mm

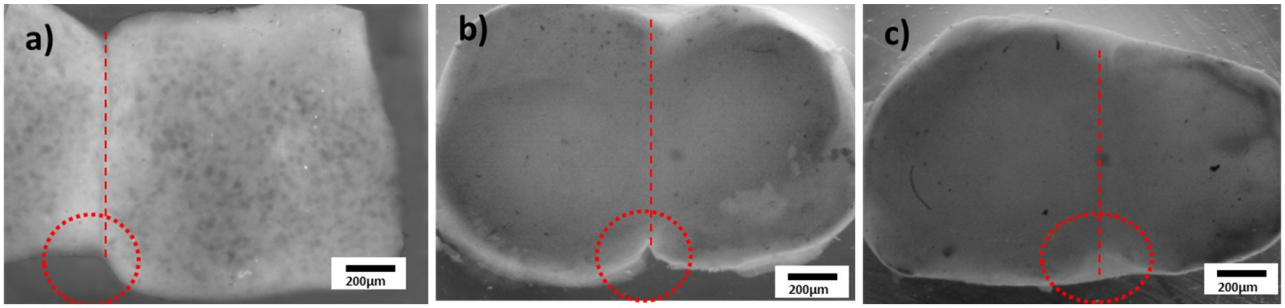

Fig. 2: Macrographs of macrotissues after 1 week of wounding (a); after 2 weeks of wounding (b); after 3 weeks of wounding (c). Original magnification 10X and scale bar, 200µm).

3.3.2 Morphological evaluation of wound closure

To detect possible differences between samples at different healing times, tissues were analyzed by histological staining and the complete repair verified. We chose the 3-week time

point, after the initial wound. In the panel reported in figure 3, histological images of Hematoxylin-Eosin (Fig. 3a, c, e) and Masson's Trichrome (Fig.b, d, f) concerning human dermis equivalent at three times of healing have been shown. At 1 week of healing, Hematoxylin-Eosin and Masson's Trichrome stain revealed a partial closure of tissue in different sections. Fibroblasts had covered wound area partially (Fig.3a, 3b), there wasn't staining in the core tissue (Fig. 3a arrow), suggesting that only external flaps repaired and cells were not infiltrated in the tissue. At 2 weeks of healing stains revealed a complete closure of tissue in different sections: fibroblasts had completely covered wound area (Fig. 3c, 3d). It is possible to note that the fibroblasts are completely immersed in collagen matrix and the elongated nuclear morphology underlines the physiological condition of the cells in their own extracellular matrix [40]. There was an intense Hematoxylin-Eosin staining (Fig. 3c) and a weak Masson's Trichrome stain (Fig. 3d) along new tissue suggesting a poor synthesis of new ECM compared to cellular number and accordingly, a poor omogeneity of extra-cellular matrix to the pre-existing matrix. It is interesting to highlight that after 3 weeks of healing the tissue is completely made-up of endogenous ECM. Stains revealed a total repair of tissue in different sections and along tissue edge (Fig. 3e, 3f). There was a uniform staining in all tissue suggesting that extra-cellular matrix completely re-established.

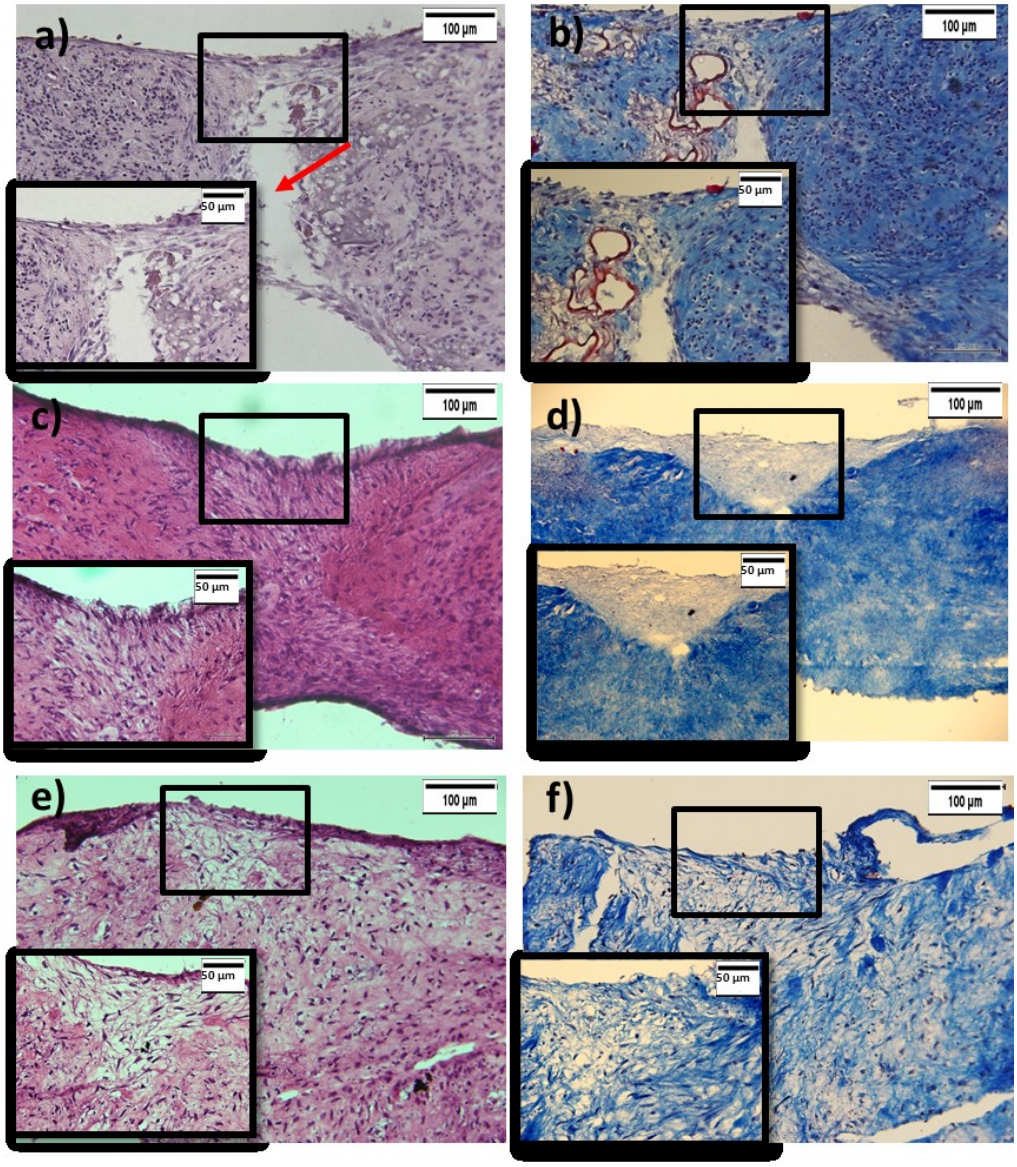

Fig .3: Hematoxylin and eosin staining and temporal sequence of micrographs showing closure progressive of wounded dermis: (a) showing alignment of cells at the wound edge and partial wound closure after 1 week of healing; (b) revealing total wound closure after 2 weeks of healing; (c) revealing the presence of a neo-ECM in neo-formed tissue after 3 weeks of healing. Original magnification-20X and 40X and scale bar, 100 and 50 µm.

3.3.3 The 3D wound model recapitulates cellular and extra-cellular matrix pathophysiological process occurring during wound healing *in vivo*

After injury, *in-vivo* wound healing follows a series of tightly regulated, sequential events, one of these is granulation tissue formation. Granulation tissue matrix is rich in fibronectin and hyaluronic acid and fibroblasts differentiated [14]. To demonstrate granulation tissue synthesis

in our 3D-HDE wound model, we evaluated Hyaluronic acid and fibronectin up-regulation and fibroblasts differentiation. In particular in images 4 and images 6 is shown HA (red) and fibronectin (red) signals respectively. Moreover presence of myofibroblasts were confirmed by staining for α-SMA in fig. 2 (blue), network of neo-collagen were exploiting by multiphoton microscopy with Second Harmonic Generation (SHG) analysis.

- *HA expression*.

After injury, *in-vivo* wound healing follows a series of tightly regulated, sequential events, one of these is granulation tissue formation. Granulation tissue matrix is rich in fibronectin and hyaluronic acid. HA is a glycosaminoglycan usually content in skin at basal levels but it is further elevated transiently in granulation tissue during the wound healing process [17]. To demonstrate typical presence of proteoglycans in our platform and its capability to generate granulation tissue during a repair process, we evaluated hyaluronic acid production in the neo-forming and undamaged matrix 1, 2, and 3 weeks after wounding. Levels of HA are detectable both in wound area than in area away from physical damage (Fig.4). At beginning of process, levels of HA increase in the wound area (stain in red) (Fig. 4a, 4b) and quantitative analysis – by using ImageJ - demonstrate high statistically significant between cut and control ($p_{value} < 0.001$ by performing an ANOVA-Tukey HSD test.) (Fig. 5, box). With the culture time, this difference was even more pronounced and quantitative analysis demonstrated a low and continuous production of HA in undamaged matrix (Fig. 4d) and a peak in wound area (Fig. 5, box). The level of proteoglycan was significantly increased at 2 weeks after injury compared to levels at 1 week. This difference was detected again compared at 2 and 3 weeks after wounding: the two values are statistically highly different with a $p<0.001$ by performing an ANOVA-Tukey HSD test (Fig. 5, box). At the end of process,

HA levels were present (Fig. 4d, e) but decreased significantly and there aren't statistically different between cut and control (Fig. 5, box).

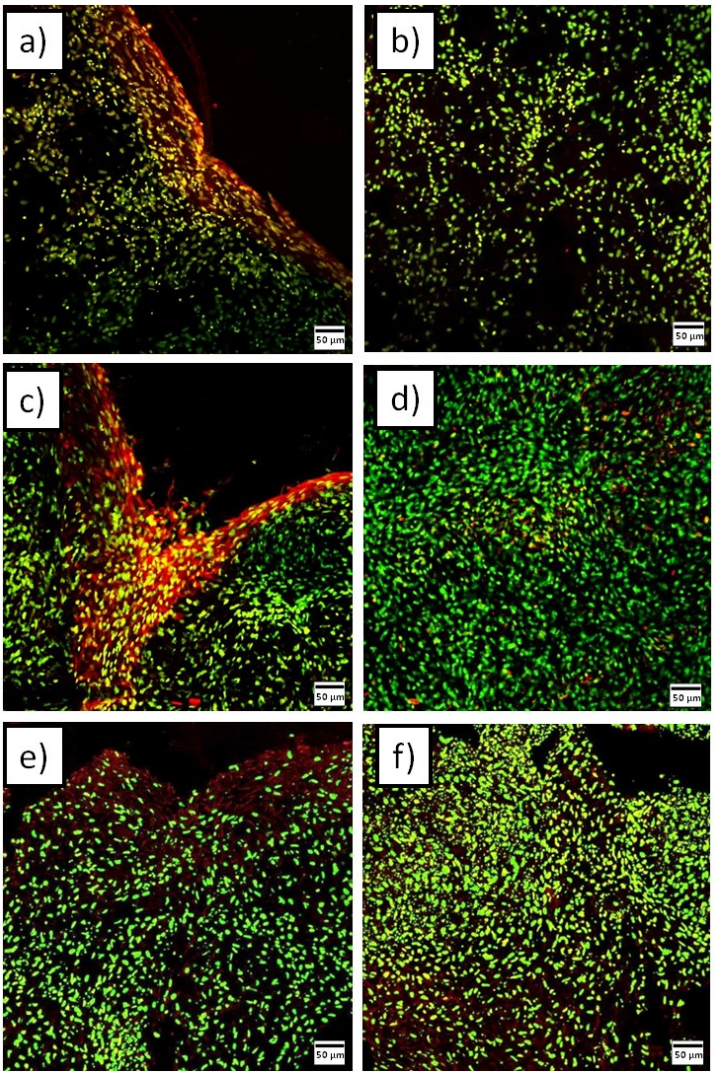

Fig.4: immunofluorescence analysis of: (a) wounded area of dermis equivalent 1 week after wounding; (b) unwounded area of dermis model (CTRL) 1 week after wounding; (c) wounded area of dermis equivalent 2 weeks after wounding; (d) unwounded area of dermis model (CTRL) 2 weeks after wounding; (e) wounded area of dermis equivalent 3 weeks after wounding; (f) unwounded area of dermis model (CTRL) 3 weeks after wounding. Frozen sections were immunostained for Hyaluronic acid and Sytox Green as nuclear stain. Scale bar, 50µm.

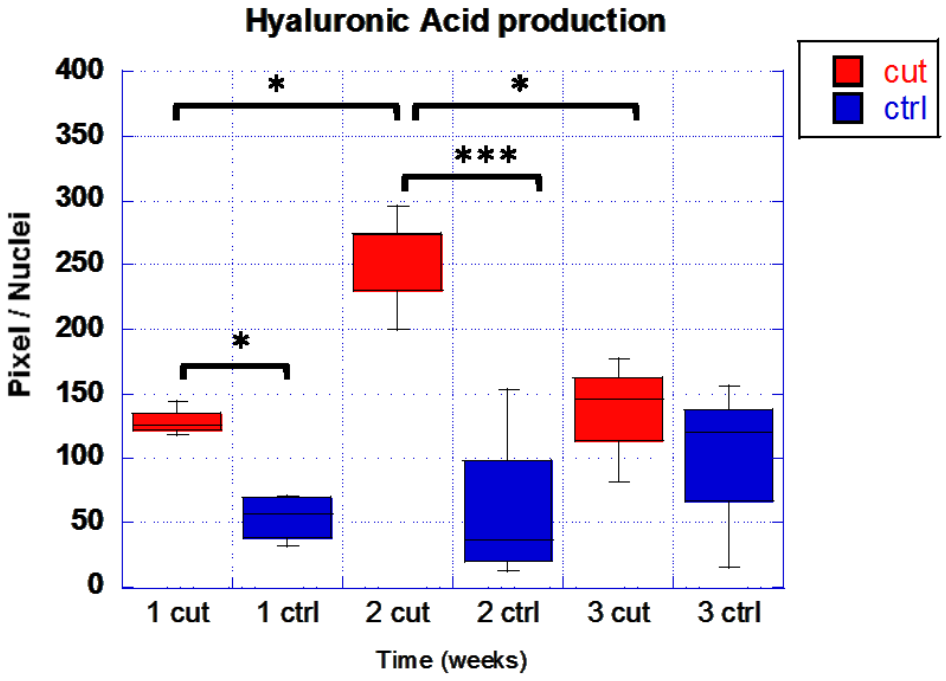

Fig.5: Hyaluronic acid production expressed in pixel/nuclei in neo-formed tissues and undamaged tissues at 1, 2 and 3 weeks of healing. Control represents the corresponding undamaged tissue of dermis equivalent. $p < 0,05$. All bars are 50 µm.

- *Fibronectin expression*.

To better define nature of granulation tissue in our organotypic model, we evaluated fibronectin (FN) production in the neo-forming matrix and in area away from physical damage 1, 2, and 3 weeks after wounding too (Fig.6). Fibronectin, a predominant type of provisional matrix protein, directs wound fibroblast migration into the fibrin clot [14]. Levels of FN are detectable both in wound area than in area away from physical damage. Low levels of FN are detectable in all time in undamaged matrix (Fig.6b, d, f). In the center of control the intensity of fibronectin signal is almost absent, but it is easily detected on the edge, this suggests that where the dermis is anchored on the grid the cells are able to produce more fibronectin and also the network of these proteins is more similar to native dermis. At beginning of process,

levels of FN increase in the wound area (stain in red) (Fig. 6a, 6b) and quantitative analysis – by using ImageJ - demonstrate high statistically significant between cut and control ($p_{value} <$ 0.001 by performing an ANOVA-Tukey HSD test.)(Fig. 7, box). With progressing time, this difference was even more pronounced and quantitative analysis demonstrated a high and continuous production of FN in undamaged matrix (Fig. 6d) (Fig. 7, box). The level of fibronectin was increased at 2 weeks after injury compared to levels at 1 week. This difference was even more pronounced at 3 weeks after wounding. In the end of process, FN levels were detected (Fig. 4d, e) and increased significantly (Fig. 7, box).

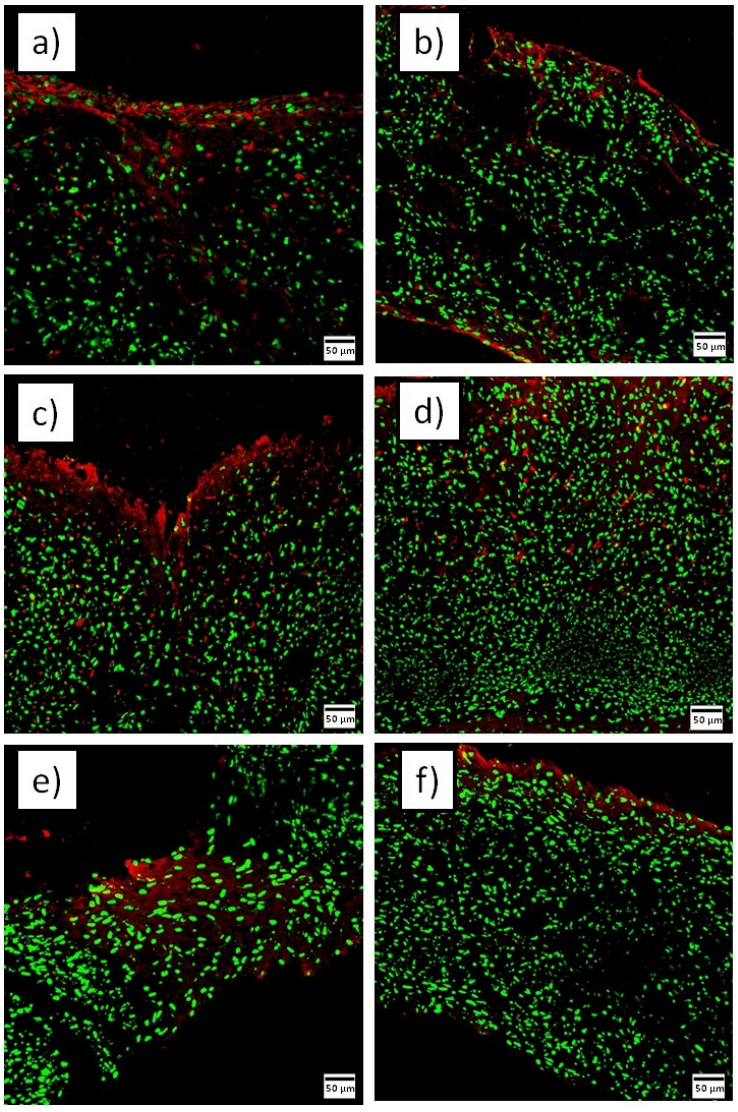

Fig.6: immunofluorescence analysis of: (a) wounded area of dermis equivalent 1 week after wounding; (b) unwounded area of dermis model (CTRL) 1 week after wounding; (c) wounded area of dermis equivalent 2 weeks after wounding; (d) unwounded area of dermis model (CTRL) 2 weeks after wounding; (e) wounded area of dermis equivalent 3 weeks after wounding; (f) unwounded area of dermis model (CTRL) 3 weeks after wounding. Frozen sections were immunostained for Fibronectin and Sytox Green as nuclear stain. Scale bar, 50µm.

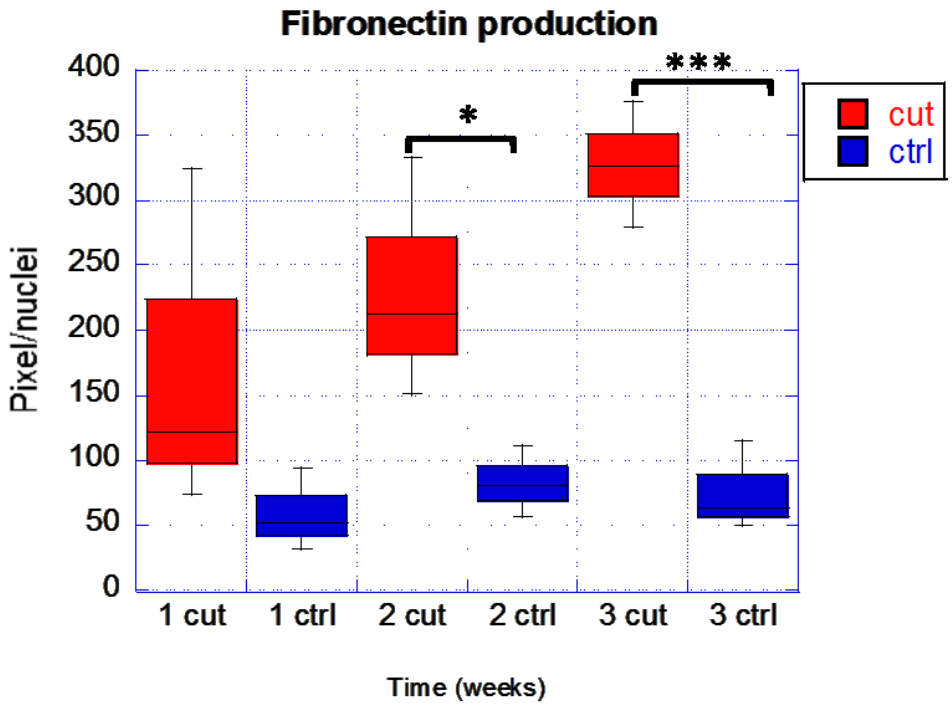

Fig.7: Fibronectin production expressed in pixel/nuclei in neo-formed tissues and undamaged tissues at 1, 2 and 3 weeks of healing. Control represents the corresponding undamaged tissue of dermis equivalent. $p < 0,05$. All bars are 50 µm.

- *α-SMA expression*.

In a tissue damaged, fibroblasts are activated and migrate in the wound area where they differentiate into α-smooth muscle actin (α-SMA)-expressing myofibroblasts. Fibroblasts undergo a series of phenotypic changes during granulation tissue formation and assume some characteristics of smooth muscle cells to become actin- rich myofibroblasts. The

appearance of myofibroblasts corresponds to the start of collagen-rich granulation tissue contraction [14]. In this purpose, to understand cellular reply to a physical damage in organotypic dermis construct and better demonstrate granulation tissue formation, we also analyzed fibroblasts answer (alpha-Smooth muscle actin expression) in the neo-forming and undamaged matrix 1, 2, and 3 weeks after wounding (Fig.8). 1 week after wounding, cells in the wound area showed an initial production of α-SMA (stain in blue) (Fig.8a). In figure is reported marker expression both in wound area than in area away from physical damage (Fig. 8a, b). α-SMA expressed only in wound area, values are next to zero in undamaged matrix (Fig.8b, d, f). There is high statistical significance between cut and control with a $p_{value} < 0.001$ by performing an ANOVA-Tukey HSD test (Fig. 9, box). With progressing time (2 weeks after cut), this difference was even more pronounced compared at 2 weeks after injury: the expression of differentiation marker advanced always only in wound area. Figures 8 relieve the strongest signal at this time. αSMA expression was transient and it was almost no detectable when healing process is exhausted(Fig. 9, box). Figures relieve a transient expression of signal.

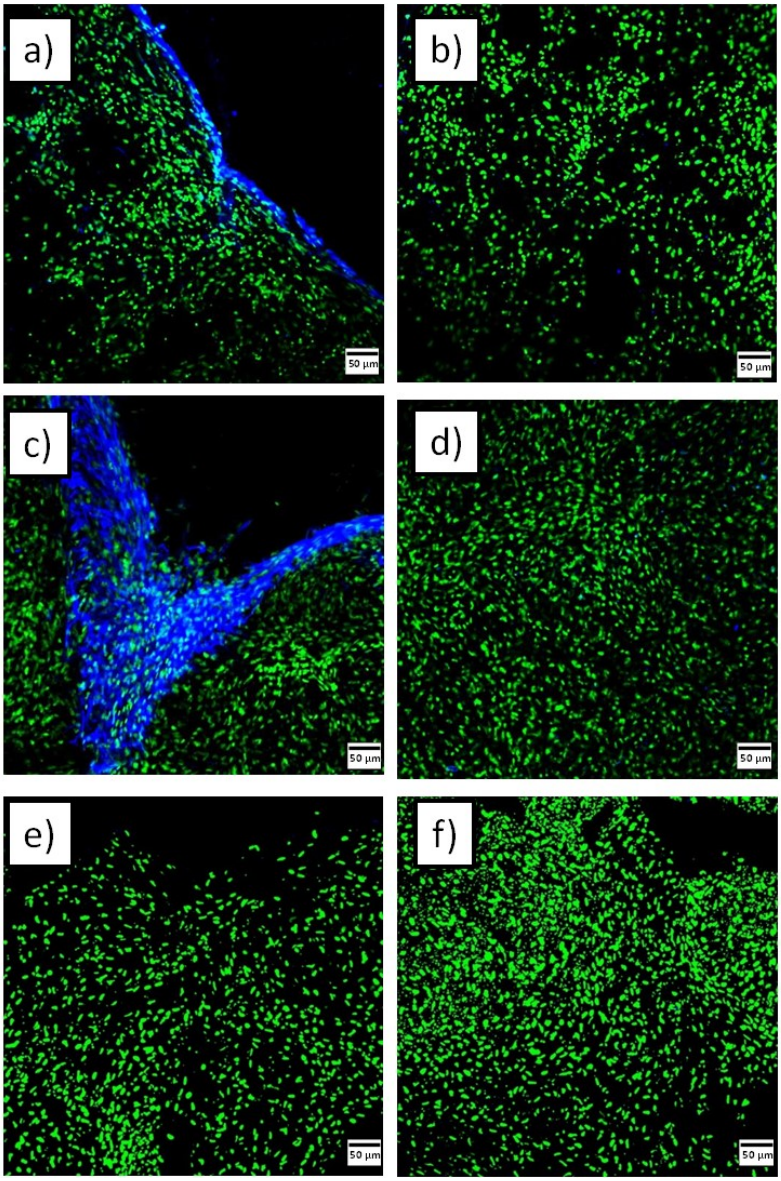

Fig.8: immunofluorescence analysis of: (a) wounded area of dermis equivalent 1 week after wounding; (b) unwounded area of dermis model (CTRL) 1 week after wounding; (c) wounded area of dermis equivalent 2 weeks after wounding; (d) unwounded area of dermis model (CTRL) 2 weeks after wounding; (e) wounded area of dermis equivalent 3 weeks after wounding; (f) unwounded area of dermis model (CTRL) 3 weeks after wounding. Frozen sections were immunostained for α-SMA and Sytox Green as nuclear stain. Scale bar, 50µm.

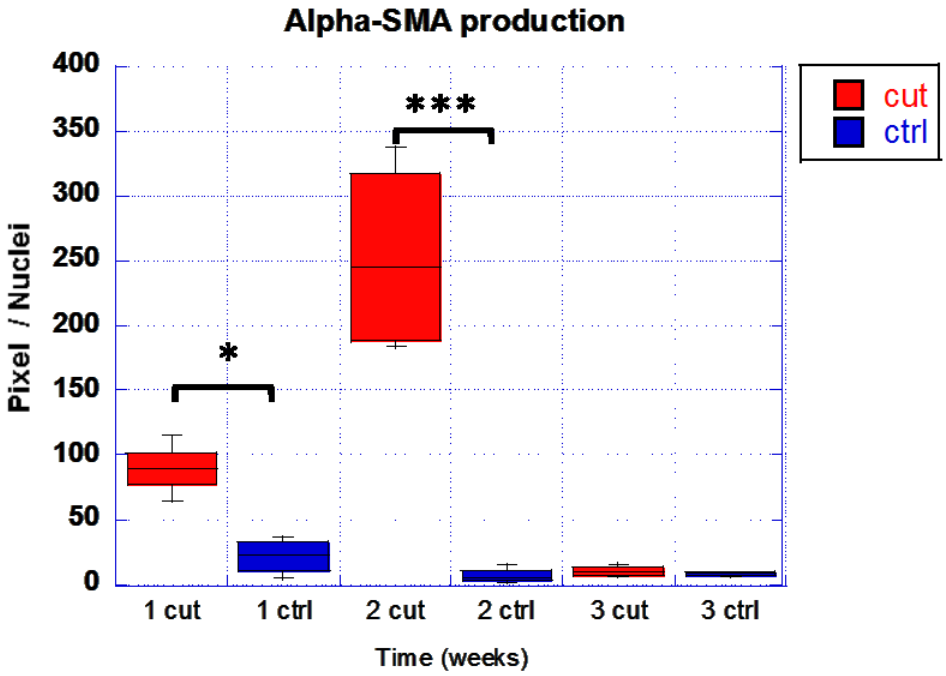

Fig.9: α-SMA production expressed in pixel/nuclei in neo-formed tissues and undamaged tissues at 1, 2 and 3 weeks of healing. Control represents the corresponding undamaged tissue of dermis equivalent. $p < 0,05$. All bars are 50 µm.

- *SHG analysis.*

The structure of collagen fibrils was observed by MPM that allowed visualize unstained collagen structure by exploiting SHG. SHG analysis was exploited to investigate the tissue capability to secrete new collagen, in this perspective SHG analysis and α-SMA (Fig. 10 d, e, f) signals were combined. In this purpose SHG imaging was performed on neo-forming ECM in order to highlight collagen timing production in wound edge. At the beginning of the process fibroblasts differentiate into myofibroblasts and migrate into the empty space between the two edges of primary stroma using the primary stroma as a scaffold for their migration (Fig. 10a, 10d). By the 14th day myofibroblasts stopped to migrate, reaching the final number (Fig. 10b) and in the wound edge it is possible to observe an initial SHG signal that

displays a less dense and organized matrix compared to mature stroma of undamaged control (control is part of the 3D-HDE, far from the wound). In details, at time 1 week, collagen in wound area wasn't detected (Fig.10d). The signal of collagen is detected only at 2 weeks after wounding in wound area, by using SHG analysis (Fig. 10e). At this time, wound area is fully of differentiated cells (Fig.10b) and low immature collagen (Fig.10e). Indeed intensity of signal is different between neo-forming ECM and mature stroma of undamaged control at this time: in pre-formed ECM it is possible to distinguish presence of mature collagen while in neo-forming ECM it is possible to distinguish fibrils of the collagen but they are not still completely organized. At 3 weeks after wounding, once contribute to connective tissue remodeling by exerting traction forces, myofibroblasts regressed and disappeared by apoptosis (Fig. 10c) on wound [41]; the two matrices are comparable and there are not differences between the wound-area matrix and the pre-formed matrix of tissue (Fig. 10e).

At least, number cells *per* Area in neo-formed tissue and in pre-existing tissue at two and three weeks after wounding were estimated (Fig. 10 h, 10i) by using ImageJ software. Results obtained at two weeks are statistically no different (Fig. 11). Unsurprisingly, statistical analysis showed a significant difference between results obtained in cut and control at three weeks after wounding. Numbers cells per Area weren't estimated at 1 week: tissue is not fully repaired.

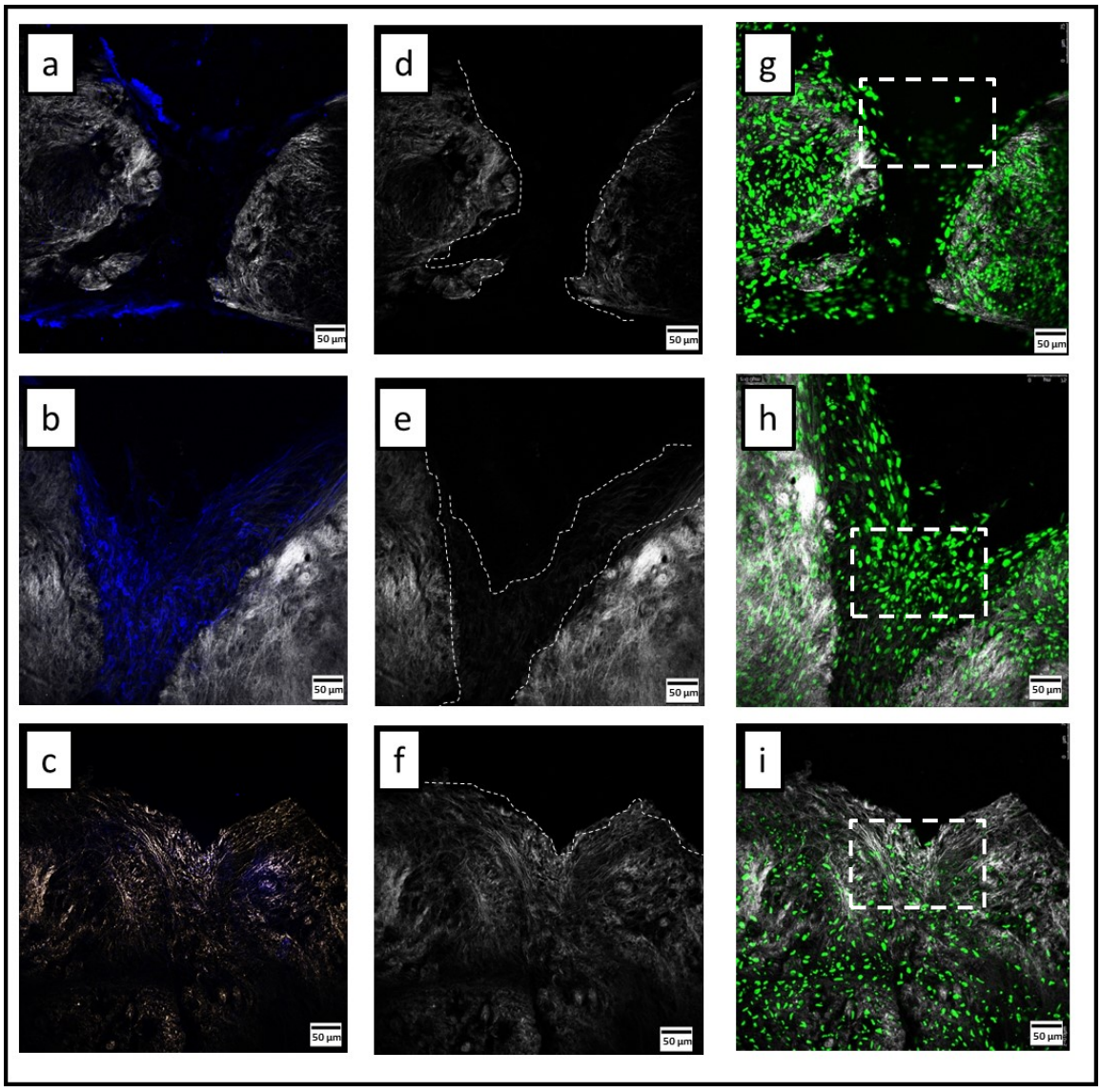

Fig.10: immunofluorescence of α-SMA analysis and second harmonic generation (SHG) of: (a) wounded area of dermis equivalent 1 week after wounding; (b) wounded area of dermis model 2 weeks after wounding; (c) wounded area of dermis equivalent 3 weeks after wounding. Second harmonic generation (SHG) of: (d) wounded area of dermis equivalent 1 week after wounding; (e) wounded area of dermis model 2 weeks after wounding; (f) wounded area of dermis equivalent 3 weeks after wounding. Second harmonic generation (SHG) and Sytox Green of: (g) wounded area of dermis equivalent 1 week after wounding; (h) wounded area of dermis model 2 weeks after wounding; (i) wounded area of dermis equivalent 3 weeks after wounding. Frozen sections were immunostained for collagen detection. Scale bar, 50µm.

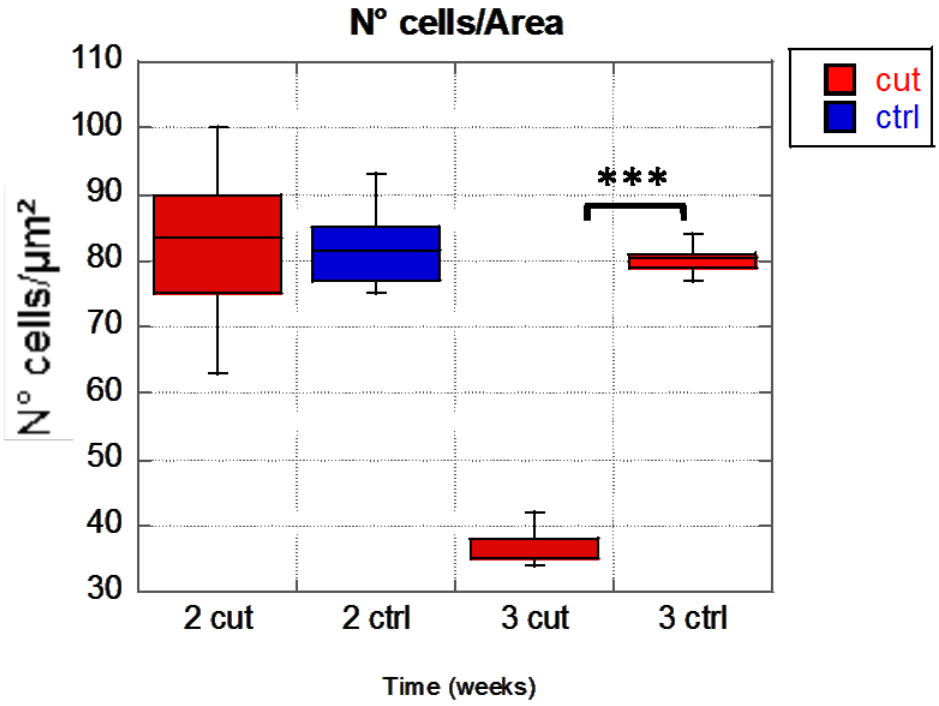

Fig.11: Number of cells per Area expressed in N° nuclei/µm² in neo-formed tissues and undamaged tissues at 2 and 3 weeks of healing. Control represents the corresponding undamaged tissue of dermis equivalent. $p < 0,05$. All bars are 50 µm.

3.3.4 ECM composition and remodelling

We investigated the 3D architecture of neo-formed matrix to assess the self-repair capability of tissue and the remodeling matrix after wounding in our model. We obtained such information mainly from scanning electron microscopy (SEM) of the samples ECM close to the wound and ECM far from the wound. By means of SEM is possible to obtain important morphological information into the three-dimensional (3D) arrangement of stroma structures. The morphology, remodeling and distribution of collagen were examined and compared to the control at 1, 2 and 3 weeks after wounding. Matrix 0-50 µm away from cut (Fig. 12, red arrow and box) were considered as neo-formed matrix and were used for these studies to demonstrate stroma answering capability –of our dermal platform – to a physical damage;

core organotypic model, ECM more than 500 µm away from cut (Fig. 12, blue arrow and box), were considered as pre-formed/undamaged matrix (control).

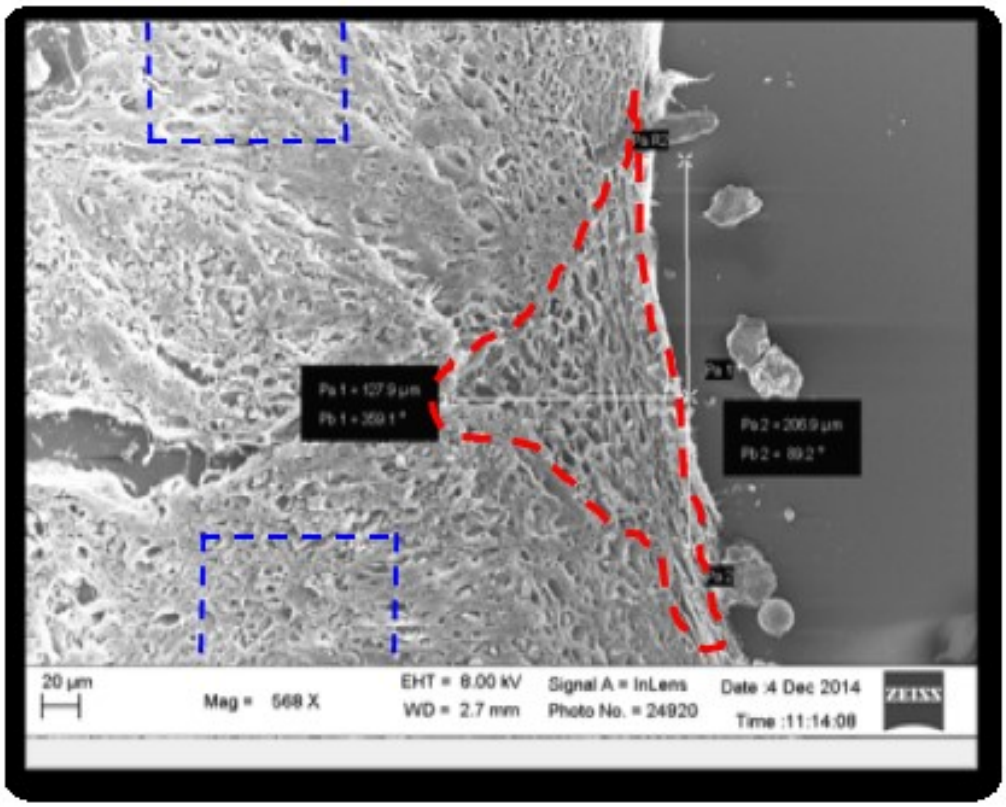

Fig. 12: Scanning electron images at 568 magnification illustrate 3D dermis equivalent and its subdivisions to detect and analyze neo-formed matrix (red box) and pre-formed matrix (blue box) for quantitative analyses. Scale bars, 20 µm.

Parameters were defined in which the x directions were parallel to cut imaging into tissue slices, y directions were perpendicular to cut imaging into tissue slices aligned and the z direction was vertical (perpendicular to the imaging plane in the circumferential direction) and corresponding to thickness of 3D model (Fig. 13).

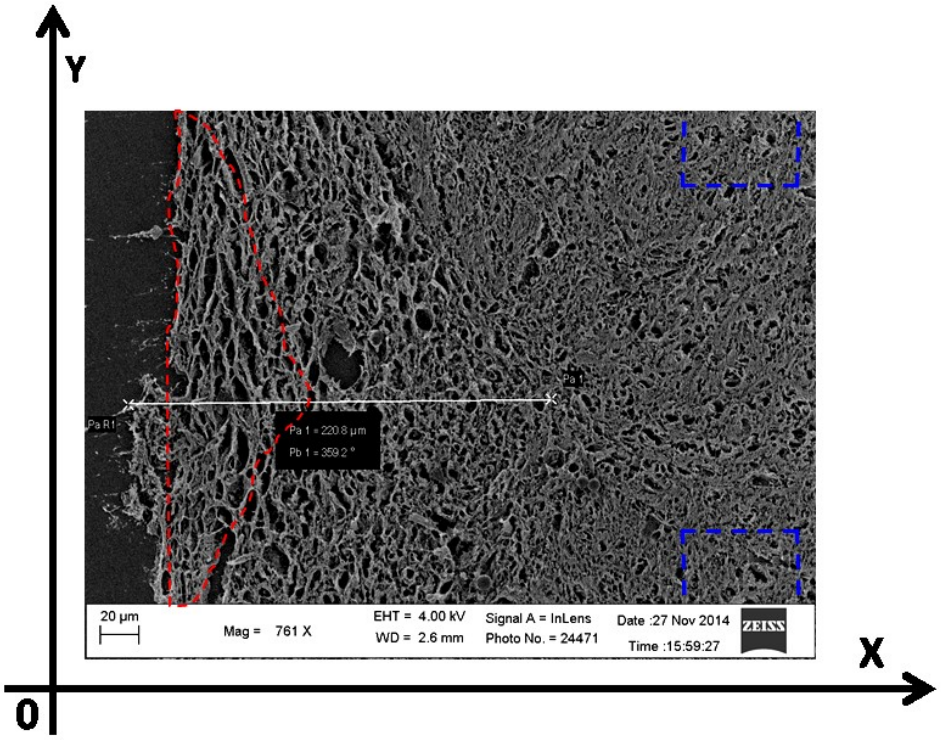

Fig. 13: Scanning electron images at 761 magnification illustrate division wounded dermis equivalent added in a Cartesian system. X-axis is the cut direction. All images for CT-Fire and ImageJ elaboration were taken with this cut direction and considering this as x-axis. Scale bars, 20 µm.

SEM data revealed two different levels of stromal organization: collagen fibrils and fibril bundles (Fig. 13). Indeed, at contrary of SHG analysis, collagen in wound area was already detected at time 1 week after wounding by SEM analysis (Fig. 14a, arrow): images detected a fully cellularised neo-matrix with a really low amount of collagen fibrils (first level of stromal organization). The collagen fibrils constitute the smallest structure of the collagen organization which could be observed by electron microscopy. The transverse and longitudinal sections of the damaged tissue show a considerable variation in collagen organization but not in diameter of the fibrils during healing time into a neo-formed matrix (Fig. 14a, 14c, 14e) and into an increasingly mature matrix (Fig. 14b, 14d, 14f). The diameter of the fibrils of dermal equivalent

in neo-formed matrix and pre-formed matrix is found to vary respectively from 15 to 70 nm and from 20 to 120 nm. Thus, the most relevant data are not then evolution of single fibrils diameter but the matrix reorganization with consequent coalescence of the fibrils into small collagen bundles.

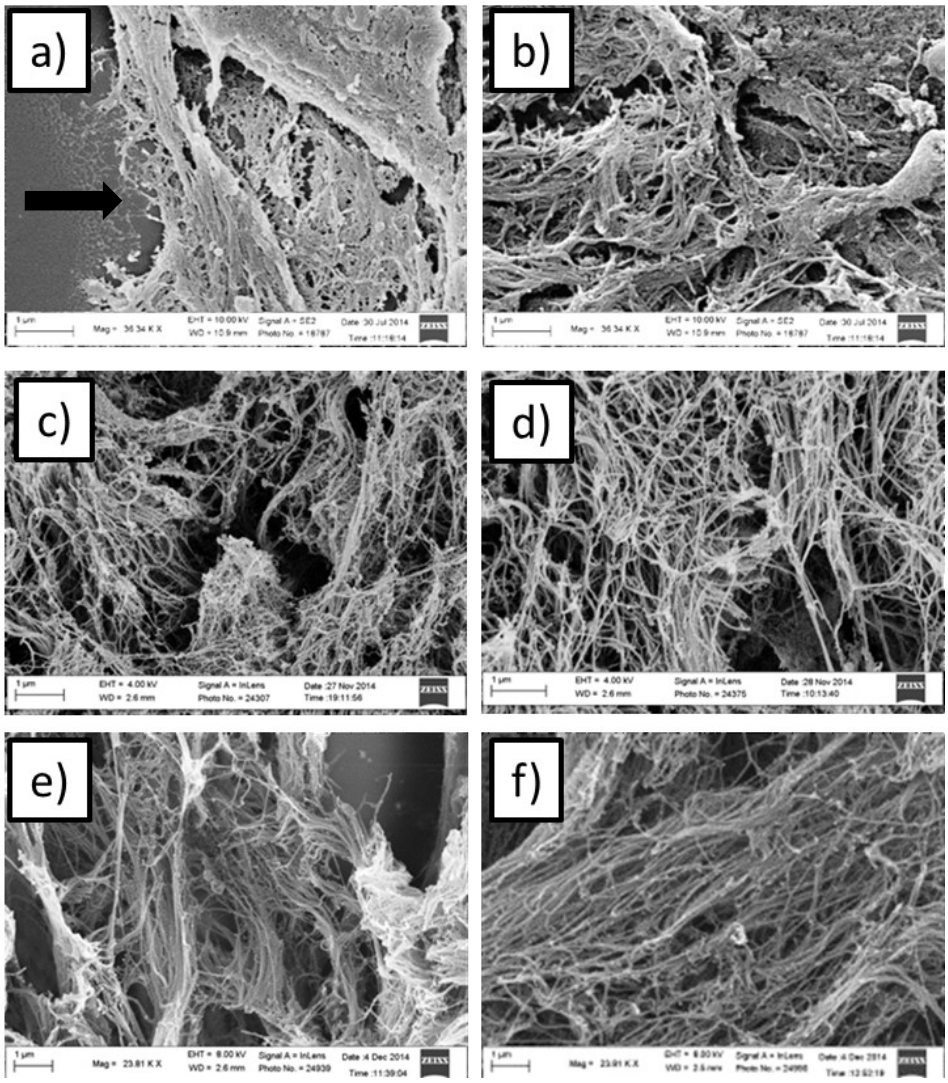

Fig. 14: Scanning electron images illustrate: (a) wounded area of dermis equivalent 1 week after wounding; (b) unwounded area of dermis model (CTRL) 1 week after wounding; (c) wounded area of dermis equivalent 2 weeks after wounding; (d) unwounded area of dermis model (CTRL) 2 weeks after wounding; (e) wounded area of dermis equivalent 3 weeks after Scale bars, 1 µm.

To learn more about matrix remodeling we evaluated collagen assembly. We investigated the bundles formation in the ECM, using SEM and ImageJ analysis. The results showed that the fibrils were organized in big groups, which occurred in extended channels. These groups of fibrils are termed 'collagen bundles' (Fig. 15). At the beginning the number of bundles is really low, within the new stroma at 1 week after wounding, there were very few single collagen fibrils in the extracellular space. At two weeks after wounding, matrix assembled and the bundles are well defined in wound area (Fig. 15). It is important to note that ECM profiles are fibrils in transverse section. It was not possible to count entire fibrils or bundles because some are too long to be contained within the SEM volumes we studied. In 3 weeks after wounding, collagen bundles are even bigger and even more assembled (Fig. 15). Analysis of SEM images demonstrated that diameter collagen bundles increased during development, with mean bundles diameter increasing from 141.28 nm ± 22.5 nm at 2 weeks of maturation (2 weeks after wounding), to 365.81 ± 94.8 nm at 7 weeks of maturation (undamaged matrix 3 weeks after wounding) (Fig. 15). Notably, the increase in collagen bundles diameter occurred uniformly throughout the ECM and even if was not confined to collagen bundles close to wound edge, it is more and more pronounced in neo-formed matrix. Indeed in such zone there is high statistical significance between neo-formed and mature matrix with a $p_{value} < 0.001$ by performing an ANOVA-Tukey HSD test. With progressing healing-time (3 weeks after cut), this difference with mature matrix was less pronounced compared at 2 weeks after injury but always present. Furthermore there is high statistical significance between neo-formed matrix at 2 and 3 weeks after wounding. This simple, key observation is critical to understanding how collagen bundles growth in diameter depend upon the distance from the

cut. Analysis of the bundles showed a pronounced increase in the bundles formation profiles after 2 weeks of healing. After 6 weeks of maturation (mature matrix in undamaged control at 2 weeks of healing) the ECM assembling reaches a steady-state (Fig. 14, $p_{value} < 0.001$).

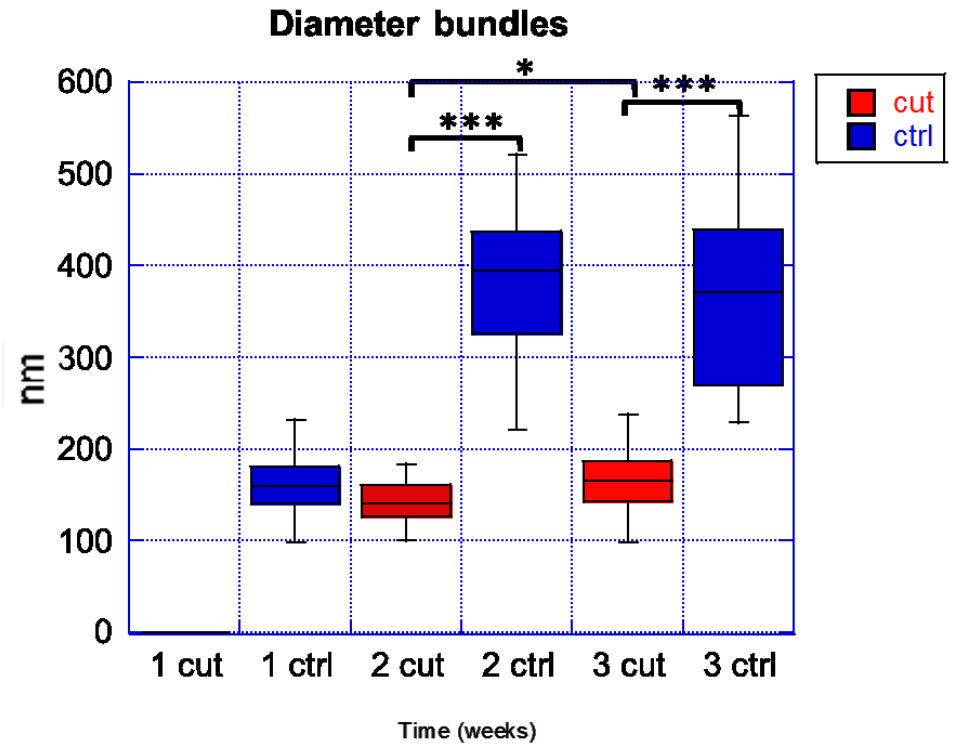

Fig. 15: Box of the diameter of collagen bundles in undamaged tissue at 1 week of healing and in neo-formed tissues and undamaged tissues at 2 and 3 weeks of healing. Control represents the corresponding undamaged tissue of dermis equivalent (box blue). $p < 0,05$. All bars are 1 µm.

At least, fibrils collagen distribution was evaluated. The microscopy studies and fiber tracking were performed on combining image acquisition by SEM and the CT-FIRE algorithm. Fibers are extracted using an automated tracking algorithm called fiber extraction (FIRE) and angle collagen fibers were obtained. Collagen fibers orientation analysis were carried out at 2 and 3

weeks and neo-formed and relate mature matrix were compared at each time as reported in figures 16 and 17. During the process of assembly, changes in collagen orientation are revealed. This analysis compares the empirical fits of four differents matrix – whose values close to 0 and 180 indicate a co-alignment with the cut direction and a parallel direction – and the normal (gaussian) distribution for fibers distribution changes using chi-square goodness-of-fit tests. Interestingly, neo-formed matrix and pre-existing matrix – both at two than three weeks after wounding – exhibited significantly different trends (Fig16a - 17a neo-formed matrix, 16b – 17b pre-existing matrix). The data clearly show that neo-formed matrices are normally distributed. Neo-formed matrix distribution at two weeks has a $\mu = 45°$, $\sigma = 0{,}014$ and a $R^2 = 0.98$ (Fig. 16a), while at three weeks has a $\mu = 95°$, $\sigma = 0{,}04$ and a $R^2 = 0.96$ (Fig. 17a). Conversely, mature matrix at 2 and 3 weeks after wounding, displayed a broader and an indefinite distribution of orientation fibers Consequently, hasn't normally distributed ($p_{value} > 0.05$). Summarizing, high rate of collagen fibrils were oriented at 45° and at 90° respect to the cut axis in neo-formed matrix 2 and 3 weeks after wounding respectively while, undamaged tissue shows more random organization without a preferential orientation and an anisotropic structure.

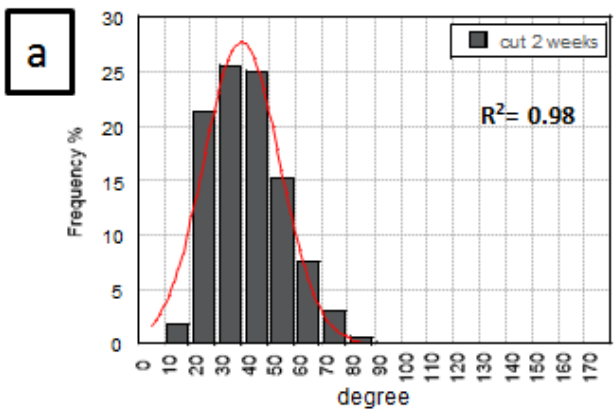

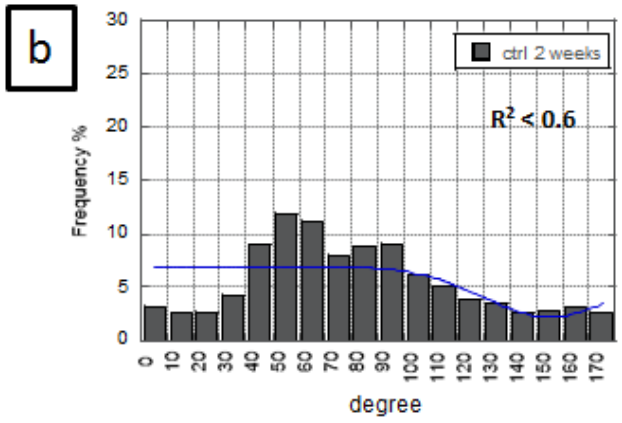

Fig. 16: Histogram of neo-formed fibers orientation along cut direction at 2 weeks of healing in (a) neo-formed tissue, (b) in pre-existing tissue. Fit with normal distribution. Range orientation angles: 0-180 degree.

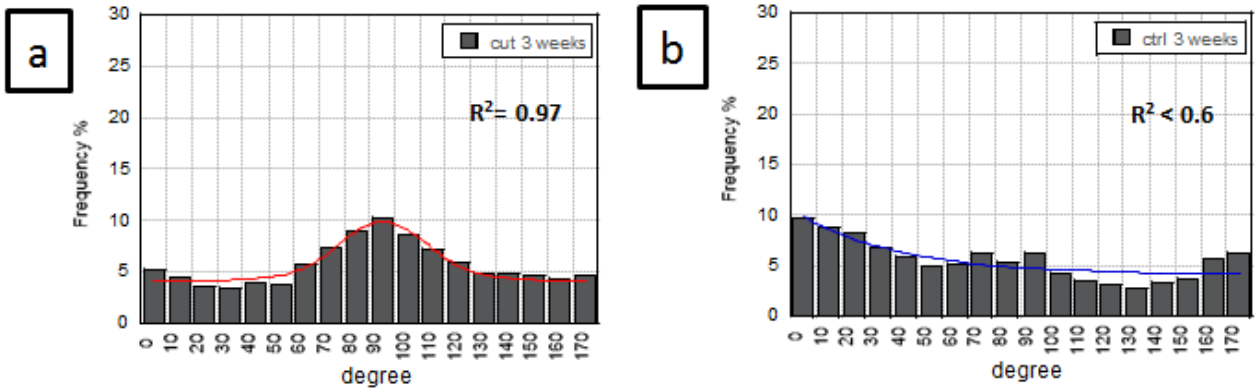

Fig. 17: Histogram of neo-formed fibers orientation along cut direction at 3 weeks of healing in (a) neo-formed tissue, (b) in pre-existing tissue. Fit with normal distribution. Range orientation angles: 0-180 degree

3.3.5 Transmission electron microscopy (TEM) investigations

TEM investigations were carried-out at three weeks after wounding to confirm collagen bundles formation, as well as the organization of these elements into an endogenous stroma when healing process is exhausted. TEM investigations confirmed the large amount of big collagen bundles in ECM with a maximum of 500 nm in diameter (Fig. 18e) and that the collagen bundle, not the collagen fibril, was the principal structure produced by the fibroblast and used in the construction of the damaged stroma after three weeks of wounding. Moreover a different tissue cellularization is verified when healing process is exhausted (look paragraph 4.3.3). As presented in figure a significant difference in cellular number, between pre-existing (Fig. 18a, 18b) and neo-formed matrix (Fig. 18c, 18d), was observed. Mature matrix consists of a surface full both of cells than ECM where fibril bundles are intimately associated and surrounded by fibroblasts (Fig. 18a, 18b). Conversely, neo-formed matrix is almost entirely rich of ECM (Fig. 18c, 18d) and poorly of cells.

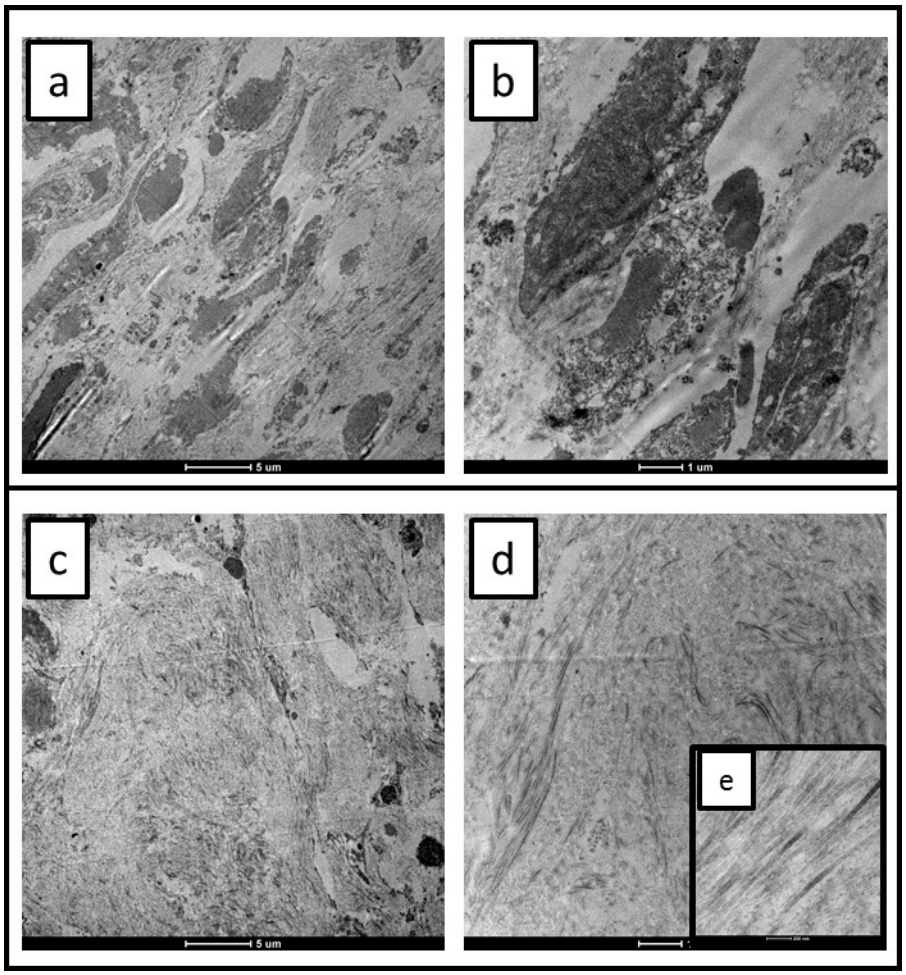

Fig. 18: Transmission electron images illustrate: (a) unwounded area of dermis equivalent 3 weeks after wounding; (b) unwounded area of dermis equivalent 3 weeks after wounding with higher magnification; (c) wounded area of dermis model 3 weeks after wounding; (d) wounded area of dermis equivalent 3 weeks after wounding with higher magnification; (e) collagen bundle formation in wounded area of dermis equivalent 3 weeks after. Scale bars, 5 µm for lowest magnification, 1 µm for higher magnification, 200 nm for collagen bundle image.

3.4 Discussions

The central question debated in the literature in skin wound healing are often reepithelialization process and mechanism of the creation and extension of the epidermal tongue [6]. But cutaneous wound healing also involves processes about dermal matrix as: provisional matrix (or granulation tissue) formation, fibroblasts infiltration and differentiation,

extracellular matrix (ECM) remodeling and scar formation [4042]. Fibroblasts represent the first population of mesenchymal stromal cells and play an essential role in regulating normal tissue homeostasis and wound repair through their synthesis of extracellular matrix (ECM) and their mechanical interactions [43]. However, the utility of these cells for wound repair therapy and *in vitro* studies of dermal repair has been limited by difficulties to incorporate these cells in a 3D architecture made-up of a responsive stroma, fully composed by endogenous ECM and not exogenous scaffold [42]. For example, Masci et al. (2016) evaluated NIH3T3 fibroblasts migration and proliferation in a type I collagen scaffold extracted by equine tendon [44]; in other works, it was used iPSC-derived fibroblasts for tissue repair and regeneration that exhibited augmented capacity to deposit collagen proteins in 2D monolayer culture [45] or it was used deepidermized dermis (DED), Glyaderm or synthetic polymers as healing model [3] [36] [46]. Also, it has been seen that an *in vitro* model of burn wound healing in human skin did not induce the differentiation of myofibroblasts [36] [10]. But, in vitro studies involving the dermal healing process are prevented by the fact that currently 3D dermal equivalent are based on collagen as exogenous scaffold and by using models that doesn't reproduce in composition and organization the extracellular space. Indeed, one of the first problem associate to use of the current *in vitro* models, is limitation in the progress of scar management consequently to the lack of physiologically relevant human models that gives the opportunity to explore the pathogenesis of scar formation. [26] [10] To derive a consistent theory of how the cellular processes of migration, proliferation, and differentiation are intertwined and how ECM answers in dermal wound healing, we proposed a novel *in vitro* tool to facilitate the study of cells and ECM in a damaged dermis that are inaccessible *in vivo* in humans and that cannot be performed using the existing *in vitro* model. Thus, once realized a 3D-HDE

constructs by a bottom-up approach [9], endogenous matrix was injured, handled gently and tissues accurately approximated in order to mimic a surgical healing [47]. In this way proliferative and remodeling phase, occurring during wound healing are recapitulated [13]. Morphologic analysis of H&E and Masson's Trichrome stained sections (Fig. 3) demonstrates tissue is able to repair itself in a short time. It is interesting to highlight that 3D construct is completely repaired and made-up of endogenous and homogeneous ECM only after 3 weeks of healing, even if wound gap is completely closed after two weeks (Fig. 2 and 3). Thus ECM remodeling begins only a few days after injury and lasts for a long period as well as *in vivo* process such as the last stage of wound repair — remodeling phase — begins 2 weeks after injury [12]. Indeed, at beginning of healing, 3D-construct recapitulate the typical steps of the proliferative phase occurring in an human dermis as the increase of hyaluronic acid (HA) and fibronectin (FN) levels and the fibroblasts differentiation [14]. In this stage, fibroblasts, which are attracted from the edge of the wound, are stimulated and some undergo a series of phenotypic changes to assume characteristics of smooth muscle cells and differentiate into myofibroblasts already from first week, and with a peak of expression at two weeks from injury [48]. Myofibroblasts are contractile cells that, over time, initialize tissue migration and contraction and bring the edges of damaged tissues together. These two cellular population interact and produce extracellular provisional matrix, mainly in the form of HA and FN [12]. Considering that current *in vitro* model doesn't correctly study fibroblasts differentiation phenomenon and considering that myofibroblasts may represent an important element in the pathogenesis of contraction, capability to detect fibroblasts differentiation is an important result in an in vitro study [49]. In this perspective, it's important highlight that repair process involved in our 3D-HDE wound model, follows a series of tightly regulated, sequential events,

as well as *in vivo* [50] [14]. At beginning, we observed granulation tissue formation: higher levels of FN and HA facilitate cell migration for subsequent collagen production and assembling at two and three weeks. In details, we observed a moderate increase of HA and FN at beginning of process (HA is synthetized after 4 weeks of *in vivo* injury and FN, which is poor at resisting injury, *in vivo* provides the main structural support for the wound clot) and an high increase in levels of HA and FN at 2 weeks of healing. We also observed transient levels of alpha-SMA and myofibroblasts detection only at one and two weeks of healing in the wound area. This is a relevant data in the light of the fact, it is well accepted that myofibroblasts appear temporarily in granulation tissue during wound healing and are absent in a normal scar [14,49]but are present permanently in hypertrophic scars [28,51] and other fibrotic settings [49,52]. After two weeks of healing, this provisional matrix is replaced by the collagen to provide strength to the wounded area, the ECM that replaced granulation tissue, is similar but not equivalent to that found in normal tissue. These data was confirmed by SEM investigations carried out at two and three weeks of healing – by SHG analysis. The presence of new endogenous collagen at different timing of α-SMA expression, suggested that cells not only migrated and differentiated but also works correctly. To the best of our knowledge, no other 3D-HDE recapitulates granulation tissue formation and spontaneously synthetized large amount of collagen bundles. Flasza et al, for example, realized a 3D scaffold composed of a provisional matrix human fibrin, into which fibroblasts are initially embedded and then, induce collagen deposition only by supplementary media with factors such as TGF-β, insulin, ascorbate and plasmin [53]. Others works used 3D scaffolds supplemented with collagen, glycosaminoglycans (GAGs) (hyaluronic acid and proteoglycans), fibronectin, and growth factors [11]. Conversely, our organotypic construct not only results in the formation of granulation tissue but also allows

possibility to evaluate remodeling phase. Indeed, once granulation tissue is realized and healing process is exhausted (at two weeks of healing), α-SMA wasn't anymore detected (Fig. 10), cells in the wound undergo apoptosis, fibroblasts commence the synthesis and assembly of extracellular matrix, and the provisional extracellular matrix is gradually replaced with a collagenous matrix as literature reports [13]. To verify scar formation, we investigated the 3D architecture of this neo-formed matrix and assess the tissue capability to reestablish and remodeling matrix after injury comparing neo-formed tissue with an undamaged tissue. We demonstrated that later in wound healing as remodeling occurs, it is possible detected formation of collagen bundles. Indeed we observed a complex organization after two weeks of healing (consequently two weeks of maturation) and an increase of collagen bundles diameter during development. Notably, the increase in collagen bundles diameter occurred uniformly throughout the ECM and even if was not confined to collagen bundles close to wound edge, it is more and more pronounced in neo-formed matrix. With progressing healing-time (3 weeks after cut), this difference with mature matrix was less pronounced but always present and relevant compared at 2 weeks after injury. This simple, key observation is critical to understanding how collagen bundles growth in assembling depend upon the distance from the cut. Analysis of the bundles showed a pronounced increase in the bundles formation profiles after 2 weeks of healing that continues more and more at three weeks, conversely mature matrix of undamaged tissue is in steady-state and it is possible a balance between matrix degradation and remodeling. Thus, matrix remodeling starts and keeps going over three weeks when healing process is exhausted as well as *in vivo* happen: the third stage of wound repair — remodeling — begins 2 weeks after injury and lasts for weeks or more; during this stage, all of the processes activated after injury wind down and cease [12 54]. This

continuous remodeling is confirmed by analysis of fibers orientation. At an early stage of remodeling phase collagen fibers are mostly aligned at 45° to the wound because of tissue works to complete healing and fill wound (Fig. 16); conversely at three weeks, collagen fibers are mostly aligned perpendicular to the wound. No preferential orientation was detected in undamaged matrices but an anisotropic distribution is observed. A random-like structure organization and an anisotropic aspect is typical in normal skin and is the first difference evaluated between a normal human skin and a scar [55]. The most significant difference between normal tissue and scar tissue seems to be the orientation of the fibrous matrix [56]. A cutaneous scar is a macroscopic fibrous disturbance in the normal tissue architecture and occurs in the setting of both surgical and traumatic wounds: it is the normal outcome of the wound-healing process and occurs after trauma, injury or surgery to any tissue or organ in the body [57]. Such scars are consequence of a repair mechanism that replaces the missing normal tissue with an extracellular matrix consisting predominantly of excessive levels of fibronectin and collagen types I and III strongly oriented [58]. Scar formation when healing process is exhausted was ultimately demonstrated in our 3D-HDE wound model too. To this end, ECM deposition and remodeling within both the wound region and healthy peripheral tissue are considered. We have already mentioned a preferential distribution of collagen fibers both at two and three weeks after wounding in the wound region. From literatures we know that human scar have greater collagen density because of less cellularization and more alignment than normal tissue, although the alignment is parallel to the skin and consequently perpendicular to the cut. This preferential fibers orientation is the most significant difference between scar and normal tissue [56] [59]. Our data suggest that neo-formed tissue after three weeks of healing have typical scar features as: poor cellularization, high levels of fibronectin

(FN doesn't results in a transient overexpression as HA), preferentially fibers orientation approximately at 90° to the cut. In figure 19 reported representative images of neo-formed matrix/scar and pre-existing matrix/normal tissue and recapitulate the central characteristics of a scar. Histological differences define scar from normal/undamaged tissue: the normal pattern of collagen fiber bundles from lost dermis is replaced with collagen fiber bundles arranged in array parallel to the surface and perpendicular to cut. SHG and immunofluorescence techniques prove differences in ECM organization and composition between the two matrices and detected levels of FN higher in neo-formed matrix than in undamaged tissue. SEM and TEM investigations confirm a preferential fibers orientation in a scar poor of cells. Thus, the new ECM that replaced granulation tissue when healing is exhausted is characterized by a new architecture that differs from the original in fiber orientation, fibronectin expression and cellularization: all typical aspects of a normal scar occurring during *in vivo* healing process. The 3D-HDE tissue capabilities to induce fibroblasts differentiation and granulation tissue and scar formation are even more relevant at light of the last three decades of literatures reported and confirmed that the early gestation fetus has the remarkable ability to heal skin wounds without scar. Since that time, research demonstrated in general that fetal skin contains more hyaluronic acid than adult skin [57], that the hyaluronic acid content of the extracellular matrix is increased more rapidly than in adult wounds [57] and that, in embryonic scar-free healing wounds, are present more primitive fibroblasts and consequently, lower levels of myofibroblasts than in adult scar-forming wounds [58] [14] [22]. Because these differences, several investigators have proposed a role of hyaluronic acid in scarless healing and many studies are trying to investigate fibroblasts differentiation process [60] [61] [62] but many more studies are needed. We think that our organotypic 3D-model is a good

platform to investigate scar formation thanks to their ability to induce fibroblasts differentiation, to promote granulation tissue formation – at same *in vivo* timing – and to induce scar formation.

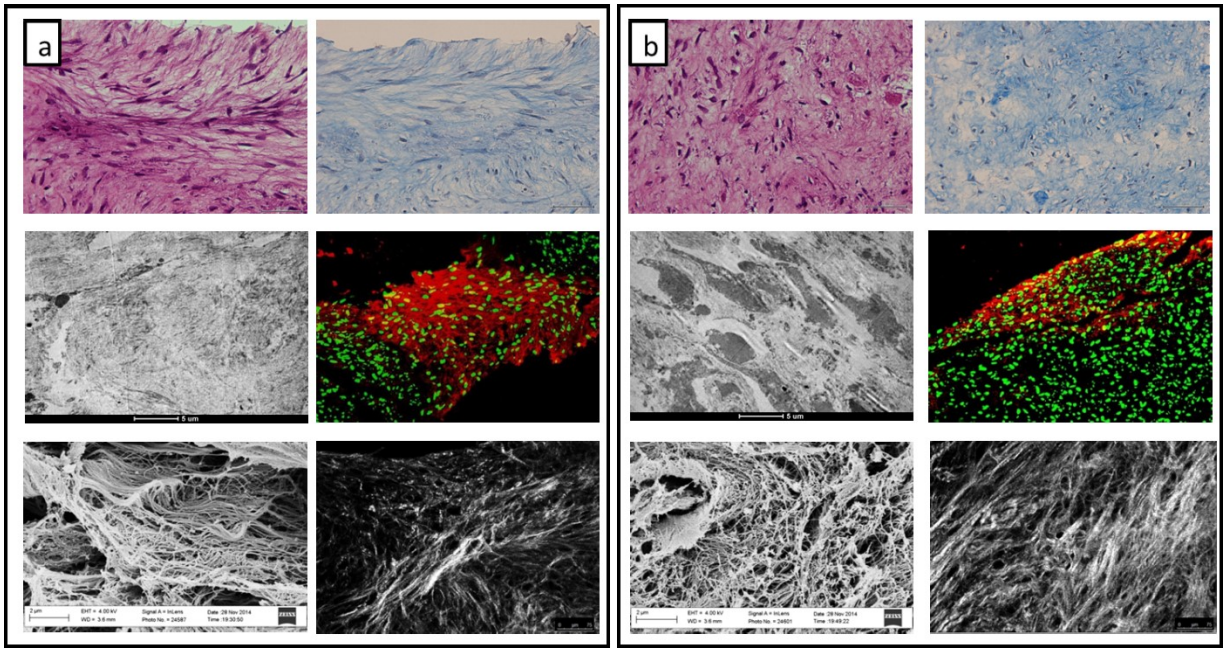

Fig. 19: 3D-dermis equivalent 3 weeks after wounding (a) neo-formed tissue, (b) pre-existing tissue. Images of: HE stain, Masson' Trichrome stain, TEM invastigation, immunofluorescence of Fibronectin and Sytox Green, SEM investigation, SHG.

3.5 CONCLUSION

The model proposed, due to its endogenous nature, could represent a valuable tool to study tissue status *in vitro* at both a cellular and an extra-cellular level after a physical damage. Our study paves the way to the development of a new class of *in vitro* tissue models that correctly reproduce in composition and organization the extracellular space. Such model would lead to the possibility of studying *in vitro* the effects of variations in human dermis on selected

aspects of both cellular and extracellular components. Specifics repair phenomena such as formation of granulation tissue and matrix remodeling with scar formation are recapitulated in our model at the same *in vivo* timing. Moreover it has been reported that wound contraction and scar formation in an *in vivo* model could be prevented with a responsive substitute dermal matrix seeded with skin cells, but not with unseeded similar matrices [4] but, to date, no gold standard exists for the treatment and study of scar tissue. In this perspective, our 3D-HDE wound model could be a valid platform to study scar formation mechanism and could be possible to use the human dermal equivalent model as novel platform to test dermal wound therapies and for the prevention or treatment of dermal scarring.

3.6 References

1. Harrison CA, Ph D, Gossiel F, et al. Use of an in Vitro Model of Tissue-Engineered Skin to Investigate the Mechanism of Skin Graft Contraction. 2006;12(11).

2. Eves P, Katerinaki E, Simpson C, et al. Melanoma invasion in reconstructed human skin is influenced by skin cells--investigation of the role of proteolytic enzymes. *Clin Exp Metastasis*. 2003;20(8):685-700. http://www.ncbi.nlm.nih.gov/pubmed/14713103.

3. Van Kilsdonk JWJ, Van Den Bogaard EH, Jansen P a M, Bos C, Bergers M, Schalkwijk J. An in vitro wound healing model for evaluation of dermal substitutes. *Wound Repair Regen*. 2013;21(6):890-896. doi:10.1111/wrr.12086.

4. Auger FA, Lacroix D, Germain L. Skin substitutes and wound healing. *Skin Pharmacol Physiol*. 2009;22(2):94-102. doi:10.1159/000178868.

5. Richards S, Ph D, Leavesley DI, Ph D, Upton Z, Ph D. Development of a Three-Dimensional Human Skin Novel Wound Healing Therapies. 2010;16(5).

6. Safferling K, S??tterlin T, Westphal K, et al. Wound healing revised: A novel reepithelialization mechanism revealed by in vitro and in silico models. *J Cell Biol*. 2013;203(4):691-709. doi:10.1083/jcb.201212020.

7. Geer DJ, Swartz DD, Andreadis ST. In Vivo Model of Wound Healing Based on Transplanted Tissue-Engineered Skin. 2004;10(7).

8. Kairuz E, Upton Z, Dawson R a, Malda J. Hyperbaric oxygen stimulates epidermal reconstruction in human skin equivalents. *Wound Repair Regen*. 2007;15(2):266-274. doi:10.1111/j.1524-475X.2007.00215.x.

9. Palmiero C, Imparato G, Urciuolo F, Netti P. Engineered dermal equivalent tissue in vitro by assembly of microtissue precursors. *Acta Biomater*. 2010;6(7):2548-2553.

doi:10.1016/j.actbio.2010.01.026.

10. Middelkoop E, Bogaerdt AJ Van Den, Ulrich MM, Meeting S. Artificial dermis and cellular aspects of scar formation. 2006;(2):1-14.

11. Debels H, Hamdi M, Abberton K, Morrison W. Dermal matrices and bioengineered skin substitutes: a critical review of current options. *Plast Reconstr surgery Glob open*. 2015;3(1):e284. doi:10.1097/GOX.0000000000000219.

12. Gurtner GC, Werner S, Barrandon Y, Longaker MT. Wound repair and regeneration. *Nature*. 2008;453(7193):314-321. doi:10.1038/nature07039.

13. Adam J. Singer RAFC. Cutaneous wound healing. 1999.

14. Hari G. Garg MTL. *Scarless in Wound Healing*. Vol 133.; 2000. doi:10.1016/B978-0-444-62644-8.00008-X.

15. S. K., Masur, H. S., Dewak, T. T. D. Myofibroblasts differentiate from fibroblasts when plated at low density. 1996;93(April):4219-4223.

16. Micallef L, Vedrenne N, Billet F, Coulomb B, Darby I a, Desmoulière A. The myofibroblast, multiple origins for major roles in normal and pathological tissue repair. *Fibrogenesis Tissue Repair*. 2012;5 Suppl 1(Suppl 1):S5. doi:10.1186/1755-1536-5-S1-S5.

17. Balaji S, Vaikunth SS, Lang SA, et al. Tissue-engineered provisional matrix as a novel approach to enhance diabetic wound healing. *Wound Repair Regen*. 2012;20(1):15-27. doi:10.1111/j.1524-475X.2011.00750.x.

18. Road O. Biological implications of a discrete mathematical model for collagen deposition and alignment in dermal wound repair. 2001;(2000):379-393.

19. Metcalfe AD, Ferguson MWJ. Bioengineering skin using mechanisms of regeneration and repair. *Biomaterials*. 2007;28(34):5100-5113. doi:10.1016/j.biomaterials.2007.07.031.

20. J. J. LONGACRE HK, Berry H. A., Johnson D, Wiethe D., Chunekamrai M., Ramnath R. THE RELATION OF THE ULTRASTRUCTURE OF COLLAGEN TO SCAR FORMATION AND ITS SURGICAL MANAGEMENT. 1966;(December).

21. Zuijlen PPM Van, Gardien KLM, Jaspers MEH, et al. Tissue engineering in burn scar reconstruction. *Burn Trauma*. 2015;(2015):1-11. doi:10.1186/s41038-015-0017-5.

22. Coolen NA, Schouten KCWM, Boekema BKHL, Middelkoop E, Ulrich MMW. Wound healing in a fetal, adult, and scar tissue model: A comparative study. *Wound Repair Regen*. 2010;18(3):291-301. doi:10.1111/j.1524-475X.2010.00585.x.

23. El-Ghalbzouri A, Gibbs S, Lamme E, Van Blitterswijk CA, Ponec M. Effect of fibroblasts on epidermal regeneration. *Br J Dermatol*. 2002;147(2):230-243. doi:10.1046/j.1365-2133.2002.04871.x.

24. Fernandes H, Moroni L, van Blitterswijk C, de Boer J. Extracellular matrix and tissue engineering applications. *J Mater Chem*. 2009;19:5474. doi:10.1039/b822177d.

25. Selman Sakar M, Eyckmans J, Pieters R, Eberli D, Nelson BJ, Chen CS. Cellular forces and matrix assembly coordinate fibrous tissue repair. *Nat Commun*. 2016;7:1-8. doi:10.1038/ncomms11036.

26. van den Broek LJ, Niessen FB, Scheper RJ, Gibbs S. Development, validation and testing of a human tissue engineered hypertrophic scar model. *ALTEX*. 2012;29(4):389-402. doi:10.14573/altex.2012.4.389.

27. Longaker MT, Whitby DJ, Ferguson MW, Lorenz HP, Harrison MR, Adzick NS. Adult skin wounds in the fetal environment heal with scar formation. *Ann Surg*. 1994;219(1):65-72. doi:10.1097/00000658-199401000-00011.

28. Seo BF, Lee JY, Jung SN. Models of abnormal scarring. *Biomed Res Int*. 2013;2013.

doi:10.1155/2013/423147.

29. Lin RY, Sullivan KM, Argenta PA, Meuli M, Lorenz HP, Adzick NS. Exogenous transforming growth factor-beta amplifies its own expression and induces scar formation in a model of human fetal skin repair. *Ann Surg*. 1995;222(2):146-154. doi:10.1097/00000658-199508000-00006.

30. Klinge U, Klosterhalfen B, Birkenhauer V, Junge K, Conze J, Schumpelick V. Impact of polymer pore size on the interface scar formation in a rat model. *J Surg Res*. 2002;103(2):208-214. doi:10.1006/jsre.2002.6358.

31. Kloeters O, Tandara A, Mustoe TA. Hypertrophic scar model in the rabbit ear: A reproducible model for studying scar tissue behavior with new observations on silicone gel sheeting for scar reduction. *Wound Repair Regen*. 2007;15(SUPPL. 1):40-45. doi:10.1111/j.1524-475X.2007.00224.x.

32. Groeber, Florian, Holeiter, Monika, Hampel, Martina, Hinderer, Svenja, Schenke-Layland, Katja. Skin tissue engineering — In vivo and in vitro applications. *Adv Drug Deliv Rev*. 2011;63(4-5):352-366. doi:10.1016/j.addr.2011.01.005.

33. Broek LJ Van Den, Limandjaja GC, Niessen FB, Gibbs S. Human hypertrophic and keloid scar models : principles , limitations and future challenges from a tissue engineering perspective. *Exp Dermatol*. 2014:382-386. doi:10.1111/exd.12419.

34. Reijnders CMA, van Lier A, Roffel S, Kramer D, Scheper RJ, Gibbs S. Development of a Full-Thickness Human Skin Equivalent In Vitro Model Derived from TERT-Immortalized Keratinocytes and Fibroblasts. *Tissue Eng Part A*. 2015;21(17-18):2448-2459. doi:10.1089/ten.TEA.2015.0139.

35. Tom VJ, Steinmetz MP, Miller JH, Doller CM, Silver J. Studies on the Development and

Behavior of the Dystrophic Growth Cone, the Hallmark of Regeneration Failure, in an In Vitro Model of the Glial Scar and after Spinal Cord Injury. *J Neurosci*. 2004;24(29):6531-6539. doi:10.1523/JNEUROSCI.0994-04.2004.

36. Vincent C., Martijn B A, Michiel C E. MMW, Middelkoop E. Biological background of dermal substitutes. *Burns*. 2010;36(3):305-321. doi:10.1016/j.burns.2009.07.012.

37. Zhu X, Zhuo S, Zheng L. Characteristics of scar margin dynamic with time based on multiphoton microscopy. 2011:239-245. doi:10.1007/s10103-010-0851-4.

38. Stein AM, Vader DA, Jawerth LM, Weitz DA, Sander LM. An algorithm for extracting the network geometry of three-dimensional collagen gels. *J Microsc*. 2008;232(3):463-475. doi:10.1111/j.1365-2818.2008.02141.x.

39. Bredfeldt JS, Liu Y, Pehlke CA, et al. Computational segmentation of collagen fibers from second-harmonic generation images of breast cancer. *J Biomed Opt*. 2014;19(1):016007. doi:10.1117/1.JBO.19.1.016007.

40. Krafts KP. Tissue repair: The hidden drama. *Organogenesis*. 2010;6(4):225-233. doi:10.4161/org6.4.12555.

41. Hinz B, Phan SH, Thannickal VJ, et al. Recent Developments in Myofibroblast Biology. *Am J Pathol*. 2012;180(4):1340-1355. doi:10.1016/j.ajpath.2012.02.004.

42. De Jesus AM, Aghvami M, Sander EA. A Combined In Vitro Imaging and Multi-Scale Modeling System for Studying the Role of Cell Matrix Interactions in Cutaneous Wound Healing. *PLoS One*. 2016;11(2):e0148254. doi:10.1371/journal.pone.0148254.

43. Thangapazham R, Darling T, Meyerle J. Alteration of Skin Properties with Autologous Dermal Fibroblasts. *Int J Mol Sci*. 2014;15(5):8407-8427. doi:10.3390/ijms15058407.

44. Masci VL, Taddei AR, Gambellini G, Giorgi F, Fausto AM. Ultrastructural investigation

on fibroblast interaction with collagen scaffold. *J Biomed Mater Res - Part A*. 2016;104(1):272-282. doi:10.1002/jbm.a.35563.

45. Shamis Y, J. Hewitt K, Bear SE, et al. IPSC-derived fibroblasts demonstrate augmented production and assembly of extracellular matrix proteins. *Vitr Cell Dev Biol - Anim*. 2012;48(2):112-122. doi:10.1007/s11626-011-9478-4.

46. Sriram G, Dykas MM, Ramasamy S, et al. Reconstructing human skin equivalents on fibrin-based dermal matrix. *Mater Today*. 2016;00(00):14-15. doi:10.1016/j.mattod.2016.01.015.

47. Carolyn Ramsey and Fran Koch. The Role of Sutures in Wound Healing. 2001. www.infectioncontroltoday.com.

48. Desmoulière A, Darby I, Gabbiani G. Normal and pathologic soft tissue remodeling: role of the myofibroblast, with special emphasis on liver and kidney fibrosis. *Lab Invest*. 2003;83(12):1689-1707. doi:10.1097/01.LAB.0000101911.53973.90.

49. Ehrlich HP, Desmoulière A, Diegelmann RF, et al. Morphological and immunochemical differences between keloid and hypertrophic scar. *Am J Pathol*. 1994;145(1):105-113. http://www.pubmedcentral.nih.gov/articlerender.fcgi?artid=1887298&tool=pmcentrez&rendertype=abstract.

50. Xie Y. Ex Vivo Investigation of Novel Wound. *Life Sci*. 2008;(November).

51. Tuan TL, Nichter LS. The molecular basis of keloid and hypertrophic scar formation. *Mol Med Today*. 1998;4(January):19-24. doi:10.1016/S1357-4310(97)80541-2.

52. Butler PD, Ly DP, Longaker MT, Yang GP. Use of Organotypic Co-culture to Study Keloid Biology. *Am J Surg*. 2009;195(2):144-148. doi:10.1016/j.amjsurg.2007.10.003.Use.

53. Flasza-Baron M, Kemp P, Shering D, Marshall D, Denham Z, Johnson PA.

Development and manufacture of a human living dermal equivalent (ICX-SKN). *Eur Cells Mater*. 2008;16(SUPPL. 3):3. doi:10.2217/17460751.2.6.903.

54. Szabowski a, Maas-Szabowski N, Andrecht S, et al. c-Jun and JunB antagonistically control cytokine-regulated mesenchymal-epidermal interaction in skin. *Cell*. 2000;103(5):745-755. doi:10.1016/S0092-8674(00)00178-1.

55. Verhaegen PDHM, Res EM, Van Engelen A, Middelkoop E, van Zuijlen PPM. A reliable, non-invasive measurement tool for anisotropy in normal skin and scar tissue. *Ski Res Technol*. 2010;16(3):325-331. doi:10.1111/j.1600-0846.2010.00436.x.

56. McDougall S, Dallon J, Sherratt J, Maini P. Fibroblast migration and collagen deposition during dermal wound healing: mathematical modelling and clinical implications. *Philos Trans A Math Phys Eng Sci*. 2006;364(1843):1385-1405. doi:10.1098/rsta.2006.1773.

57. Larson BJ, Longaker MT, Lorenz HP. Scarless fetal wound healing: a basic science review. *Plast Reconstr Surg*. 2010;126(4):1172-1180. doi:10.1097/PRS.0b013e3181eae781.

58. Ferguson MWJ, O'Kane S. Scar-free healing: from embryonic mechanisms to adult therapeutic intervention. *Philos Trans R Soc Lond B Biol Sci*. 2004;359(1445):839-850. doi:10.1098/rstb.2004.1475.

59. Dallon JC, Sherratt J a, Maini PK. Mathematical modelling of extracellular matrix dynamics using discrete cells: fiber orientation and tissue regeneration. *J Theor Biol*. 1999;199(4):449-471. doi:10.1006/jtbi.1999.0971.

60. Cliff WJ, Chir B, Phil D, et al. Myofibroblasts in human granulation tissue. :55-67.

61. Wang X, Wei F, Luo F, Huang K, Xie Z. Induction of granulation tissue for the secretion of growth factors and the promotion of bone defect repair. *J Orthop Surg Res*. 2015;10:147. doi:10.1186/s13018-015-0287-4.

62. Berning M, Prätzel-Wunder S, Bickenbach JR, Boukamp P. Three-Dimensional In Vitro Skin and Skin Cancer Models Based on Human Fibroblast-Derived Matrix. *Tissue Eng Part C Methods*. 2015;00(00):1-13. doi:10.1089/ten.TEC.2014.0698.

4 Development of engineered 3D human skin equivalent *in vitro* model to study melanoma process

4.1 Introduction

4.1.1 *In vivo* melanoma process

Melanoma is a type of cancer that develops from the pigment-containing cells known as melanocytes [1]. This rare form of skin cancer accounts for only 4 % of all skin cancers but it causes the greatest number of skin cancer-related deaths worldwide [2] [3] . Overall, in the last years, the global incidence of melanoma is increasing, with approximately 200,000 new cases and 65,000 melanoma-associated deaths each year [3] .The primary cause of death in cutaneous melanoma are metastasis [4]. The overall survival for patients with metastatic melanoma is poor [5] and novel forms of treatment are needed considering that traditional chemotherapeutic agents fail [6]. For this reason, early detection and diagnosis is necessary [7] and the evolution of melanocytic lesion morphology remains an important diagnostic tool [1]. Currently, identification of primary cutaneous malignant melanoma (CMM) is mainly based on the famous ABCDE criteria: Asymmetry, Border, Color, Diameter, Evolution [7]. These classifications allows possibility to distinguish benign lesions, nevi, from melanomas, physicians [8] [7]. After four decades of studies, clinic-pathologic prognostic markers have been consistently identified in several studies: age at diagnosis (with worse prognosis in older patients) [3], male gender [9], growth phase (radial vs. vertical) [10], Breslow thickness (BT) [11], level of invasion [6], presence of ulceration and its extension [11], presence and density of tumor-infiltrating lymphocytes (TILs) [12], presence of microsatellites [13], presence of vascular and/or

lymphatic invasion [14], and the mitotic rate (MR) [7]. The most important of these is the Breslow index, although it is merely a measure of tumor depth and is a reflection of the changes occurring in the growth characteristics of the cells [15]. Indeed, melanoma undergoes different phases and malignancy degree related to infiltration cells capability. Presence of dysplastic nevi means presence of a premalignant lesion with a specific cytology and architecture [16]. The second step of disease is formation of malignant lesions, in this phase cells grow primarily in a horizontal direction, remaining within or near the epidermis; in this so-called radial growth phase (RGP) stage, the cells have not yet acquired metastatic capacity and are restricted to the epidermis only [16] [17–19]. Radial growth phase (RGP) melanoma cells proliferate and form nests in the epidermis, but do not invade the dermis [19,20]. In this phase, cancer cells are incapable biologically of generating metastatic events. Radial growth phase comprises neoplastic melanocytes growing in a horizontal array as single cells and small nests predominantly in an intra-epidermal location. The radial growth phase may also involve the papillary dermis [17]. As cells begin to grow into the dermis, they enter a histologically defined vertical growth phase (VGP) which has been postulated to be the first point at which the tumor gains metastatic capacity [21]. Conversely to RGP, VGP cells cross the basement membrane, invade and proliferate in the dermis [15,21]. Subsequent step is metastatic (met) melanoma formation that rapidly invades deep into the dermal compartment until arriving into organs [22]. Migration and dermis invasion are the result of a specific interaction between tumoral and stromal cells [23] in which where cells lose their epithelial features including their sheet-like architecture and polarity. Cells also develop a mesenchymal phenotype, taking on a spindle-like, fusiform morphology, become motile, and start expressing mesenchymal markers [24] [25] like: lumican, glypican, N-cadherin, osteonectin (SPARC), osteopontin,

metalloproteinases, integrins [26–32]. A relevant phenomena during switch RGP-VGP is the switch of cadherins (calcium-dependent molecules which belong part of adherens junctions family): loss of E-cadherins with gain of alternate neural isoforms (N-cadherin) [15 33].

In the last years, a key genetic alteration has been identified in melanoma progression [34–37]. In each case, the first step is the activation of a single 'driver' oncogene subsequently, additional genetic alterations occur such as additional driver mutations or heterozygous loss of suppressors [38 31]. In 40%-60% of melanoma cases, oncogene BRAF is involved and activated with specific mutation $BRAF^{V600E}$ [39]. This oncogene known to be critical for the proliferation and survival of melanoma cells through activation of the RAF/MEK/ERK mitogen activated protein kinase pathway (MAPK) [39 40 41]. For this reason BRAF is an attractive target for anti-melanoma therapy [42]. In this perspective, several BRAF inhibitors are currently being tested; for example, the BRAF inhibitors RAF-265 (Novartis), PLX4032 (Plexxikon/Roche), and GSK2118436 (GSK) are in advanced stages of clinical trials (ClinicalTrials.gov). Encouraging results from a clinical trial with the BRAF inhibitor PLX4032 were recently reported [43 44 43], however, most patients who initially responded to treatment with PLX4032 relapsed, suggesting that chronic treatment with BRAF inhibitors is associated with development of drug resistance [39 38]. Thus, other studies and researches are the key to destroy this disease.

4.1.2 Engineered melanoma models

Cutaneous malignant melanomas represent an important clinical problem because of its high capacity to metastasize [45]. Currently melanoma is still studied *in vitro* using 2D cell cultures, spheroids or co-cultures in 3D microenvironement [46–48]. Obviously, conventional 2D cell culture

is not representative of the cellular environment: tissue-specific architecture, mechanical and biochemical cues as well as cell–cell communication are lost when 2D models were used [49]. The lack of 3D structure is more and more relevant in case of melanoma studies because the first problem of this cancer is precisely invasion and infiltrative capability of cells. Thus, microenvironement is fundamental to fabricate valid platform of study and screening. Typical human skin reconstructs consist of artificial skin fabricated from isolated cutaneous cell populations [50–53]. The reconstructs comprise a stratified, terminally differentiated epidermal compartment and a dermal compartment consisting of fibroblasts embedded in exogenous collagen [54]. The co-culture of keratinocytes and melanoma cells induce fabrication of a tumor skin and can be used as an alternative to animal testing for studies melanoma invasion [47]. Tissue culture of melanoma cells also induces a different epidermis structure and phenotype depending of grade malignancy of the cell lines used. Different studies compared the phenotypes and the behavior of melanoma cells derived from primary and metastatic sites in order to study the biological properties of melanoma cells from different stages of progression were used [20,5556]. Different research groups demonstrated that, in 3D skin model, melanoma cells lines displayed characteristics that are consistent with the original tumors from which they are derived, such as their motility and invasiveness. For example, cell lines derived from RGP primary melanoma are unable to invade the dermis, indeed in RGP melanoma reconstructs, fibroblasts and keratinocytes can still form an intact basement membrane [57]. Conversely, when VGP metastatic melanoma cells were incorporated into skin reconstructs, they displayed rapid proliferation and aggressive invasive growth deep into the dermis [58].

Accordingly, we developed a complex three-dimensional (3D) human skin equivalent model in which the organized 3D architecture of the native skin is reproduced. Purpose of our work

was analysed a disease that mainly adversely affect epidermis. In this perspective, human melanoma cell lines derived from primary sites were added to this 3D engineered skin model.

4.2 Fabrication and characterization of tumor tissue micromodules

4.2.1 Materials and methods

Cell expansion and melanoma-μTP-culture

A375-1619 (ATCC® CRL-1619™) were sub-cultured onto 150mm^2 Petri dishes in culture medium (Eagle's BSS minimum essential medium containing 10% fetal bovine serum, 100 μg/ml^{-1} L-glutamine, 100U/ml^{-1} penicillin/ streptomycin, and 0.1mM nonessential amino acids). Cells were maintained at 37 ° C in humidified atmosphere containing 5% CO2. A375 of passages 4–7 were used. Gelatine microbeads having a diameter of 75–150 μm, stabilized by 4% of glyceraldehyde were fabricated by means of a modified double emulsion technique (O/ W/O) as previously reported [14]. The resulting microspheres were filtered and washed with acetone and then dried at room temperature. To make the HD-μTP, spinner flask bioreactor (250 ml, CELLSPIN, Integra Bio-sciences) was inoculated with a cell density of 105 cell ml^{-1} and a gelatine microbeads density of 2mgml^{-1} in order to obtain an initial ratio of 10 cells per microbead. Two separate experiments were carried out. Previously the culture suspension was stirred intermittently at 30 rpm (5 min stirring and 30 min static incubation) or the first 6 h post-inoculation to allow cell adhesion, and then continuously at 30 rpm for the entire duration of the process. Then, the culture suspension was stirred intermittently at 30 rpm (5 min stirring and 30 min static incubation) for the entire duration of the process. All cultures were maintained at 37 ° C in a humidified 5% CO2 incubator. The culture medium was replenished on the first day and every 2 days until the end of the experiments.

A375-μTP proliferation and aggregation

To evaluate the aggregation capability of the A375-μTP both in continuous than discontinuous stirring conditions, aliquots of 1ml containing μTP were collected at each time point (days 1, 3, 5, 6, 7, 8 and 10) from the spinner culture and placed under microscope (Olympus CK X41). The acquired images were processed by using ImageJ® software. At the same times, 3 aliquots of 300 μl each were transferred to a cell culture dish having and the number of A375-μTP were counted using a microscope. After that, the suspension was placed in a 1.5 ml eppendorf tube, gently washed twice with PBS and then treated with the yellow tetrazolium MTT (3-(4, 5-dimethylthiazolyl-2)-2, 5-diphenyltetrazolium bromide) to performed cell proliferation assay.

Histological analysis

At culture day 6, and 9 (discontinuous stirring conditions), aliquots of 1ml were collected from the spinner culture and the A375- μTP were stained with N-cadherin (1:100, monoclonal, Abcam) and SYTOX® Green (INVITROGEN) for the detection of tumor adherens junctions protein and cell nuclei, respectively. The A375- μTP were fixed with 4% paraformaldehyde and rinsed twice with PBS buffer. Immunofluorescences were performed on paraffin-embedded tissue sections with sodium antigen retrieval. Then the samples were stained overnight with N-cadherin at 4° C. Alexa-fluor 594 (1:500, Abcam) was used as secondary antibody. Then samples were incubated with SYTOX® Green stock solution (10 mg ml−1 in dimethyl sulfoxide), diluted in PBS (1/500 v/v) for 10 min at 37 ° C.). Samples were investigated by using confocal microscopy (TCS SP5 II Leica, Milano, Italy).

4.2.2 Results and discussions

In this work melanoma microtissues were engineered and used as micromodules to evaluate melanoma cells adhesion capability. Cell-scaffold aggregation and N-cadherin expression were analysed for the investigation. A375-μTPs were fabricated by culturing melanoma cells within gelatine porous microbeads in a dynamic spinner culture [13, 14]. The same methods was already used to obtain HDF-μTP, and have previously proved that, under such configuration, the interaction arising among fibroblasts and the surface of the gelatin microscaffolds induce cell-scaffold aggregation and collagen production [59]. A375-μTP evolution was evaluated during 10 days of the spinner culture both in continuous than discontinuous stirring conditions. Figure 1 reports the time evolution of cells showing if cells assembled around microbeads. At day 7 of spinner culture in continuous stirring conditions, tumor-μTPs are not assembled (Fig. 1a), conversely the number of cells per A375-μTP increased during all 10 days of spinner culture (figure 1B), starting from 10 cells per A375-μTP up to 200 cells per A375-μTP in discontinuous stirring conditions. Imparato et al. (2013) have previously proved that the interaction arising among fibroblasts and the surface of the gelatin microscaffolds, triggered mechano-transduction pathways involved in the collagen remodeling and, as consequence, fibroblasts synthesized new collagen molecules that were then assembled within the pore spaces and on the surfaces of the gelatin microscaffold inducing HD-μTPs assembling. Studies demonstrated that A375 do not product collagen (the glue of this system) [60]. Reasons to μTP aggregation are to be sought in heterotypic cell aggregation capability. Immunofluorescence (figures 2) revealed that A375-μTP express N-cadherin. N-Cadherin is a cell adhesion protein and member of catenin family. Cadherins are a family of glycoproteins involved in the Ca2+-dependent cell-cell

adhesion mechanism. It has been demonstrated that N-Cadherin mediated both homotypic than heterotypic aggregation among melanoma cells and have a relevant role in melanoma progression [61]. Thus cell-scaffold aggregation and consequently tumor μTP formation is due to protein adhesion expression. At least MTT assay was used for measuring cell viability and activation in the assessment of compatibility between cells and biomaterials. Relationship between cell number and μTP aggregation was tested during entire experiment. Figure 3 shows that the absorbance was directly proportional to the number of cells: A375 cell in tumor-μTP are activated and vital and consequently biocompatible to porous scaffold [62]. These previous analysis have been the starting point for the development of full-thickness melanoma model. Indeed biocompatibility of melanoma cells with porous gelatin beads is necessary for their future use in a 3D *in vitro* melanoma model realized by the same scaffold.

4.3 Engineered melanoma model

4.3.1 Materials and methods

Fabrication of 3D Human dermis equivalent endogenous Biohybrid

Spinner cell culture: macroporous gelatine microbeads were obtained by using a double emulsion technique. Glyceraldehydes have been used as gelatine crosslinker at 4% w/w of the microbeads. The microbeads/fibroblasts cultures were propagated intermittently at 30 rpm (5 min stirring and 30 min static incubation) for the first 6h post-inoculation for cell adhesion, and then continuously agitated at 30 rpm in spinner flasks (100 ml, Bellco). The spinner cultures were incubated at 37 ° C in 5% CO2. Tissue equivalent assembly: tissue precursors obtained by previous step have been injected in maturation chamber to allow their

molding in disc-shaped construct (1 mm in thickness, 5 mm in diameter). After 4 weeks of culture, under dynamic conditions, the biohybrid obtained has been removed from the maturation chamber and seeded with keratinocytes in order to obtain the epithelial layer (for details look chapter 2).

Keratinocyte and fibroblast extraction

Human keratinocytes and fibroblasts were isolated from human foreskins after routine with the informed consent of the patient.

Day 1: separation of dermis from epidermis. Skin sample derived from reduction surgery with the informed consent of the patient. Take some ml of the transport solution as sterility control and incubate it in a culture flask over night at 37° C. Rinse the biopsy 3 times with PBS, remove the PBS but leave a little bit to avoid the biopsy to run dry. Remove hairs from the top and all fat and tissue remnants from the bottom side (the better you remove the fat/tissue remnants from the bottom side the easier the separation of dermis from epidermis will be the next day).Rinse with PBS again, till the PBS stays clear (about 3 times). Determine the size of the "purified" skin (important for the amount of enzymes dispase needed; do not determine the size before having removed all the fat because the skin will enlarge after the tissue remnants are removed). Cut skin into strips of about 3 mm width. Transfer strips into new small petri dish, wash with PBS (important: do not use PBS with calcium and magnesium at this step). Incubate skin strips with Dispase solution (2 U/mL; about 5-10 ml for 6 cm^2 of skin) that all strips are covered with it and incubate over night for 16 h.

Day 2: fibroblast and keratinocyte extraction. Check after 16 h if epidermis has removed from dermis (you can see this at the edge where epidermis is partly detached from dermis). Once digestion completed, skin strips was transferred to PBS. Separate epidermis from dermis with tweezers and storing temporarily dermal tissue at 4° C in cold PBS.

For keratinocytes extraction wash epidermal parts with PBS. Cut epidermis into small pieces (they should be about 4 mm). Transfer pieces into 5 mL of pre-heated Trypsin/EDTA at 0,05%, wash petri dish with another 5 mL Trypsin/EDTA and transfer it to the tube. Incubate Trypsin/EDTA (with cut epidermal pieces) for 5 min at 37° C water bath, vortex shortly every 1-2 min (important: the water bath temperature has to be 37° C, therefore do not place large cold flasks into it as this would reduce the temperature). Stop enzyme reaction by using FBS.

Resuspend solution for 5 min (plastic single-use pipette) to separate cell clumps Strain solution by transferring it to new tube through cell strainer. Use the same pipette with prepared 10 mL PBS solution to wash the tube, the single-use pipette and finally transfer solution through cell strainer, too. Centrifuge: 5 min 1200 rpm. Resuspend cells in culture media and count cells. Seed cells into flasks: $8*10^3$ cells per cm^2. Important: full medium change after 4 h. (prepuce) or 24 h (adult skin). After 3 days 2nd medium change (cells should feature characteristic morphology now). Let cells culture up to 80% confluency before freezing (not more as keratinocytes will start to differentiate). Precaution to take during cell extraction: age of donor, gender, amount of cells extracted. Keratinocytes were grown in KGM™-2 culture media. The growth medium contains the base medium, separate vial of calcium chloride and other supplement mix that are: BPE (bovine pitutary extract), hEGF, insulin (recombinant human), hydrocortisone, GA-1000 (gentamicin, amphotericin-B),

epinephrine and transferrin. The formulation is optimised for initial seeding of 5000 cells / cm^2 up to sub-confluence.

For fibroblast extraction dermal tissue scraped eight times on the both surfaces of dermal piece in PBS solution to remove endothelial cells. Take the dermal pieces, cut them in small pieces and put in 30 ml collagenase A solution (ROCHE) at concentration of 2mg/ml for 40 minutes at 37° C. After stop the collagenase solution with FBS and centrifuge 5 min 1200 rpm and resuspend the piece in a little volume of EMEM. Eagle's BSS Minimum Essential Medium containing 20% fetal bovine serum, 100 mg/mL L-glutamine, 100 U/mL penicillin/streptomycin, and 0,1 mM Non Essential Amino Acids). In this in this way occurs the migration of fibroblasts on the surface of the petri.

Cell culture

Fibroblasts were grown in enriched Eagle's BSS Minimum Essential Medium (EMEM) until full-confluence. Keratinocytes were grown KGM™-2 culture media (PromoCeLL). Melanoma cell lines were purchased from ATCC. The A375 (ATCC® CRL-1619™)) are primary melanoma and derived from skin. Melanoma cells were grown in the same medium as fibroblast supplemented with 10% of fetal bovine serum until a semi-confluence. One day before seeding, melanoma cells were grown in the same medium as keratinocytes. All cells were grown at 37° C in 5% CO2 atmosphere.

In Vitro Reconstruction of Human 3D Skin and Melanoma

Dermal reconstruction was realized as previously described. For epidermal realization, the mature dermal reconstructs were extracted from maturation chamber, rinsed and left in petri dish for 24 h before the use.

For healthy epidermal reconstruction, dilute human fibronectin (Sigma Aldrich) in sterile balanced salt solution e concentration of 50 µg/ml than coat the dermis equivalent surface with a minimal volume (about 10 µl for single well). Allow to air dry for at least 45 minutes at room temperature. Wash the keratinocyte 3 or 4 times with PBS/EDTA 0.01 M leaving in contact for a few second and after. Keratinocyte colonies were detached by using trypsin/EDTA for 5 min at 37° C. Gently resuspend cells in culture media, count cells and add the appropriate number of cells to a 15-mL tube so that there will be enough cells (400,000 cells/insert) to seed onto the desired number of inserts. Centrifuge at 1200 rpm for 5 min. At this time, cells can be seeded directly onto the dermis equivalent. Resuspend the keratinocytes pellet in a small volume needed for plating onto the matrix. It is important to resuspend cells in a small volume as 140000 cells will be seeded onto the small surface area of the connective tissue (5 mm diameter). This is performed by using a sterile, plastic 200 µL pipet to add 50 µL keratinocytes media to the 15 mL tube per 140000 keratinocytes present. Gently dislodge the cell pellet and transfer it to a 1.5 mL sterile Eppendorf tube with a 1 mL pipet. Gently resuspend the cell pellet in the eppendorf tube with a 200 µL pipet until it is cloudy and well suspended and transfer 10 µL of the cell suspension to the middle of tissue. Do not touch for 10 min to allow the cells attachment. Incubate at 37° C for 2,5/3 h by adding only a drop of culture media each 10 minutes to allow the keratinocytes to fully adhere. At this point, in reference to the procedure used, the operator must continue to use

the culture media related. Cultures are fed every 2 d in submerged condition for one week. Then, cultures are raised to the air/liquid interface by adding only 1 ml to the bottom of the well so that the bottom of the insert just contacts the interface with the media for two weeks. Additional feedings with KGM-2 culture media without EGF and BPE but with CaCl2 concentration of 1.88 mM: media are performed for 6 day.

For incorporation of melanomas, cells were seeded together with keratinocytes onto dermal reconstructs at two different concentrations: 1:5 and 1:10 ratio of melanoma cells to keratinocytes. A375 (1619) centrifuge at 900 rpm for 4 min. Culture conditions were the same as for reconstructs containing keratinocytes alone.. All experiments were performed in triplicate. Tumor growth was monitored for 3 weeks evaluating reconstructed skin at: 1 week sub-merged, 1 week air-liquid interface, 2 weeks air-liquid interface.

Histological and immunohistochemical analysis of composites

Tumor growth was monitored for 3 weeks. Morphological analyzes were performed on histological section at 6 days of submerged conditions, and at 6 and 12 days after air-liquid interface transfer. For further visualization of epithelial structures, tissues were rinse gently in PBS, detached from metallic grid by using a thin palette and fixed with 10% neutral-buffered formalin fixative for 2–4 h. Healthy and tumor tissues were subsequently stained with H&E and cleared in xylene. Whole mounts were mounted with Permount and photographed under 20× and 40× magnifications. Immunofluorescences were performed on paraffin-embedded tissue sections with sodium antigen retrieval, followed by detection with secondary antibodies (anti-mouse 488 or anti-rabbit 546; Abcam). Paraffin sections were stained with primary

antibody for E-cadherin (1:100, monoclonal, Abcam), K14 (1:1000, polyclonal, Covance), K10 (1:500, polyclonal, Covance), P63 (1:50, monoclonal, Abcam) and filaggrin (1:200, polyclonal, Sigma) after citrate antigen retrieval, to detect epithelial markers. Paraffin sections were stained with primary antibody for S-100 (1:100, Abcam) and CD146 (1:100, Abcam) after citrate antigen retrieval, to detect melanoma markers. The secondary antibodies used were: Alexa fluor 647 goat anti-mouse (Life Techologies, Milano, Italy) and Alexa fluor 546 anti-Rabbit Anti-Sheep IgG H&L (Abcam). SYTOX® Green (INVITROGEN) for the detection of cell nuclei was used. Immunohistochemistry was performed on paraffin-embedded tissue sections with sodium antigen retrieval, followed by detection with biotinylated secondary antibodies and visualization with DAB substrate (Vector Laboratories). Antibody used on paraffin-embedded healthy and tumor tissues sections was N-cadherin (1:100; Abcam). Samples were investigated by using confocal microscopy (TCS SP5 II Leica, Milano, Italy). A375-μTP and human skin were used as positive controls.

4.3.2 Results and discussions

We previously reported on the importance of cell-ECM (native BM) and cell–cell (interactions between fibroblasts, keratinocytes, melanocytes and melanoma cells) communication in a 3D reconstructed skin model, and we showed how disruptions in these forms of communication can alter cell biology within this model [7,17]. In this study we further investigated the role of skin cells and BM components on melanoma biology and invasive ability in reconstructed human skin. In this perspective, we first fabricated a human skin reconstructs resembled the architecture of skin *in situ*. The dermal equivalent contained endogenous extracellular matrix (composed by mostly collagen but also fibronectin, hyaluronic acid and neutral mucin as

described in chapter 3) with interspersed fibroblasts. To fabricate an engineered skin model, single-cell suspensions of normal human keratinocytes were seeded onto endogenous dermis. In order to fabricate an engineered melanoma model, single-cell suspensions of normal human keratinocytes and A375 human melanoma cells derived from RGP were seeded. Two different cellular ratios of keratinocytes and A375s were evaluated: 1:5 and 1:10. The first experimental set-up with higher tumor density (1:5) presented an epithelial cells behaviour that was incapability to generate an epidermis. Figure 1 shows how epithelium was not yet formed after 2 weeks of air-liquid interface of culture. We supposed that number of melanoma cells was too high to obtain a correctly structured epithelium because of the higher replication rate and aggressiveness of A375s respect to the ones of keratinocytes.

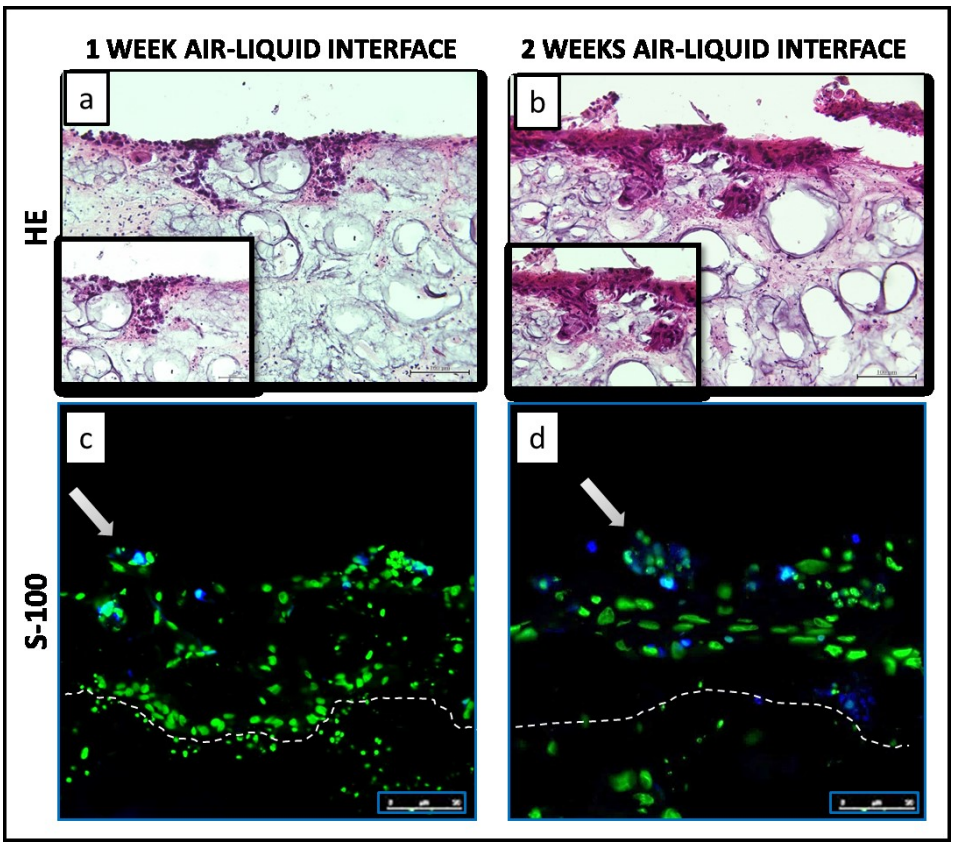

Fig .1: HE stain and Immunofluorescence of human skin equivalent in engineered melanoma model at (a) 1 week air-liquid interface culture (b,) 2 weeks air-liquid interface culture. 1° condition of experimental set-up: ratio Ker: A375 = 5:1. Paraffin section were immunostained for S-100 and Sytox Green as nuclear stain. Scale bar, 50 and 100 µm.

Subsequently, single-cell suspensions of normal human keratinocytes and A375 human melanoma cells were seeded at the ratio of 1:10 onto endogenous dermis. According to ATCC, A375-1619 cell line was derived from human melanoma skin with an epithelial morphology. The resultant tissues were allowed to grow and differentiate in serum-free medium to form 3D-highly differentiated, full-thickness, skin-like tissues. Reconstituted human epidermis was studied at 6^{th} days of submerged conditions and at 6^{th} and 12^{th} days starting from the air–liquid interface transfer. Figure 2 shows the appearance and histology of composites containing only foreskin-derived keratinocytes and co-culture both keratinocytes than melanoma-derived A375. HE stain reveals that during submersion conditions in both healthy and tumor conditions, keratinocytes are not able to synthesize some keratin polypeptides. Thus, their differentiation results uncompleted, because of the culture microenvironment used, that provides environmental conditions dramatically different from those occurring *in vivo* (Fig. 2a and 2d). Conversely, morphology analysis of healthy epidermis related to foreskin-derived keratinocytes showed a structured multilayered epithelium at day 6 (Fig. 2b), evolving at day 12 or air-liquid interface (Fig. 2c) to an organize epithelium composed of basal layer, spinosum, granulosum and corneum stratum, similar to that of a human skin. Figure 2c shows various layers of progressively flattening keratinocytes with less prominent nuclei and constituted by a high keratin content stratum spinosum. In contrast, analysis of engineered tumor epidermis obtained from foreskin-derived keratinocytes and melanoma-derived A375 revealed unstructured tissue (Fig. 2e), followed by an evolution to a flat and degenerative tissue at day 12 (Fig. 2f). The figure shows formation of a barely stratified epithelium, displaying a less pronounced red fuchsia color than the one related to the healthy tissue at 12 days after air-liquid interface (Fig. 2c and 2f). Morphological analysis

also reveals a clusters organization of A375 that does not permit a good epidermal fabrication; RGP melanoma cells formed nests within the epidermis and band-like tumor cell aggregates. When melanoma cells were incorporated into skin reconstructs, they displayed rapid proliferation and aggressive invasive growth deep into full epithelium. We speculated that the majority of A375 cells could be located on the surface of the epithelial layer or between basal epidermal layer and basement membrane after the end of the two weeks of air-liquid interface transfer. RGP primary melanoma cells in these layers could be disposed as individual cells and as small nests at the epidermal-dermal junction. Moreover, morphological analysis detected a low production of cutaneous appendage with a 3:1 ratio of healthy tissue to melanoma tissue. These data and the lack of competence for invasive growth into the dermis were confirmed by immunohistochemical analysis.

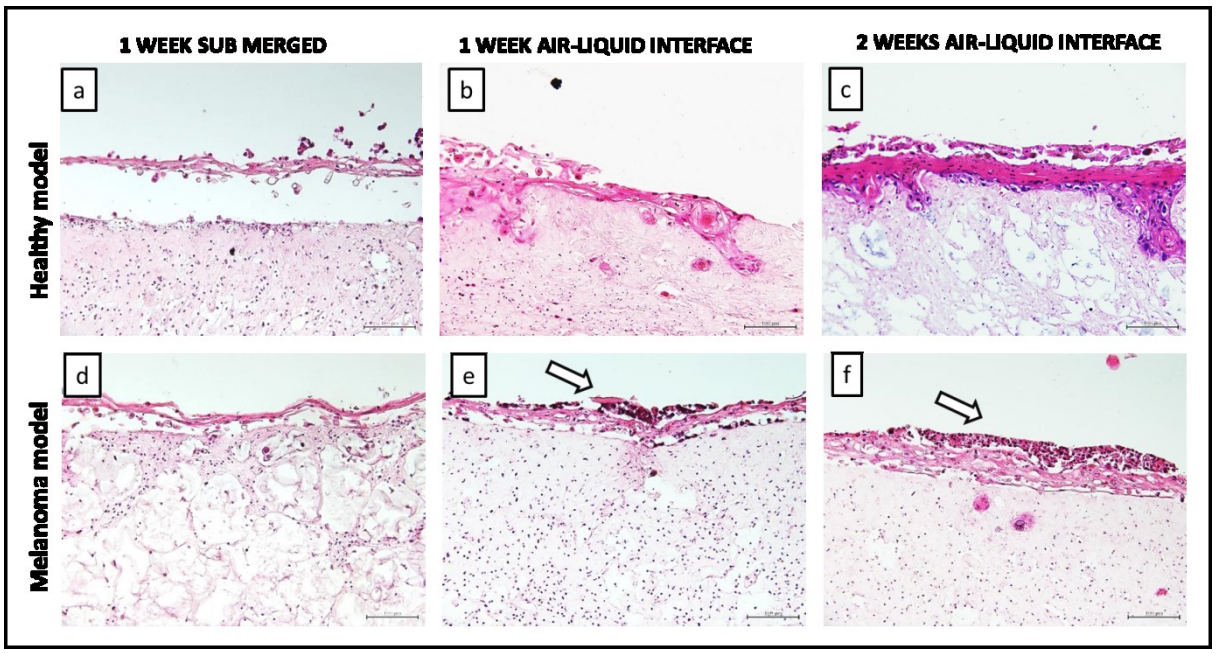

Fig .2: HE stain of human skin equivalent in engineered healthy model at (a) 1 week submerged culture, (b) 1 week air-liquid interface culture, (c) 2 weeks air-liquid interface culture; HE stain of human skin equivalent in engineered melanoma model at (d) 1 week submerged culture, (e) 1 week air-liquid interface culture, (f)2 weeks air-liquid interface culture. Scale bar, 100 µm.

To understand how the collectively migrating cells form a multilayered epithelium, we analyzed keratinocyte differentiation in both healthy and melanoma engineered tissues in submerged conditions and at 6 and 12 days after air-liquid interface transfer. Based on immunological staining with antibodies for human keratin 14 (k14), keratin 10 (k10) and filaggrin, the state of differentiation of the healthy epidermal layer differed to that visible in melanoma construct. K14, typically detected at the stratum basale in human skin, was present in the spinous layer only in submerged culture conditions in both healthy engineered and melanoma engineered skins, as reported in Fig. 3a and Fig. 3d, respectively. Progressive time K14 was present in the well-polarized stratum basale in engineered healthy model, as well as in normal epidermal differentiation (Fig. 3b, 3c). Conversely, increased levels were observed in melanoma model: after 2 weeks of culture at the air-liquid interface K14 was expressed in the upper layers too (Fig. 3e, 3f).

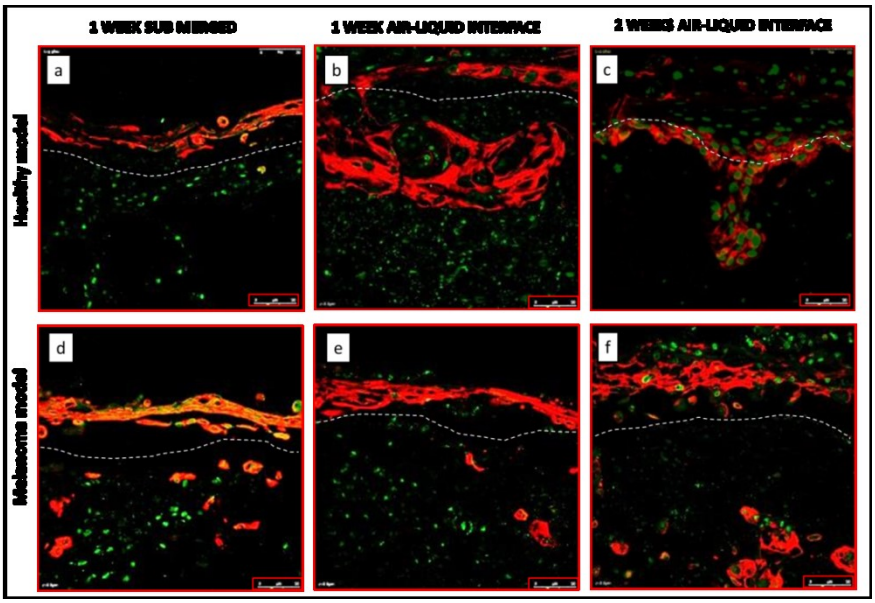

Fig .3: Immunofluorescence of human skin equivalent in engineered healthy model at (a) 1 week submerged culture, (b) 1 week air-liquid interface culture, (c) 2 weeks air-liquid interface culture; Immunofluorescence of human skin equivalent in engineered melanoma model at (d) 1 week submerged culture, (e) 1 week air-liquid interface culture, (f)2 weeks air-liquid interface culture. Paraffin sections were immunostained for K14 and Sytox Green as nuclear stain. Scale bar, 50µm.

K10 levels also exhibited significant differences between the two models (Figure 4) at the 6th, 10th and 15th day of culture. After 1 week of growth in submerged conditions, keratinocytes showed a really low expression of K10 toward the tip of the epidermis in both models (Fig. 4a, 4d). At the later time (12th and 18th days), the expression of differentiation marker progressively increased (Fig. 4b, 4e). After 2 weeks of culture at the air-liquid interface, K10 was expressed in all suprabasal epidermal layers of healthy epidermal reconstructed skin (Fig. 4c) indicating a progressive differentiation process. At this time, organotypic model seeded with A375s cocultured with keratinocytes expressed lower levels of K10 (Fig. 4f), reflecting a less differentiated status. In our model, A375 melanoma cells seem to prevent epithelial differentiation.

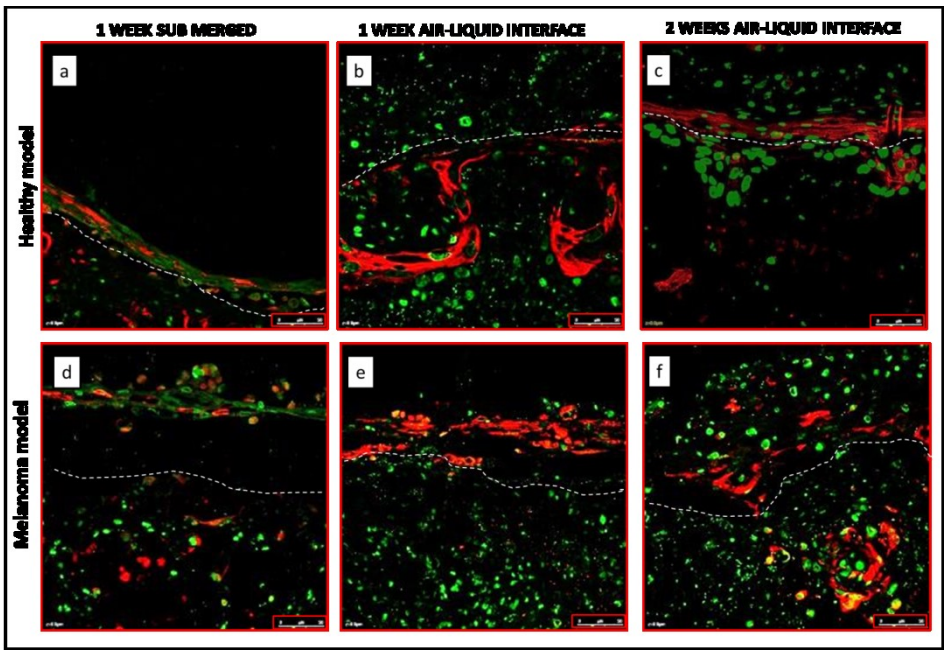

Fig .4: Immunofluorescence of human skin equivalent in engineered healthy model at (a) 1 week submerged culture, (b) 1 week air-liquid interface culture, (c) 2 weeks air-liquid interface culture; Immunofluorescence of human skin equivalent in engineered melanoma model at (d) 1 week submerged culture, (e) 1 week air-liquid interface culture, (f)2 weeks air-liquid interface culture. Paraffin sections were immunostained for K10 and Sytox Green as nuclear stain. Scale bar, 50µm.

These data were confirmed by filaggrin detection: with progressive time, the expression of K14 and K10 are down regulated in the upper layers, while structural proteins, such as filaggrin, are upregulated in engineered in our healthy model as well as *in vivo*. Indeed, between days 6 and 12 after air-liquid interface transfer, filaggrin expression increased in foreskin-keratinocytes-derived model, indicating a progressive differentiation process (Fig. 5b, 5c). Thus, filaggrin expression, whose signal was detectable only in the upper layers of epidermis, displayed a correct and a well-differentiated epidermis. Conversely, no filaggrin expression was revealed by the same analysis in the melanoma model (Fig. 5d, 5e, 5f).

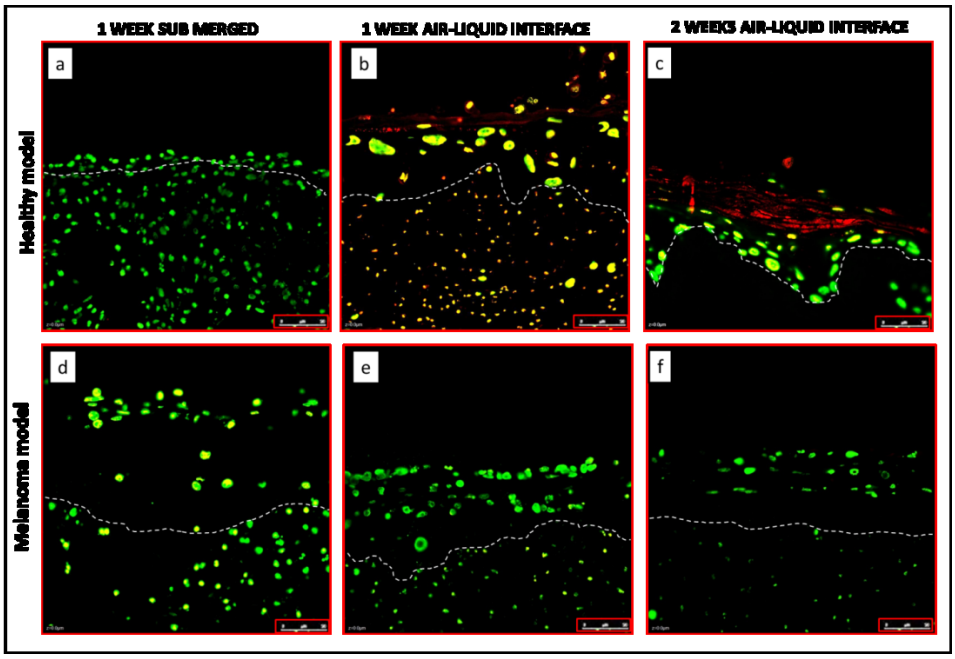

Fig .5: Immunofluorescence of human skin equivalent in engineered healthy model at (a) 1 week submerged culture, (b) 1 week air-liquid interface culture, (c) 2 weeks air-liquid interface culture; Immunofluorescence of human skin equivalent in engineered melanoma model at (d) 1 week submerged culture, (e) 1 week air-liquid interface culture, (f)2 weeks air-liquid interface culture. Paraffin sections were immunostained for Filaggrin and Sytox Green as nuclear stain. Scale bar, 50µm.

To investigate the reason of lack epidermis differentiation in melanoma model, we examined the epithelial cell capability to express p63. Analysis at submerged conditions and 1 and 2

weeks after air-liquid interface transfer, relieve that p63 is regular expressed in healthy model (Fig. 6a, 6b, 6c) and is completely absent in melanoma model (Fig. 6d, 6e, 6f). Figure 6c shows that P63/K10 signals exhibits a differentiation patterns in healthy model equal to normal human epidermis (K10 that identifies the suprabasal cells, is located above the p63 signal) and also figure 6f shows a total absence of P63 expression in melanoma model. Previous studies established that p63 is required in development for proper epidermal stratification and differentiation [63]. Truong et al. (2016) have been demonstrated that p63-deficient primary human keratinocytes exhibited hypoproliferation. In details simultaneous p63 and p53 knockdown rescued the cell proliferation defect of p63 knockdown alone but failed to restore differentiation, suggesting that defects in epidermal proliferation and differentiation are mediated via p53-dependent and -independent mechanisms, respectively [64]. These considerations explain the low and absent signals of K10 and filaggrin, respectively, in melanoma model. Also, the basal keratin 14, which are expressed throughout the epithelium of regenerating tissue, was not altered because of p63 may not directly regulate expression of these proteins in this setting [60,64]. Together, these results suggest that the lack of epithelial differentiation in melanoma model could be attributed to A375 cells capability to inhibit the production of P63 in keratinocytes.

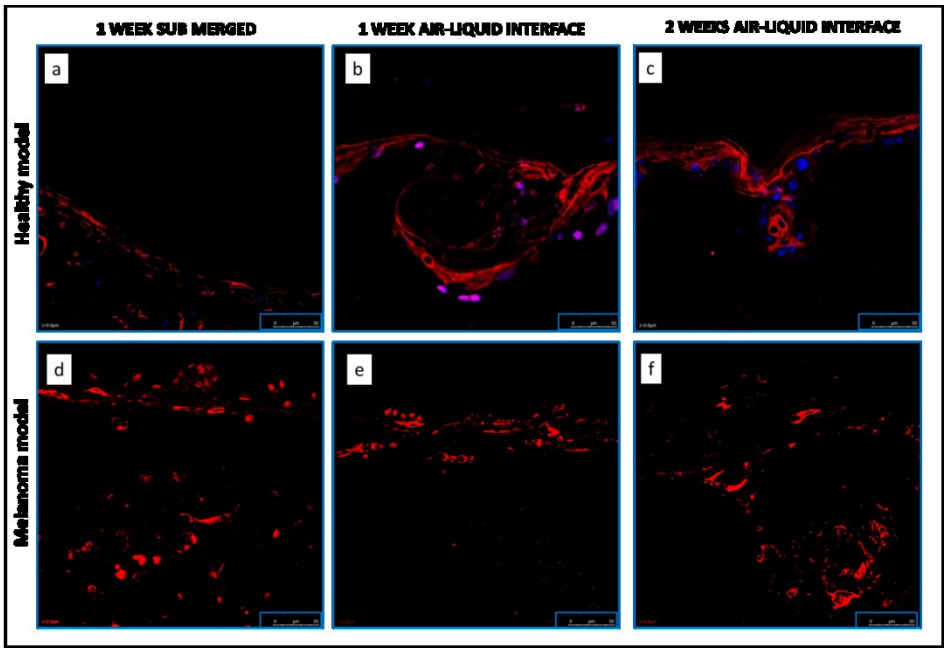

Fig .6: Immunofluorescence of human skin equivalent in engineered healthy model at (a) 1 week submerged culture, (b) 1 week air-liquid interface culture, (c) 2 weeks air-liquid interface culture; Immunofluorescence of human skin equivalent in engineered melanoma model at (d) 1 week submerged culture, (e) 1 week air-liquid interface culture, (f)2 weeks air-liquid interface culture. Paraffin sections were immunostained for P63 (blue) and K10 (red). Scale bar, 50µm.

In the last decades the role E-cadherin in epidermal differentiation process has been demonstrated. Experimental evidence indicates that epidermal deletion of the cell-cell adhesion protein, E-cadherin, results in delayed progression of epidermal differentiation [65]. E-cadherin is necessary for epidermal differentiation, and the loss of this protein mediated adhesion shifts the homeostatic balance toward proliferation [66]. Thus, further investigations on differentiation process were carried out by monitoring cadherins expression in both systems (Fig. 7 and Fig. 8). E-cadherin was immunolocalized in basal and suprabasal cells of the engineered normal model, showing functional adherens junctions and microfilaments in the full length of the engineered tissue (Fig. 7a, 7b, 7c). E-cadherin was strongly expressed in basal keratinocytes and specialized epithelial structures. A natural gradient of E-cadherin

mediated adhesion exists within the normal engineered epidermis such that increasing adhesion correlates with the progression of time and, consequently, differentiation (Fig. 7). Therefore, E-cadherin mediated adhesion may function as a microenvironmental cue to promote epidermal differentiation. Investigations of E-cadherin expression in melanoma model (Fig. 8), reveals that the levels of expression were significantly different among cells of the healthy and tumor engineered models at each time of detection (Fig. 8a, 8b, 8c). The expression levels resulted significantly lower in tumor engineered model and cells in the upper layer of epidermis did not express E-cadherin at 1 and 2 weeks of air-liquid interface (Fig. 8b, 8c). We already demonstrated that epithelial cells in the melanoma model do not differentiated and realize corneum stratum, moreover the analysis revealed the presence of nucleic cells in the upper layer of epidermis of engineered melanoma model. In order to understand the nature of these cells, N-cadherin expression was investigated and compared with E-cadherin expression. IHC of N-cadherin revealed a positive signal in tumor model exactly in correspondence of negative E-cadherin-cells (Fig. 8a, 8b, 8c compared with 8d, 8e, 8f respectively, arrow). N-cadherin was not detected in healthy model at any time (Fig. 7d, 7e, 7f). The biology of tumour invasion and metastasis is a multistep process, dependent on the outcome of a series of interactions between tumour cells and host cells or tissues. These phases include growth, angiogenesis, detachment, migration and release, as well as survival and migration of the metastasis, followed by invasion and implantation. Invasion itself is a complex process involving proteolysis of tissue barriers, as well as alteration in cell/cell and cell/matrix interactions. Increasing evidence implicates reduced expression of E-cadherin with increased metastatic potential of epithelial cancers. Despite the loss of E-cadherin expression by melanoma cells, cells in tumor model express high levels of N-cadherin as well as *in vivo*

happen [29,30,66,67]. It have been demonstrated that the switching of cadherin subtypes during melanoma development allows melanoma cells to interact directly with other N-cadherin-expressing cells, such as fibroblasts, thus affecting tumor-host cell adhesion, tumor cell invasion and migration, and gene expression [26]. Potential role of N-cadherin in the development and progression of melanoma is widely demonstrated. N-Cadherin mediating homotypic and heterotypic aggregation improve cells ability to migrate through basement membrane [68,69].

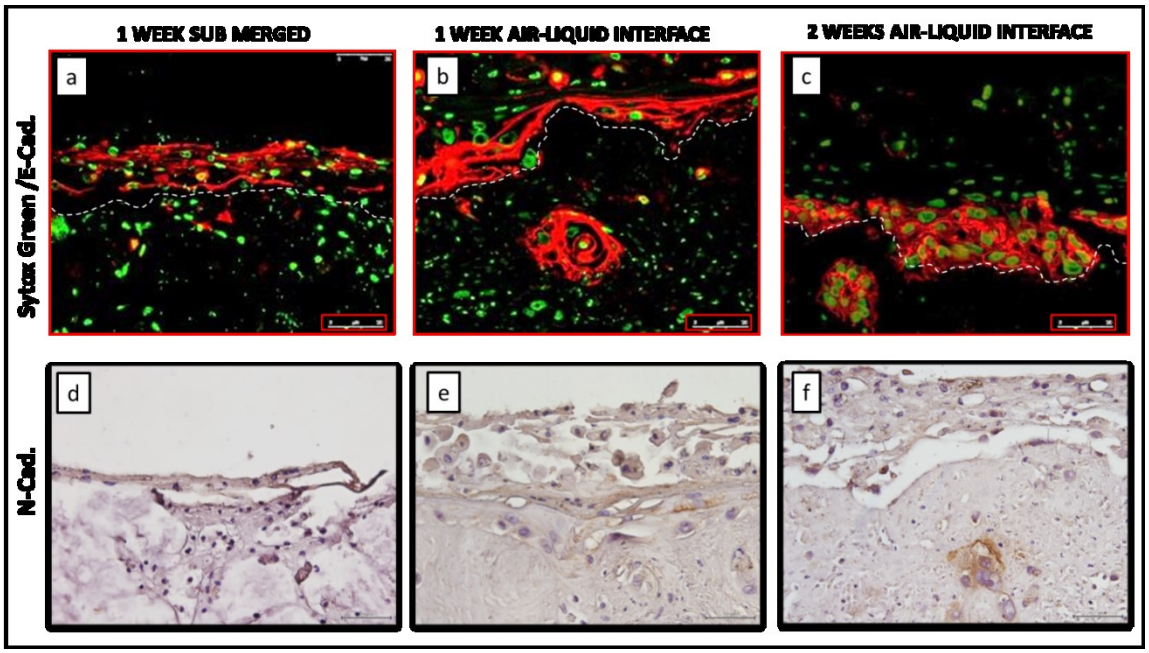

Fig .7: Immunofluorescence of human skin equivalent in engineered healthy model at (a) 1 week submerged culture, (b) 1 week air-liquid interface culture, (c) 2 weeks air-liquid interface culture; paraffin sections were immunostained for E-cadherin and Sytox Green as nuclear stain. Immunohistochemistry of human skin equivalent in engineered healthy model at (d) 1 week submerged culture, (e) 1 week air-liquid interface culture, (f) 2 weeks air-liquid interface culture; paraffin sections were immunostained for N-cadherin. Scale bar, 50µm.

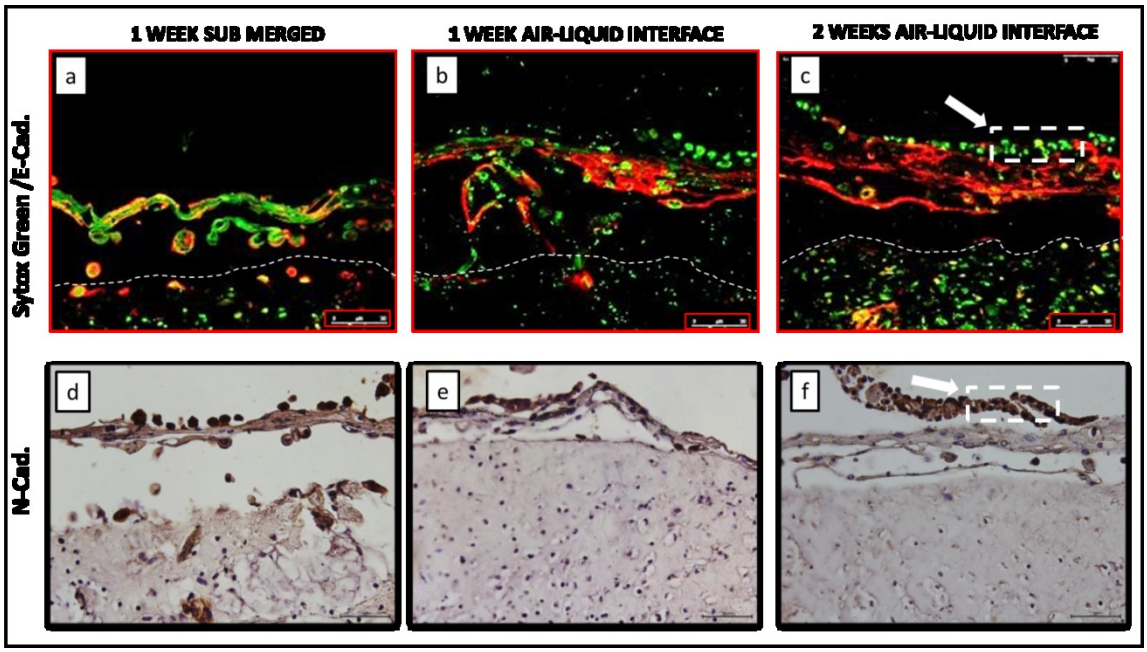

Fig .8: Immunofluorescence of human skin equivalent in engineered melanoma model at (a) 1 week submerged culture, (b) 1 week air-liquid interface culture, (c) 2 weeks air-liquid interface culture; paraffin sections were immunostained for E-cadherin and Sytox Green as nuclear stain. Immunohistochemistry of human skin equivalent in engineered melanoma model at (d) 1 week submerged culture, (e) 1 week air-liquid interface culture, (f) 2 weeks air-liquid interface culture; paraffin sections were immunostained for N-cadherin. Scale bar, 50µm.

These considerations are a proof that the tumor cells in melanoma model could be acquired a radial growth phenotype as well as *in vivo*. This could be explained the presence of cells with an intense dark color in HE stain (Fig. 2e, 2f, arrows) – indicating presence of A375 melanoma cells – at the epidermal-dermal junction. At this point, we confirmed tumor nature of these cells and, consequently, the localization of melanoma cells within the organotypic model by immunohistochemical analysis for the expression of the S100 and CD146 proteins. The cells presenting clusters organization, isolated from the tumor model, showed a significantly high expression of S100 and CD146 (Fig. 9). Conversely, healthy model does not express these two markers (data not shows). These results demonstrated clusters organization of A375 and formation of nests on top of epidermis. Moreover, Fig. 9b, 9e display

a rapid proliferation and aggressive invasive growth deep into full epithelium still after 1 week of air-liquid transfer. Data confirmed that at the end of a two weeks culture period, the majority of A375 cells are located on the surface of the epithelial layer and between basal epidermal layer and basement membrane (Fig. 9c, 9f). A375-RGP primary melanoma cells are disposed as a continuous layer of cells and as small nests at the epidermal-dermal junction. Detection of S-100 and CD146 also permitted to investigate cutaneous appendage nature. As previously mentioned, HE stain revealed the presence of epithelial cyst-like inclusions in their dermal portion; in addition, the number of cutaneous appendage decreased in engineered tumor model. Indeed, this cyst-forming capability was rarely observed in tissues composed both of keratinocytes than A375. We demonstrated that all cysts in dermis compartment are healthy and only composed by keratinocytes (Fig. 10, arrows). A375s formed cell nests within the epidermal layer but showed no propensity for dermal invasion. In engineered tumor model, A375 cells derived from primary tumor sites formed large compact (Fig. 9c, 9f) and small aggregates (Fig. 10a, 10c, 10e) over the basal layer of the reconstructed epidermis. However, they did not spread into the dermis (Fig. 10b, 10d, 10f). Similar results were already reported in literature in the presence of melanoma cells from primary tumor, where intra-epidermally growing nodules were bordered by an intact basement membrane but they did not disintegrate it [57,70,71].

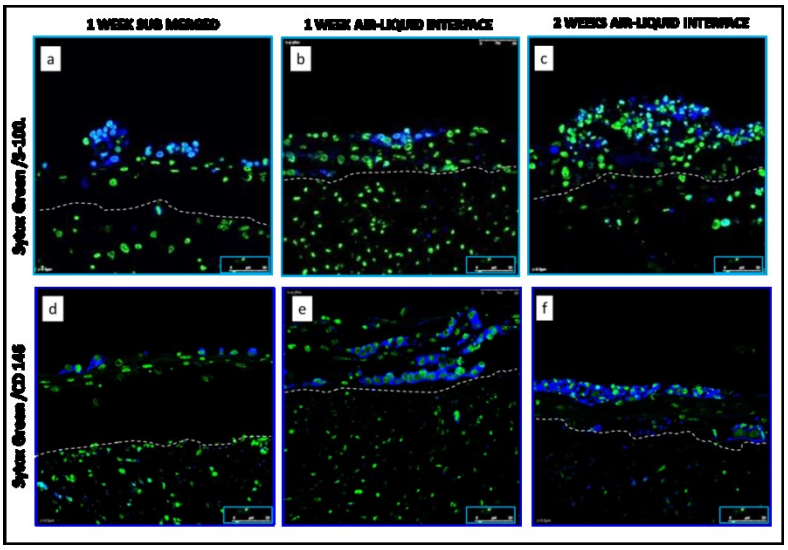

Fig .9: Immunofluorescence of human skin equivalent in engineered melanoma model at (a) 1 week submerged culture, (b) 1 week air-liquid interface culture, (c) 2 weeks air-liquid interface culture; paraffin sections were immunostained for S-100 and Sytox Green as nuclear stain. Immunofluorescence of human skin equivalent in engineered melanoma model at (a) 1 week submerged culture, (b) 1 week air-liquid interface culture, (c) 2 weeks air-liquid interface culture; paraffin sections were immunostained for CD146 and Sytox Green as nuclear stain. Scale bar, 50 µm.

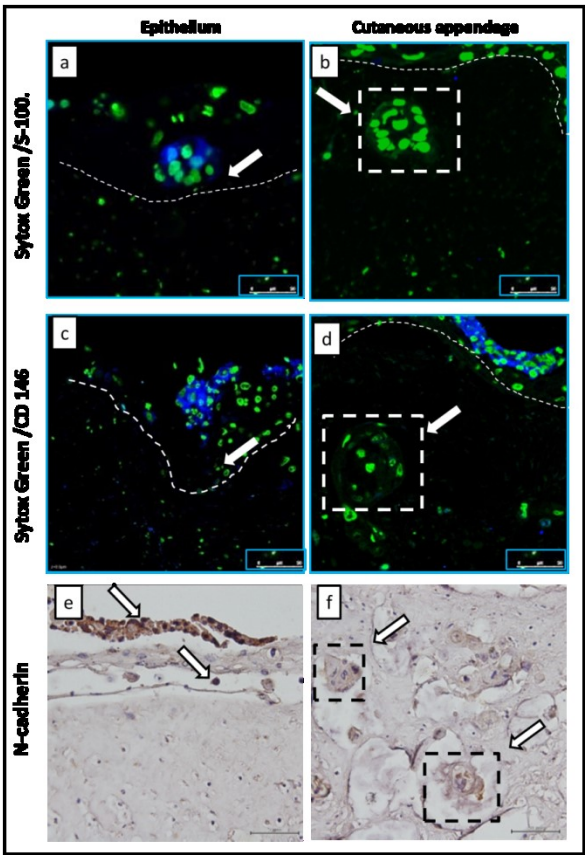

Fig .10: Investigations of cutaneous appendage in melanoma model after 2 weeks of air-liquid interface transfer. Paraffin sections were immunostained for S-100 and Sytox Green as nuclear stain in epithelium (a) and in dermis (b). Paraffin sections were immunostained for CD146 and Sytox Green as nuclear stain in epithelium (c) and in dermis (d). IHC of Paraffin sections for N-cadherin in epithelium (e) and in dermis (f). Scale bar, 50 µm.

The ability of melanoma cells from primary tumor to migrate into the epidermal layers leads to a radial invasion [57]. Over the years, in many *in vitro* melanoma studies have already been used 3D engineered models to look at the invasive behaviour of different metastatic human melanoma cell lines and different interaction with skin keratinocytes and fibroblasts. Commonly, the growth patterns of melanoma cells representing different stages of tumor progression was analysed by comparing the phenotypes and the behavior of melanoma cells derived from primary and metastatic sites [55–58,72]. The results have been demonstrated that non-metastatic melanoma cell lines are incapable of dermal invasion [57], whereas metastatic cell lines breached the BM and readily invaded the dermis [58] . Moreover, it has been recently observed that invasive capacity of melanoma cells is strongly dependent on the presence or absence of a BM too. Indeed, under certain circumstances, high metastatic cells also failed to invade the dermis when BM structure was confirmed. For examples, in the presence of a BM a significantly reduction of A375-SM invasion was observed [55,70,71]. Therefore BM results in a functional barrier for melanoma invasion for both tumor cell lines. Degradation of the basement membrane has also been correlated with the metastatic potential of tumor cells [70]. As generally reported [71] , tumor cells have been considered to be invasive if they are capable of overcoming basement membrane barriers alone. Taking into account the incapability of A375s to infiltrate dermis (Fig. 10 arrow), we focused analyses on basement membrane detection in the tumor model through immunohistochemical localization of laminin. Laminin is a glycoprotein that is present in the basal membrane and is considered as a biochemical equivalent of the anchoring filaments fixing basal keratinocytes to the basement membrane [73]. As a readily detectable basement membrane component, laminin can be used as a marker for presence of intact or degraded basement membrane during tumorigenesis [74]. Figure 11

reveals that the expression was continuous around the basement membrane in healthy model (Fig. 11a, 11b, 11c) and discontinuous and frequently frammented in melanoma model (Fig. 11d, 11e, 11f). Engineered healthy model showed more laminin expression and nothing loss of continuity compared to melanoma model, whose higher loss of continuity suggests a greater enzymatic degradation of basement membrane components. Comparing cutaneous appendage formation with basement membrane localization, we definily demonstrate that A375s cysts are localated just over basement membrane, as well as reported by Gibot et al. (2013), highlighting formation of small aggregates over the basal layer of the reconstructed epidermis, without spreading into the dermis [72]. The aggressive nature of this cell line well fitted with its *in vivo* characterisation [75].

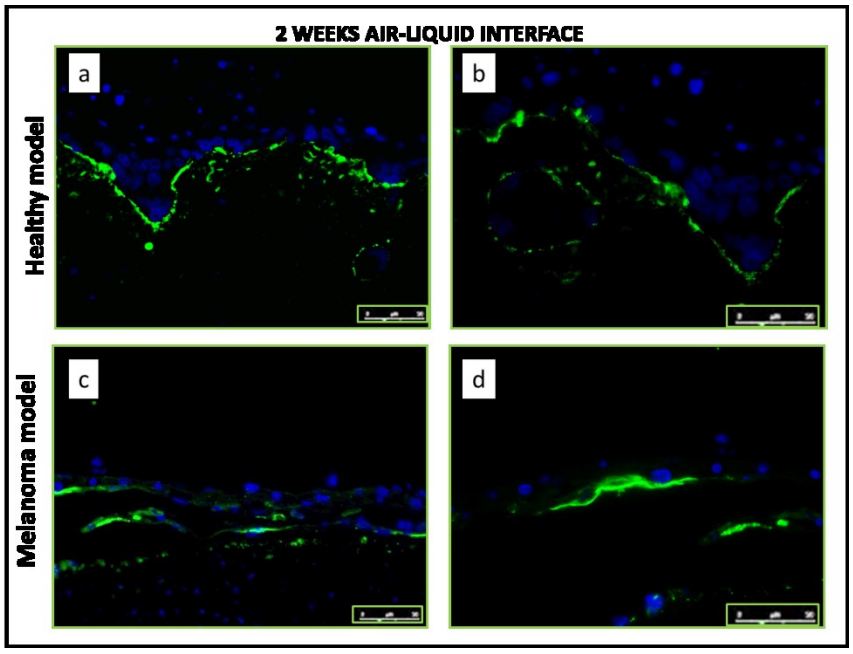

Fig .11: Immunofluorescence of human skin equivalent in engineered healthy model at 2 weeks air-liquid interface culture at low (a) and high (b) magnification. Immunofluorescence of human skin equivalent in engineered melanoma model at 2 weeks air-liquid interface culture at low (c) and high (d) magnification. Paraffin sections were immunostained for laminin V and DAPI as nuclear stain. Scale bar, 50µm.

Finally our data demonstrate that the engineered healthy model derived from foreskin keratinocytes showed a structured multilayered epithelium at day 6, evolving at day 12 to an organized epithelium similar to that of a human skin. Conversely, the present 3D culture model of skin melanoma revealed unstructured and disorganised epidermal tissue, including tardive cutaneous appendage formation at day 6, followed by an evolution to a flat and degenerative tissue at day 12. Engineered tumor model also exhibited good stability and well recapitulated radial growth phase phenotype, exhibiting the biological characteristics of proliferation and invasion of RGP (according to ATCC, A375-1619 derived from human melanoma epithelium). Melanoma cells not spreaded into the dermis but interfere with epidermal differentiation preventing p63 expression and destroying BM. The slightly less intense and dispersed basal membrane staining, observed where it is in direct contact with A375 cell nodules, could be explained by the loss of contact between the basal membrane and the epidermal basal cells that are directly responsible for its generation.

4.4 Conclusions

We fabricated a 3D human skin equivalent (3D-HSE) model with an endogenous stroma as dermis component (see chapter 2) to study an aggressive and rare form of skin cancer: melanoma. We underlined the importance of cell-ECM – with native basement membrane (BM) – and cell–cell (interactions between fibroblasts, keratinocytes, melanocytes and melanoma cells) communication involved in carcinogenesis. The disruptions in these forms of communication can alter cell biology of human skin [7,17]. Consequently, we investigated the role of skin cells and BM components on melanoma biology and invasive ability in reconstructed

human skin equivalent. We first made-up and characterized a human skin model that resembled the architecture of skin *in situ*, than we carried out an analogous procedure for the equivalent engineered tumor model. On the basis of our results, we can assert that there is communication between skin cells and melanoma cells and the outcome is dictated by the nature of the melanoma cells. Thus, the bioengineered 3D melanoma skin model may become a valuable tool to investigate the underlying mechanics of melanoma infiltration. The proposed study does not recapitulate yet melanoma metastasis process as a whole, however, the present engineered 3D tissue represents a reliable model for investigating the phenotype and behavior of melanoma cells derived from primary sites. Indeed, the 3D melanoma skin model is suitable to study the biological properties of radial growth phase invasion. This study represents a preliminary model for investigating all aspects of melanoma metastasis and it has great potential for improving our understanding of the interactive biology between melanoma cells and their immediate surroundings and evaluating melanoma cells influence on epidermis structure and differentiation.

4.5 References

1. Balois T, Ben Amar M. Morphology of melanocytic lesions in situ. Scientific reports 4:3622.c lesions in situ. *Sci Rep*. 2014;4:3622. doi:10.1038/srep03622.

2. Leight JL, Tokuda EY, Jones CE, Lin AJ, Anseth KS. Multifunctional bioscaffolds for 3D culture of melanoma cells reveal increased MMP activity and migration with BRAF kinase inhibition. *Proc Natl Acad Sci U S A*. 2015;112(17):5366-5371. doi:10.1073/pnas.1505662112.

3. Mandalà M, Massi D. Tissue prognostic biomarkers in primary cutaneous melanoma. *Virchows Arch*. 2014;464(3):265-281. doi:10.1007/s00428-013-1526-x.

4. Alonso SR, Tracey L, Ortiz P, et al. A high-throughput study in melanoma identifies epithelial-mesenchymal transition as a major determinant of metastasis. *Cancer Res*. 2007;67(7):3450-3460. doi:10.1158/0008-5472.CAN-06-3481.

5. Jemal A, Siegel R, Ward E, et al. Cancer Statistics, 2006. *CA Cancer J Clin*. 2006;56:106-130. doi:10.3322/canjclin.56.2.106.

6. Balch CM, Gershenwald JE, Soong SJ, et al. Final version of 2009 AJCC melanoma staging and classification. *J Clin Oncol*. 2009;27(36):6199-6206. doi:10.1200/JCO.2009.23.4799.

7. Bissel MJ, Radisky D. Putting tumors in context. *Nat Rev Cancer*. 2001;1(1):46-54. doi:10.1038/35094059.PUTTING.

8. Breetveld M, Richters CD, Rustemeyer T, Scheper RJ, Gibbs S. Comparison of wound closure after burn and cold injury in human skin equivalents. *J Invest Dermatol*.

2006;126(2003):1918-1921. doi:10.1038/sj.jid.5700330.

9. Huang CW, Wang CC, Jiang RS, Huang YC, Ho HC, Liu SA. The impact of tissue glue in wound healing of head and neck patients undergoing neck dissection. *Eur Arch Oto-Rhino-Laryngology*. 2016;273(1):245-250. doi:10.1007/s00405-015-3709-3.

10. Wu Y, Lin Y, Liu H, Li J. Inhibition of invasion and up-regulation of E-cadherin expression in human malignant melanoma cell line A375 by (-)-epigallocatechin-3-gallate. *J Huazhong Univ Sci Technolog Med Sci*. 2008;28(3):356-359. doi:10.1007/s11596-008-0330-3.

11. Day CL, Harrist TJ, Gorstein F, et al. Malignant melanoma. Prognostic significance of "microscopic satellites" in the reticular dermis and subcutaneous fat. *Ann Surg*. 1981;194:108-112.

12. Kawakami Y, Eliyahu S, Delgado CH, et al. Identification of a human melanoma antigen recognized by tumor-infiltrating lymphocytes associated with in vivo tumor rejection. *Proc Natl Acad Sci*. 1994;91(14):6458-6462. doi:10.1073/pnas.91.14.6458.

13. Eke I, Hehlgans S, Sandfort V, Cordes N. 3D matrix-based cell cultures: Automated analysis of tumor cell survival and proliferation. *Int J Oncol*. 2016;48(1):313-321. doi:10.3892/ijo.2015.3230.

14. González-de Arriba M, Bordel-Gómez MT, Solera JC, Sánchez-Estella J. Primary Dermal Melanoma: A Case Report and a Review of the Literature. *Actas Dermo-Sifiliográficas (English Ed*. 2013;104(6):518-522. doi:10.1016/j.adengl.2011.12.013.

15. Alonso SR, Tracey L, Ortiz P, et al. A high-throughput study in melanoma identifies

epithelial-mesenchymal transition as a major determinant of metastasis. *Cancer Res*. 2007;67(7):3450-3460. doi:10.1158/0008-5472.CAN-06-3481.

16. Johnson JP. Cell adhesion molecules in the development and progression of malignant melanoma. *Cancer Metastasis Rev*. 1999;18(3):345-357. http://www.ncbi.nlm.nih.gov/pubmed/10721489.

17. Ruiter D, Bogenrieder T, Elder D, Herlyn M. Melanoma – stroma interactions : structural and functional aspects. :35-43.

18. Lázár-Molnár E, Hegyesi H, Tóth S, Falus A. Autocrine and Paracrine Regulation By Cytokines and Growth Factors in Melanoma. *Cytokine*. 2000;12(6):547-554. doi:10.1006/cyto.1999.0614.

19. Beaumont KA, Mohana-Kumaran N, Haass NK. Modeling melanoma in vitro and in vivo. *Healthcare*. 2013;2(1):27-46. doi:10.3390/healthcare2010027.

20. Gibot L, Galbraith T, Huot J, Auger FA. Development of a tridimensional microvascularized human skin substitute to study melanoma biology. *Clin Exp Metastasis*. 2013;30(1):83-90. doi:10.1007/s10585-012-9511-3.

21. Gimotty PA, Guerry D, Ming ME, et al. Thin primary cutaneous malignant melanoma: A prognostic tree for 10-year metastasis is more accurate than American Joint Committee on cancer staging. *J Clin Oncol*. 2004;22(18):3668-3676. doi:10.1200/JCO.2004.12.015.

22. Satyamoorthy K, Meier F, Hsu MY, Berking C, Herlyn M. Human xenografts, human skin and skin reconstructs for studies in melanoma development and progression. *Cancer Metastasis Rev*. 1999;18(3):401-405. doi:10.1023/A:1006333627271.

23. Berning M, Prätzel-Wunder S, Bickenbach JR, Boukamp P. Three-Dimensional In Vitro Skin and Skin Cancer Models Based on Human Fibroblast-Derived Matrix. *Tissue Eng Part C Methods*. 2015;00(00):1-13. doi:10.1089/ten.TEC.2014.0698.

24. Li R, Liang J, Ni S, et al. A Mesenchymal-to-Epithelial Transition Initiates and Is Required for the Nuclear Reprogramming of Mouse Fibroblasts. *Cell Stem Cell*. 2010;7(1):51-63. doi:10.1016/j.stem.2010.04.014.

25. Lanti Y. *MECHANICAL PROPERTIES OF COLLAGEN FIBRILS AND ELASTIC FIBERS EXPLORED BY AFM Lanti Yang*.; 2008.

26. Girotti MR, Fernández M, López J a, et al. SPARC Promotes Cathepsin B-Mediated Melanoma Invasiveness through a Collagen I/$\alpha 2\beta 1$ Integrin Axis. *J Invest Dermatol*. 2011;131(12):2438-2447. doi:10.1038/jid.2011.239.

27. Baum CL, Arpey CJ. Normal cutaneous wound healing: clinical correlation with cellular and molecular events. *Dermatol Surg*. 2005;31(6):674-686; discussion 686. http://www.ncbi.nlm.nih.gov/entrez/query.fcgi?cmd=Retrieve&db=PubMed&dopt=Citation&list_uids=15996419.

28. Longati P, Jia X, Eimer J, et al. 3D pancreatic carcinoma spheroids induce a matrix-rich , chemoresistant phenotype offering a better model for drug testing. 2013:1-13.

29. Hazan RB, Phillips GR, Qiao RF, Norton L, Aaronson SA. Exogenous Expression of N-Cadherin in Breast Cancer Cells Induces Cell Migration , Invasion , and Metastasis. 2000;148(4):779-790.

30. The Catenin/Cadherin Adhesion System Is Localized in Synaptic Junctions Bordering

Transmitter Release Zones. 1996;135(3):767-779.

31. Elder D, Elder D. Melanoma Progression. 2016;(2015):1-8. doi:10.1016/j.pathol.2015.12.002.

32. Quintana E, Shackleton M, Sabel MS, Fullen DR, Johnson TM, Morrison SJ. Efficient tumour formation by single human melanoma cells. *Nature*. 2008;456(7222):593-598. doi:10.1038/nature07567.

33. Garimella SD, Krantz SB, Shields MA, Grippo PJ, Munshi HG. Epithelial – mesenchymal transition and pancreatic cancer progression. 2012;(15):1-9.

34. Kimata Y, Kimata YI, Shimizu Y, et al. Genetic Evidence for a Role of BiP / Kar2 That Regulates Ire1 in Response to Accumulation of Unfolded Proteins. *Mol Biol Cell*. 2003;14(February):2559-2569. doi:10.1091/mbc.E02.

35. Lever E, Sheer D. The role of nuclear organization in cancer. *J Pathol*. 2010;220(September):114-125. doi:10.1002/path.

36. Fang D, Nguyen TK, Leishear K, et al. A tumorigenic subpopulation with stem cell properties in melanomas. *Cancer Res*. 2005;65(20):9328-9337. doi:10.1158/0008-5472.CAN-05-1343.

37. Bernadette Marrero, Richard Heller. The use of an in vitro 3D melanoma model to predict in vivo plasmid transfection using electroporation. *Biomaterials*. 2012;33(10):3036-3046. doi:10.1038/nature13314.A.

38. Bottos A, Martini M, Di Nicolantonio F, et al. Targeting oncogenic serine/threonine-protein kinase BRAF in cancer cells inhibits angiogenesis and abrogates hypoxia. *Proc Natl*

Acad Sci U S A. 2012;109(6):E353-E359. doi:10.1073/pnas.1105026109.

39. Villanueva J, Vultur A, Lee JT, et al. Acquired Resistance to BRAF Inhibitors Mediated by a RAF Kinase Switch in Melanoma Can Be Overcome by Cotargeting MEK and IGF-1R/PI3K. *Cancer Cell*. 2010;18(6):683-695. doi:10.1016/j.ccr.2010.11.023.

40. Jiang CC, Lai F, Thorne RF, et al. MEK-independent survival of B-RAFV600E melanoma cells selected for resistance to apoptosis induced by the RAF inhibitor PLX4720. *Clin Cancer Res*. 2011;17(4):721-730. doi:10.1158/1078-0432.CCR-10-2225.

41. Wong K-K. Recent developments in anti-cancer agents targeting the Ras/Raf/MEK/ERK pathway. *Recent Pat Anticancer Drug Discov*. 2009;4(1):28-35. doi:10.2174/157489209787002461.

42. Liu C, Peng W, Xu C, et al. BRAF Inhibition Increases Tumor Infiltration by T cells and Enhances the Antitumor Activity of Adoptive Immunotherapy in Mice. *Clin Cancer Res*. 2013;19(2):393-403. doi:10.1158/1078-0432.CCR-12-1626.

43. Ji Z, Flaherty KT, Tsao H. Targeting the RAS pathway in melanoma. *Trends Mol Med*. 2012;18(1):27-35. doi:10.1016/j.molmed.2011.08.001.

44. Nazarian R, Shi H, Wang Q, et al. Melanomas acquire resistance to B-RAF(V600E) inhibition by RTK or N-RAS upregulation. *Nature*. 2010;468(7326):973-977. doi:10.1038/nature09626.

45. Guerriere-Kovach PM, Hunt EL, Patterson JW, Glembocki DJ, English JC, Wick MR. Primary melanoma of the skin and cutaneous melanomatous metastases: Comparative histologic features and immunophenotypes. *Am J Clin Pathol*. 2004;122(1):70-77.

doi:10.1309/R8N1-CN04-KKFV-6M7T.

46. Beaumont KA, Mohana-Kumaran N, Haass NK. Modeling melanoma in vitro and in vivo. *Healthcare*. 2013;2(1):27-46. doi:10.3390/healthcare2010027.

47. Mertsching H, Weimer M, Kersen S, Brunner H. Human skin equivalent as an alternative to animal testing. *GMS Krankenhhyg Interdiszip*. 2008;3(1):Doc11.

48. Martin I, Wendt D, Heberer M. The role of bioreactors in tissue engineering. *Trends Biotechnol*. 2004;22(2):80-86. doi:10.1016/j.tibtech.2003.12.001.

49. Groeber, Florian, Holeiter, Monika, Hampel, Martina, Hinderer, Svenja, Schenke-Layland, Katja. Skin tissue engineering — In vivo and in vitro applications. *Adv Drug Deliv Rev*. 2011;63(4-5):352-366. doi:10.1016/j.addr.2011.01.005.

50. Friedrich J, Ebner R, Kunz-Schughart LA. Experimental anti-tumor therapy in 3-D: Spheroids – old hat or new challenge? *Int J Radiat Biol*. 2007;83(11-12):849-871. doi:10.1080/09553000701727531.

51. Nyga A, Cheema U, Loizidou M. 3D tumour models: Novel in vitro approaches to cancer studies. *J Cell Commun Signal*. 2011;5(3):239-248. doi:10.1007/s12079-011-0132-4.

52. Marrero B, Heller R. The use of an invitro 3D melanoma model to predict invivo plasmid transfection using electroporation. *Biomaterials*. 2012;33(10):3036-3046. doi:10.1016/j.biomaterials.2011.12.049.

53. Kelm JM, Fussenegger M. Microscale tissue engineering using gravity-enforced cell assembly. *Trends Biotechnol*. 2004;22(4):195-202. doi:10.1016/j.tibtech.2004.02.002.

54. Kimlin LC, Casagrande G, Virador VM. In vitro three-dimensional (3D) models in cancer research: An update. *Mol Carcinog*. 2013;52(3):167-182. doi:10.1002/mc.21844.

55. Eves P, Katerinaki E, Simpson C, et al. Melanoma invasion in reconstructed human skin is influenced by skin cells--investigation of the role of proteolytic enzymes. *Clin Exp Metastasis*. 2003;20(8):685-700. http://www.ncbi.nlm.nih.gov/pubmed/14713103.

56. Corporation M. Reconstructed Human Skin Model to Study Melanoma at Different Stages of Progression. 2011:1-5.

57. Van Kilsdon, Bergers M, Van Kempen, Schalkwijk J, GW. S. Keratinocytes drive melanoma invasion in a reconstructed skin model. *Melanoma Res*. 2010;20(5):372-380.

58. Meier F, Nesbit M, Hsu MY, et al. Human melanoma progression in skin reconstructs : biological significance of bFGF. *Am J Pathol*. 2000;156(1):193-200. doi:10.1016/S0002-9440(10)64719-0.

59. Imparato G, Urciuolo F, Casale C, Netti PA. The role of microscaffold properties in controlling the collagen assembly in 3D dermis equivalent using modular tissue engineering. *Biomaterials*. 2013;(34):7851-7861.

60. Hsieh J, Chen S, Cheng S. Molecular Profiling of A375 Human Malignant Melanoma Cells Treated with Kojic Acid and Arbutin. *Biol Chem*. 2011;3.

61. McCrea PD, Gu D. The catenin family at a glance. *J Cell Sci*. 2010;123(5):637-642. doi:10.1242/jcs.039842.

62. Ciapetti G, Cenni E, Pratelli L, Pizzoferrato A. In vitro evaluation of cell/biomaterial interaction by MTT assay. *Biomaterials*. 1993;14(5):359-364. doi:10.1016/0142-

9612(93)90055-7.

63. Mohapatra S, Coppola D, Riker AI, Pledger WJ. Roscovitine inhibits differentiation and invasion in a three-dimensional skin reconstruction model of metastatic melanoma. *Mol Cancer Res*. 2007;5(2):145-151. doi:10.1158/1541-7786.MCR-06-0300.

64. Truong AB, Kretz M, Ridky TW, Kimmel R, Khavari PA. P63 Regulates Proliferation and Differentiation of Developmentally Mature Keratinocytes. *Genes Dev*. 2016;20(22):3185-3197. doi:10.1101/gad.1463206.

65. Sanders DSA, Blessing K, Hassan GAR, Bruton R, Marsden JR, Jankowski J. Alterations in cadherin and catenin expression during the biological progression of melanocytic tumours. *Clin Pathol*. 2014;(52):151-157.

66. Calautti E, Li J, Saoncella S, Brissette JL, Goetinck PF. Phosphoinositide 3-kinase signaling to Akt promotes keratinocyte differentiation versus death. *J Biol Chem*. 2005;280(38):32856-32865. doi:10.1074/jbc.M506119200.

67. Wei CJ, Francis R, Xu X, Lo CW. Connexin43 associated with an N-cadherin-containing multiprotein complex is required for gap junction formation in NIH3T3 cells. *J Biol Chem*. 2005;280(20):19925-19936. doi:10.1074/jbc.M412921200.

68. Gang Li, Kapaettu Satyamoorthy, Herlyn M. N-Cadherin-mediated Intercellular Interactions Promote Survival and Migration of Melanoma Cells. *Cancer Res*. 2001;(17):3819-3825.

69. Takeichi M. The cadherins : cell-cell adhesion molecules controlling animal morphogenesis. 1988;655.

70. Woodward JKL, Nichols CE, Rennie IG, Parsons MA, Murray AK, Sisley K. An in vitro assay to assess uveal melanoma invasion across endothelial and basement membrane barriers. *Investig Ophthalmol Vis Sci*. 2002;43(6):1708-1714.

71. P. Eves, Layton C, S. Hedley, et al. Characterization of an in vitro model of human melanoma invasion based on reconstructed human skin. *Br J Dermatol*. 1999;(142):210-222.

72. Gibot L, Galbraith T, Huot J, Auger F a. Development of a tridimensional microvascularized human skin substitute to study melanoma biology. *Clin Exp Metastasis*. 2013;30:83-90. doi:10.1007/s10585-012-9511-3.

73. El Ghalbzouri A, Hensbergen P, Gibbs S, Kempenaar J, van der Schors R, Ponec M. Fibroblasts facilitate re-epithelialization in wounded human skin equivalents. *Lab Invest*. 2004;84:102-112. doi:10.1038/labinvest.3700014.

74. Suzuki K, Tanaka T, Enoki M, Nishida T. Coordinated reassembly of the basement membrane and junctional proteins during corneal epithelial wound healing. *Invest Ophthalmol Vis Sci*. 2000;41(9):2495-2500.

75. Herwig N, Belter B, Wolf S, Haase-Kohn C, Pietzsch J. Interaction of extracellular S100A4 with RAGE prompts prometastatic activation of A375 melanoma cells. *J Cell Mol Med*. 2016;XX(X):n/a - n/a. doi:10.1111/jcmm.12808.